IAEA-TECDOC-1385

WWER-440 fuel rod experiments under simulated dry storage conditions

INTERNATIONAL ATOMIC ENERGY AGENCY

IAEA

April 2004

FOREWORD

One of the prerequisites for confirming the safety of dry spent fuel storage technologies is the ability to predict the condition of the spent fuel during its period of storage. Experimental results are an important factor in modelling spent fuel behaviour during dry storage conditions. Accordingly, a contract with the State Scientific Centre of the Russian Federation, Scientific Research Institute for Nuclear Reactors (RIAR) in Dimitrovgrad, Russian Federation was signed in April 2001 to conduct a dry storage experiment in the hot cells at RIAR. For this experiment the following scope of work was planned: selection and certification of fuel rods for tests; dry storage tests at 350°C for two months; analysis of fuel rods after tests; dry storage tests at 390°C for two months; analysis of fuel rods after the tests; issuing of a final report on the test results.

The Government of Japan provided extra-budgetary funds for these dry storage tests of WWER-440 fuel rods to improve the safety of spent fuel storage in the Central and Eastern European countries. The activities performed under the extra-budgetary funds are consistent with the spent fuel management projects and objectives defined in the IAEA Programme. A consultants meeting held in Vienna in May 2002, discussed and finalized the results reported here. This TECDOC describes the tests, the results of the pre- and post-characterization of the test rods and evaluates the results achieved.

The IAEA wishes to express its thanks to S. Pavlov (RIAR/Russian Federation), M. Peehs (consultant/Germany), V. Smirnov (RIAR/Russian Federation), and J. Vesely (Skoda UJ/Czech Republic), who prepared this TECDOC on the basis of the original report supplied by RIAR.

The IAEA officer responsible for this publication was P. Dyck of the Division of Nuclear Fuel Cycle and Waste Technology.

CONTENTS

1. INTRODUCTION

One of the key objectives in the development of the dry storage technology for WWER-440 spent nuclear fuel is safety especially with respect to: environmental impacts; radiation to the service personnel and the public; all engineering issues like fuel handling during loading and unloading and during spent nuclear fuel (SNF) storage.

So it is necessary to predict the condition of SNF during storage and at the end of its storage period. It should be shown that the SNF can be safely handled and transported at the end of the dry storage period and will be able to withstand safely all technological operations in the back end of the fuel cycle. It is possible to make such predictions if there is a model for SNF behaviour under dry storage conditions. In order to develop such a model it is necessary to put SNF to a dry storage test, simulating the dry storage conditions. Since all material degradation processes are temperature dependant, it is sufficient to investigate the dry storage behaviour at higher temperature levels and during a shorter period of time.

The main criterion from the standpoint of preventing radioactive material releases is the fuel rod (FR) cladding integrity during dry storage. The following factors can cause FR failure:

- Thermal creep of cladding material under internal gas pressure;
- Corrosive damage of the inner and outer cladding surface;
- Hydrogen induced cladding defects;
- Stress corrosion cracking of cladding.

The most probable mechanism of FR failure is thermal creep [1, 2] resulting in cladding defects. In this connection, the maximum allowable temperature of the fuel rods under the standard storage conditions is one of the most important parameters which determine the safety of dry storage.

The following conditions and criteria of safe dry storage are considered to be generally accepted (or standard) for LWR SNF [2, 3] and applied in the Russian Federation:

- Preliminary cooling of SNF in the spent fuel pool for 5 years;
- The maximum allowable hot spot temperature of FR cladding under the standard storage conditions is 350°C;
- The maximum allowable temperature of FR cladding under the transient and emergency conditions is 450°C during 8 hours;
- The maximum allowable hoop strain of the cladding should not exceed 1% at the expiration of the storage period.

Therefore, it is necessary to test the irradiated WWER-440 FRs at temperatures common to the dry storage conditions to prove the reliable dry storage performance of spent WWER-440 fuel.

The possible FR failure caused by thermal cladding material creep under the influence of internal pressure and high temperature appears to be the main concern during long term dry storage. Therefore, it is necessary to study the behaviour of some fuel rods at different storage temperatures.

The RIAR (Research Institute for Atomic Reactors) selected FRs for testing from a fuel assembly (FA) that had experienced an average burnup of ~46 MW·d/kgU in 5 reactor cycles. The FR cladding material is Zr-1%Nb alloy. The dry storage tests were performed at 350°C for 2 months and at 390°C for another 2 months. After the 350°C test period and after the 390°C test period the SNF was inspected by non-destructive methods. The tested FRs did not show any detectable changes in optical appearance, eddy current testing, profilometry, length measurement, gamma scanning and oxide thickness measurement. In parallel, 3 FRs taken from the neighbourhood of the tested FRs were inspected by destructive methods to get the fission gas content in the SNF, the void volume and mechanical test data of fuel rods with practically identical operational performance. Detailed statistical investigation of the fuel rod diameter measurements indicated that a diameter increase of 1 to 2 μm had occurred. This value corresponds to the theoretical forecast for the diameter increase during the test. No negative effects on the FR in the test had been observed in the course of the test programme. An extrapolation of the test data for longer term storage shows that even under constant storage temperature the total strain at 350°C stays after 50 years below 1%. Assuming a temperature drop characteristic for fuel pre-cooled for five years in a dry storage cask, the total hoop strain does not exceed approximately 0.02% (too low to cause safety concerns).

2. SELECTION AND CERTIFICATION OF FUEL RODS FOR TESTING

Two WWER-440 fuel rods were selected to perform thermal testing from a fuel assembly operated during five fuel cycles in the third unit of the Kola Nuclear Power Plant (NPP). So-called "equivalent" fuel rods adjacent to the test FRs were chosen to assess mechanical properties of FR cladding and pressure of fission gas products.

2.1. MAIN DESIGN DATA ON FUEL ASSEMBLIES AND FUEL RODS

WWER-440 standard fuel assemblies consist of a top nozzle, a bottom nozzle with the bottom spacer grid to fasten FR tails, a hexagonal shroud tube and FR bundles containing the central tube, 11 spacer grids and 126 fuel rods.

Zr-1%Nb alloy was chosen as material for cladding and end-plugs of the fuel rods. Pellets sintered from uranium dioxide and enriched in ^{235}U up to 4.4% were used as fuel. The shroud tube is made from Zr-2.5%Nb alloy. The top and bottom nozzle spacer grids of the fuel assemblies are made of 08X18H10T steel. Table I includes the main design data for fuel assemblies and fuel rods and Figures 1 and 2 are the schematic representation of the WWER-440 fuel assembly and fuel rod.

Fuel rods No. 64 and No. 78 located near the central tube and in the fourth row, respectively (see Fig. 3) were selected for testing. As an equivalent to fuel rod No. 64, the fuel rods No. 52 and 65 were selected [and to fuel rod No. 78, the fuel rods No. 65 and 79]. These fuel rods consist of fuel from different batches and different cladding tubes (Table II).

Table I. Data on component parts of fuel assemblies and fuel rods

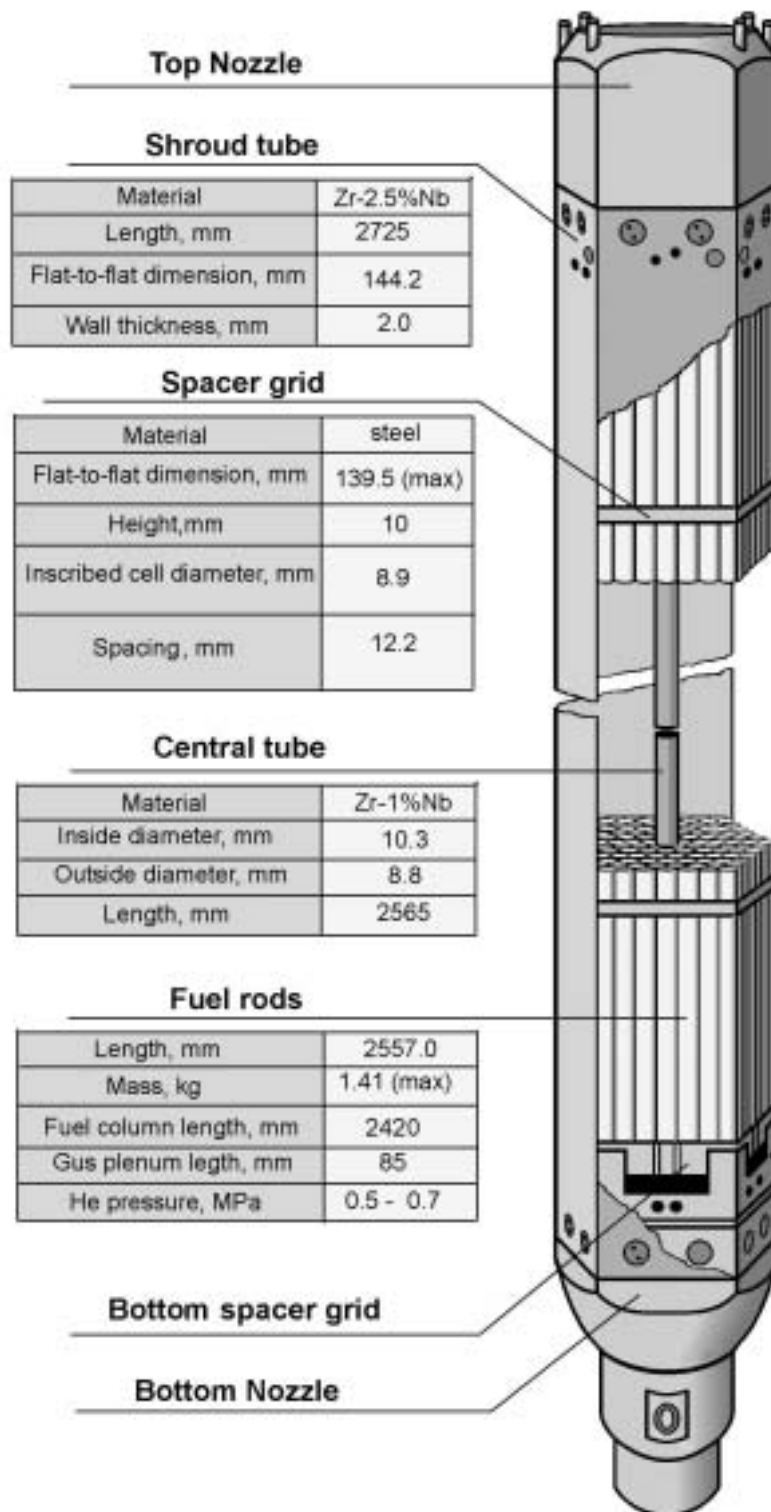| Parameter	Value
Shroud tube dimensions, mm:	
length	3 217
flat-to-flat dimension	144.2
Shroud sheet thickness, mm	2.0
Shroud fastening to the end parts	Screws (12 holes in each wrapper end)
Fuel rod length, mm	2 557
Requirement on the outside FR diameter, mm	9.1
Inside cladding diameter, mm	7.72
Cladding wall thickness, mm	0.65
Fuel pellet:	
Outside diameter, mm	7.60
Central hole diameter, mm	1.2
Height, mm	8–14
- Fuel column length, mm;	2 410–2 430
Fuel column mass, g	1087
Gas plenum, cm^3	16.7–17.2
Gas plenum length, mm	85
Helium pressure in fuel rod, MPa at ambient temperature	0.5–0.7
Helium content in gas, filling of the fuel rod, %	Not more than 99.9

Top Nozzle

Shroud tube

Material	Zr-2.5%Nb
Length, mm	2725
Flat-to-flat dimension, mm	144.2
Wall thickness, mm	2.0

Spacer grid

Material	steel
Flat-to-flat dimension, mm	139.5 (max)
Height, mm	10
Inscribed cell diameter, mm	8.9
Spacing, mm	12.2

Central tube

Material	Zr-1%Nb
Inside diameter, mm	10.3
Outside diameter, mm	8.8
Length, mm	2565

Fuel rods

Length, mm	2557.0
Mass, kg	1.41 (max)
Fuel column length, mm	2420
Gus plenum legth, mm	85
He pressure, MPa	0.5 - 0.7

Bottom spacer grid

Bottom Nozzle
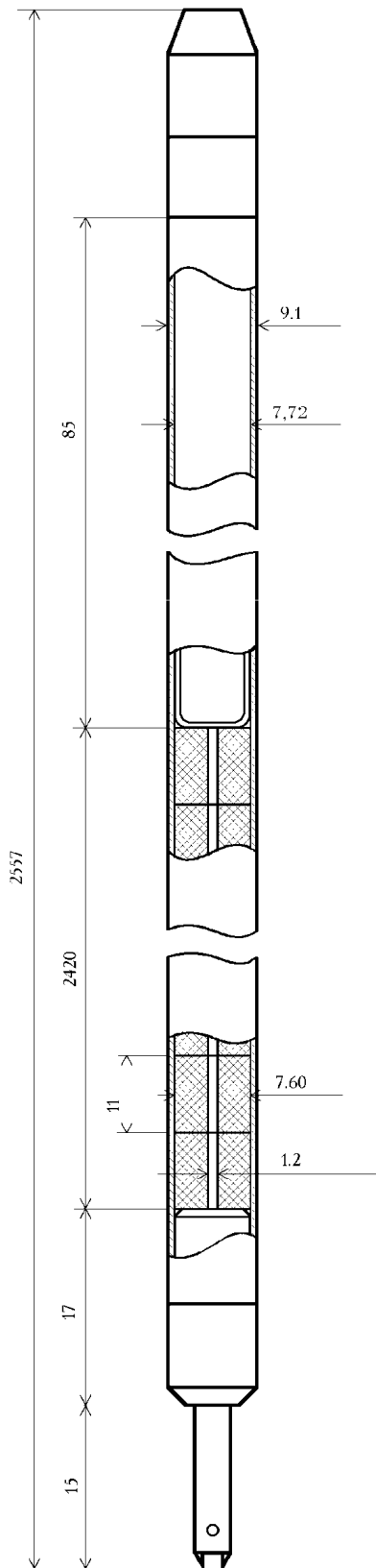
Fig. 1. WWER-440 FA schematic drawing.

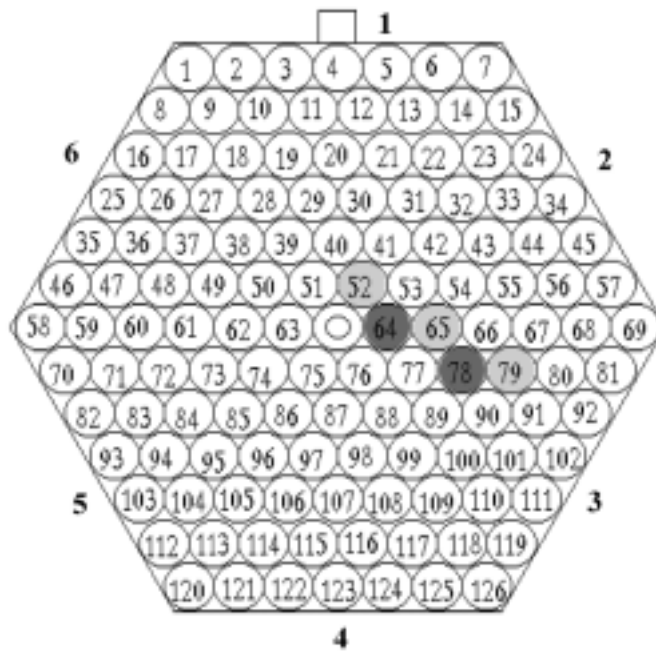*Fig. 2. WWER-440 FR schematic drawing.*

Fig. 3. Scheme of FR location in FA.

⬤ - Fuel rods picked out for testing;

⬤ - "Equivalent" fuel rods.

Table II. Numbers for fuel batches and cladding tube batches

Fuel rod numberig	Fuel batch number	Cladding tube batch number
52	1	1
64	1	1
65	1	2
78	2	3
79	2	3

Fuel data from different fuel batches and cladding tubes are given in Tables III and IV, respectively. However, both batches were fabricated to the same specification. According to the fuel data, it is evident that the fuel rods selected for testing and the fuel rods equivalent to them, did not differ significantly from each other at the fabrication date.

Table III Fuel batch parameters

Parameter	Fuel batch number	
	1	2
1. Chemical composition:		
1.1. Uranium content, %mass	87.88	87.81
1.2. ^{235}U content, % mass	4.37	4.37
1.3. ^{236}U weight, % mass	0.04	0.02
1.4. Total boron equivalent, ppm	0.70	0.65
1.5. Oxygen factor	2.002	2.001
1.6. Impurities, ppm		
1.6.1. Boron	<0.3	<0.3
1.6.2. Iron	100	70
1.6.3. Manganese	<3	<3
1.6.4. Nickel	<30	<30
1.6.5. Copper	7	11
1.6.6. Nitrogen	80	70
1.6.7. Silicon	<30	<30
1.6.8. Fluorine	<20	<20
1.6.9. Carbon	<30	<30
1.6.10. Chromium	<30	<30
2. Moisture, ppm	2–3	2–3
3. Pellet density, g/cm^3	10.5–10.7	10.5–10.7
4. Roughness value (R_a) for lateral surface of some pellets	R_a=4.10...5.85 μm	
5. Pellet length	9.30...12.52 mm	
6. Outside diameter of pellets	7.54...7.58 mm	
7. Central hole diameter of pellets	1.2–2.0 mm	
8. Facet presence in pellet	No	
9. Average grain size in the pellet material	6.6 μm	
10. Compaction resulted in resinter testing	Change of the average outside diameter is within 1.0...0.0 % (average value - 0.5 %).	

Table IV Data on cladding tubes of different batches

Parameter	Cladding Tube Batch Number		
	1	2	3
Average value of the inside cladding diameter, mm		7.76	
Impurity content in claddings made of Zr-1%Nb alloy, % nitrogen carbon hydrogen oxygen copper		6×10^{-3} 2×10^{-2} 1.5×10^{-3} 1×10^{-1} 7×10^{-3}	
Mechanical testing of claddings, yield strength in the longitudinal direction, kg/mm^2; 380°.	9.0–11.0	9.1–10.5	8.9–10.5
Ultimate strength in the transverse direction, kg/mm^2 20°	38.5–39.6	40.3–43.0	40.1–41.8
380°	19.3–20.8	19.2–21.3	18.7–19.1
Yield strength in the transverse direction, kg/mm^2 20°	35.1–36.5	37.5–40.7	35.7–37.7
380°	17.1–19.1	18.2–19.7	17.3–17.8
Total percent elongation, % 20°	31.6–38	30.0–36.0	34.8–36.4
380°	44.0–49.6	47.2–48.4	46.0–48.4
Corrosion tests, overweight, mg/m^2	13.0–15.0	14.0–16.0	15.0–20.0
Hydride orientation coefficient	0.3	0.3	0.35
Anisotropy factor	1.8	1.9	1.8

2.2. FR OPERATIONAL BACKGROUND

The selected fuel rods were incorporated into the fuel assembly that was operated in the course of 5–9 fuel loadings of the core in the third power unit of the Kola NPP. Table V and Fig. 4 show data on fuel cycles and co-ordinates for FA location in the core.

Table V Fuel Cycle dates and FA co-ordinates

Fuel cycle No.	5	6	7	8	9
Start date	24.09.86	21.08.87	07.10.88	05.10.89	02.12.90
End date	17.06.87	05.09.88	09.09.89	02.11.90	15.10.91
Co-ordinates of FA location in the core	03–54	05–54	05–54	11–54	08–57

The fuel assembly was arranged in the core in such a way that its fixture pin (edge provided with serial number, Fig.1.3) was always oriented between the first and the second semi-axes of symmetry (Fig. 4).
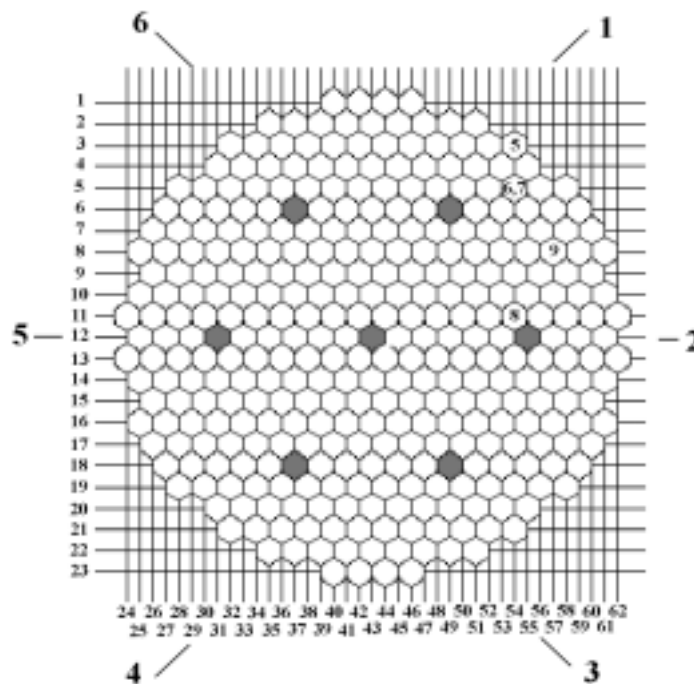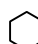
Fig. 4. FA location in the core with reference to the fuel cycle number: 1, 2...6 – core semi-axes.

⬡ - FA location in the core;
⬢ - Location of control rod clusters.

The average daily power data of the unit are given in Fig. 5 [4]. During the 5–8th fuel cycles, the control rod system was actuated 15 times. During the 9th fuel cycle, the control rod system was not actuated. The fuel assembly was not disposed close to the control rod clusters.
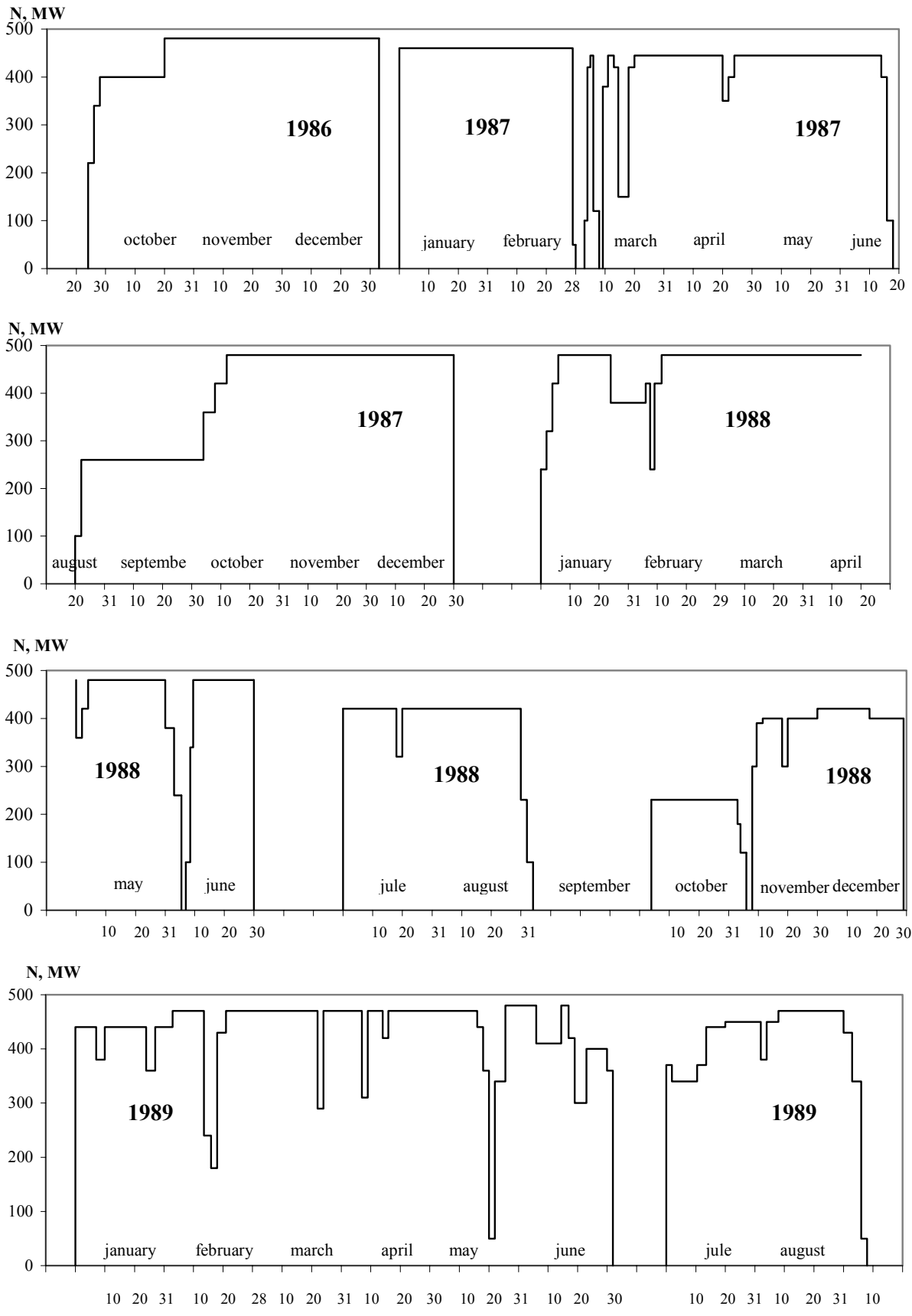
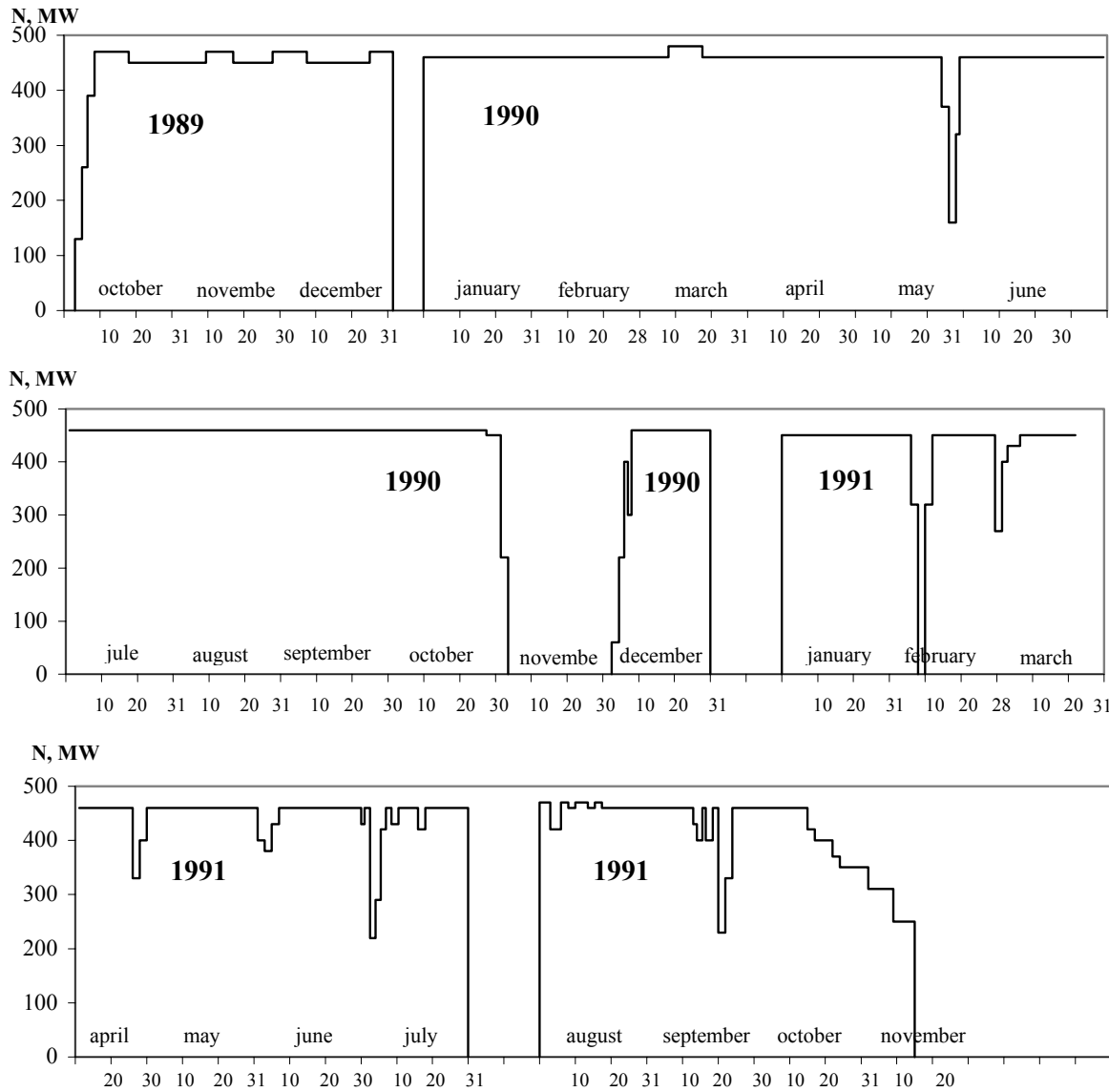*Fig. 5. Schedule of the power unit loading during 5–9 fuel cycles.*

Fig. 5. Continued.

The coolant inlet temperature and its temperature increase during different operational periods did not exceed 265 and 30°C, respectively. The primary circuit pressure was 12.5 MPa. The coolant quality was kept within the imposed standards during the FA operation.

The average calculated fuel burnup in the fuel assembly was 48.18 MW·d/kgU. The maximum linear power was achieved at the beginning of the sixth fuel cycle (Fig.1.6) and did not exceed 260W/cm. The maximum linear power decreased gradually and came to ~70W/cm at the end of the FA operation period [4]. According to the results of in-pile cladding integrity control, the fuel assembly was leak-tight at the end of the operation period.
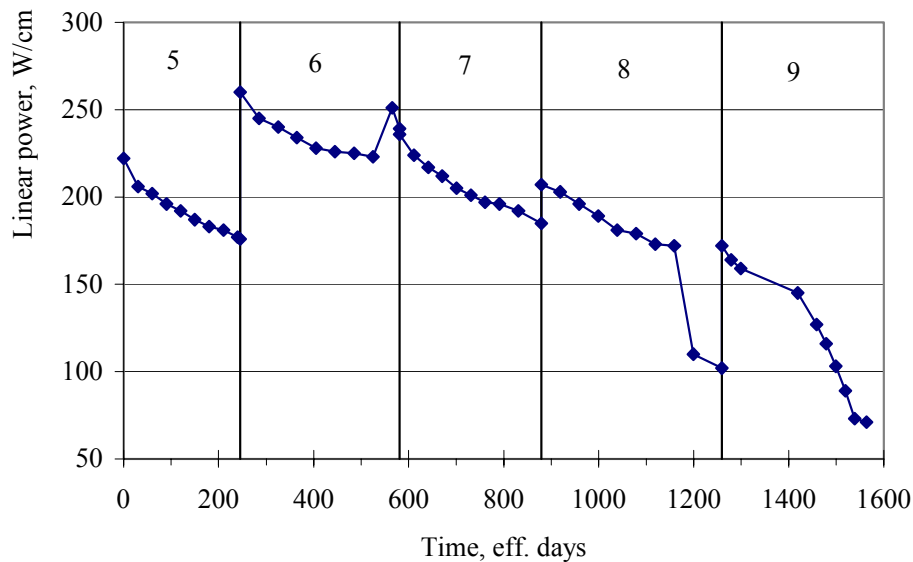
Fig. 6. The maximum FA linear power change during operation.

2.3. NON-DESTRUCTIVE EXAMINATIONS OF FUEL RODS INTENDED FOR STORAGE TESTING

The storage conditions of the fuel rods after discharge from the reactor are of great importance with regard to their technical condition before testing.

The fuel assembly removed from the reactor was cooled during two and a half years in the NPP spent fuel pool. The material of some fuel rods were examined at the Research Institute of Atomic Reactors before they were put into storage containers. The temperature of the gaseous medium (humid air) did not exceed 80°C in the containers. The storage time of the fuel rods under testing under such conditions comprised ~7 years.

The nondestructive examinations of fuel rods involved the following:

- Visual inspection;
- Leak-tight testing;
- Diameter measurement in 4 azimuthal projections;
- Length measurement;
- Eddy-current testing;
- Measurement of the oxide film thickness;
- Gamma-scanning.

-

The list of the applied techniques and their main characteristics are given in the Appendix 1.

2.3.1. Visual inspection

The outward appearance of the cladding surface for fuel rod No. 64 (Fig. 1.7) and No. 78 (Fig. 1.8) is typical for WWER-440 fuel rods after 5 fuel cycles [5]. The cladding surface is dark grey in colour at the lower part as shown in Fig. 8d. The degree of blackness goes down

as a whole in the upward direction, but the oxide profiles are also noticed in some regions (Fig. 7a and 8a).

The condition of welded joints in the neighbourhood of the upper plug (Fig. 8b) and FR fixture (Fig. 8e) is typical for WWER-440 fuel rods after five fuel cycles.

FR fixtures are undercut at the lower grid level to withdraw fuel rods from the fuel assembly, with results shown in Fig. 8e.

2.3.2. Cladding integrity control

The ^{85}Kr activity measurement technique was used for cladding integrity control (see Appendix 1). Figure 1.9 represents the gamma-radiation spectra for fuel rods No. 64, 78 and 75, respectively. Fuel rod No. 75 was punched for comparison (failed fuel rod prototype). The gamma-spectra of fuel rods No. 64 and 78 were identical practically. The area under ^{85}Kr (E_γ=514.0keV) photopeak constituted ~$1.21 \cdot 10^4$ and ~$1.20 \cdot 10^4$ pulses for these fuel rods during the exposure time of 300s. As for the failed fuel rod, the area under the photopeak constituted ~0.43×10^4 pulses, that is approximately 3 times smaller than the photopeak area of the fuel rods No. 64 and 78. So according to the obtained results, the fuel rods No. 64 and 78 were leak-tight.

2.3.3. Geometric parameters

The diameters of the fuel rods were measured in 4 azimuthal orientations with a step of 2 mm. The azimuthal orientation was made by sight in accordance with the mark placed on the upper plug of the fuel rod. Figures 10 and 11 show cladding profiles for fuel rod No. 64 and No. 78, respectively. The distribution of the average diameter along the length of these fuel rods is given in Fig. 12. They were obtained by averaging the corresponding profiles. The origin of the coordinate is at the lower end of the fuel column.

The profiles demonstrate features common to WWER-440 fuel rods. The FR cladding decreased in diameter regarding the initial value as a result of thermal creep and radiation growth. The diameter decreased to a greater extent in the central part of the fuel column.

Table VI includes the data on cladding diameter averaged in each of four orientations within the region from 500 to 1 750 mm. The average diameter values in this particular region constituted 9.042 and 9.070 mm for fuel rod No. 64 and 78, respectively.
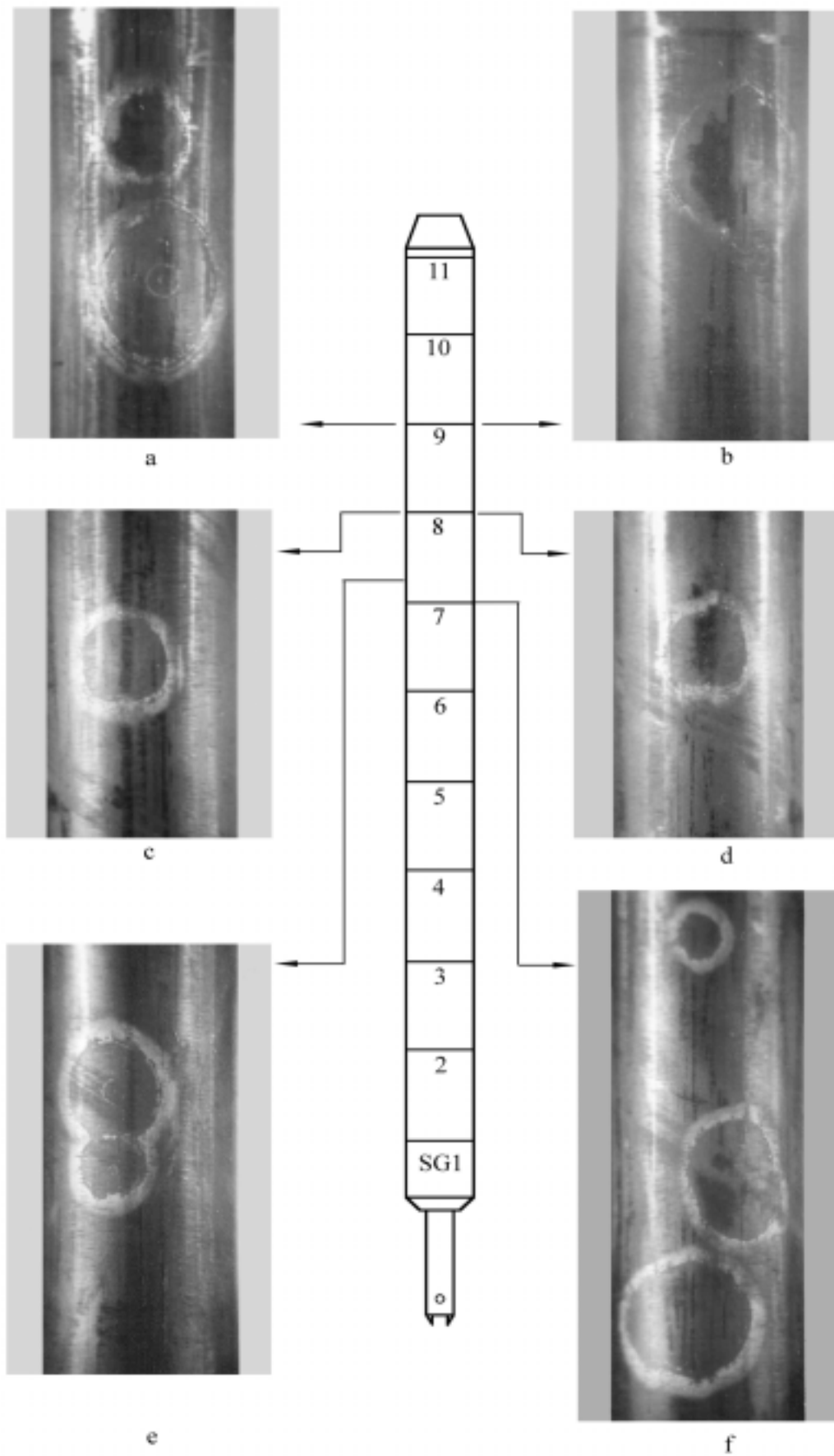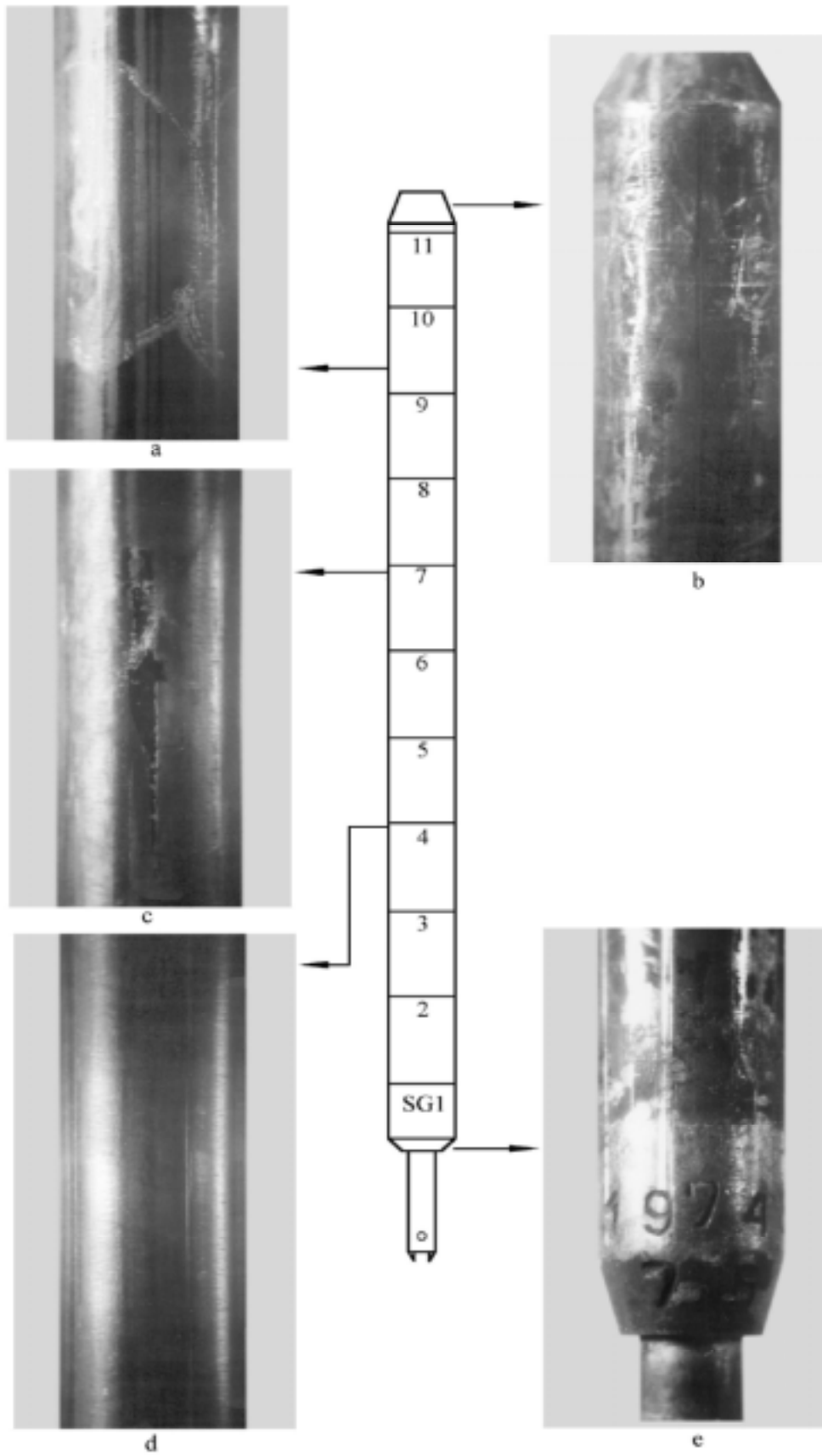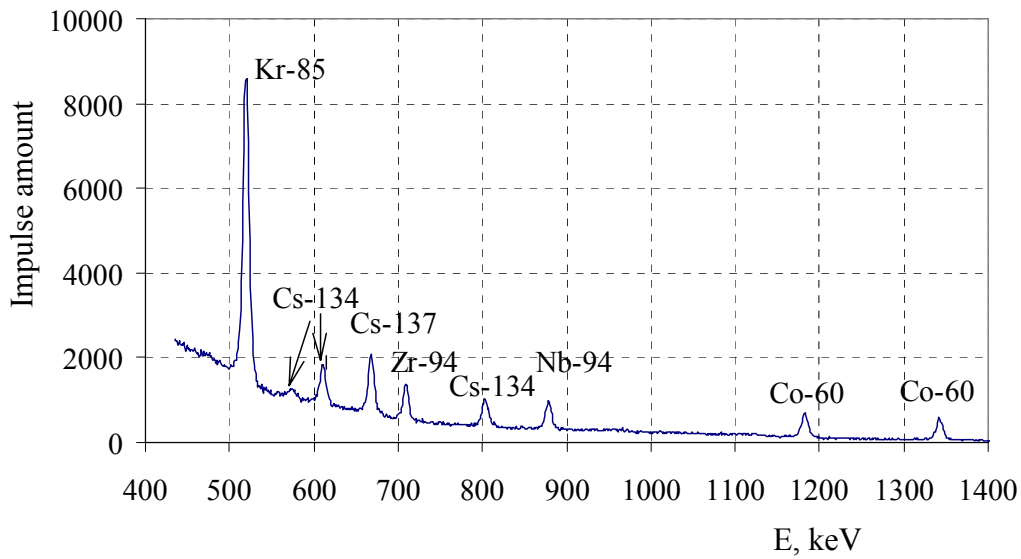
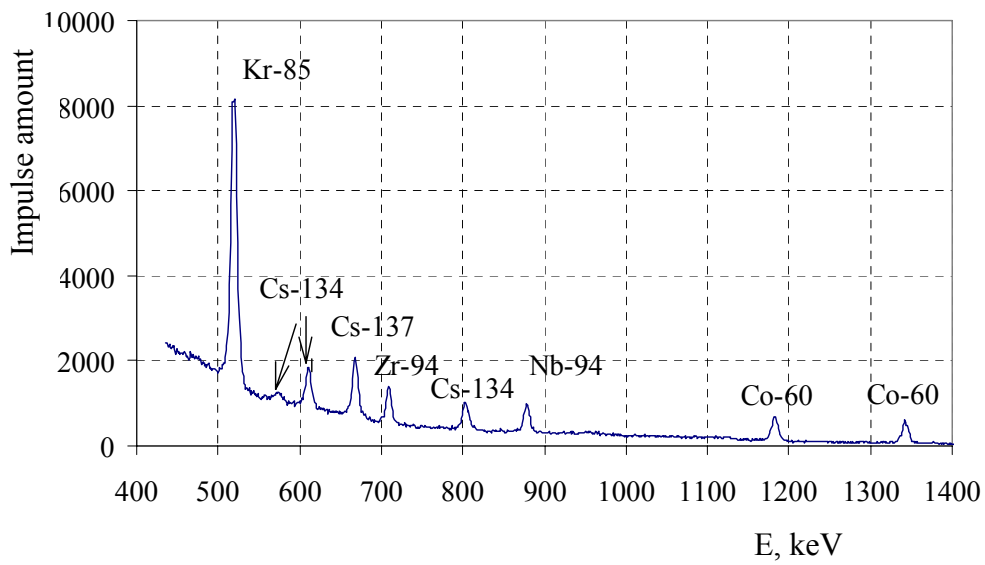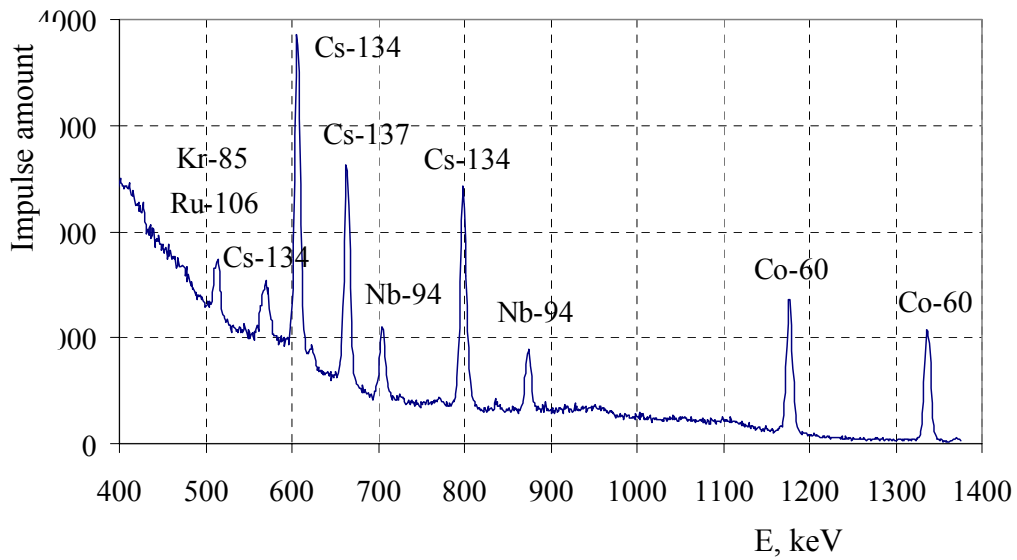*Fig. 7. Fuel rod No. 64 cladding fragments.*

Fig. 8. Fuel rod No. 78 cladding fragments.

Fig. 9. Gamma-spectra of fuel rods No.64 (a), No.78 (b) and punched one No.75 (c).

16

Table VI. Average diameter (mm) within the fuel rod region from 500 to 1750 mm

Fuel rod	Orientation			
	0°	45°	90°	135°
64	9.046	9.040	9.040	9.040
78	9.072	9.068	9.070	9.070

In doing so, the decrease in cladding diameter in the central part of fuel rod in the neighbourhood of gas plenum constituted ~0.08 and 0.07 mm for fuel rod No. 64 and No. 78, respectively.

FR lengths were measured in air and water:

- Air temperature, °C   -   35;
- Relative humidity, %   -   30-80;
- Water temperature, °C   -   30.

The average length of fuel rods constitutes the following:

For fuel rod No.64   -   L=2558.1±0.3 mm;
For fuel rod No.78   -   L=2558.4±0.3 mm.
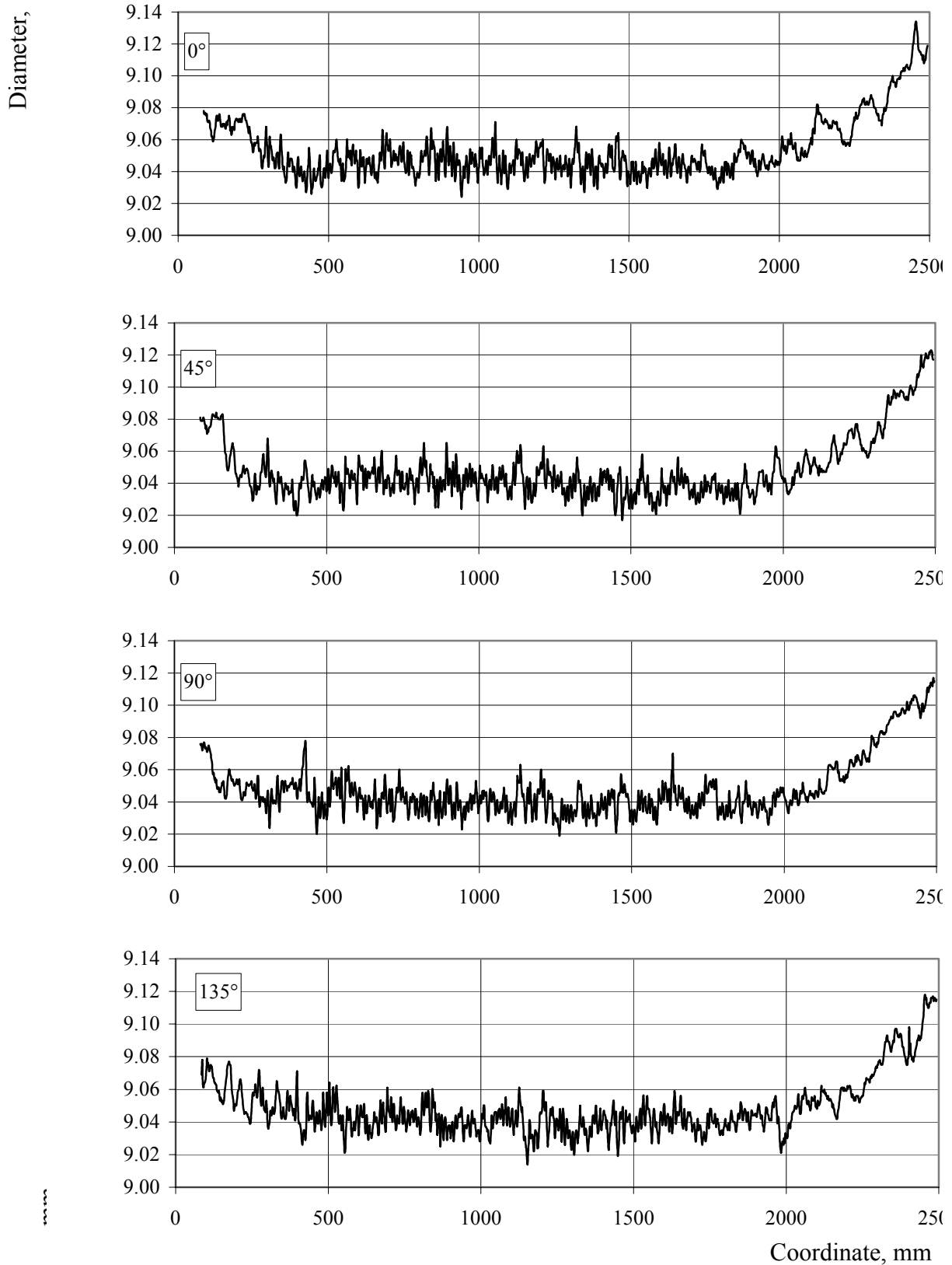
Fig. 10. The cladding profile for fuel rod No. 64 in four orientations.
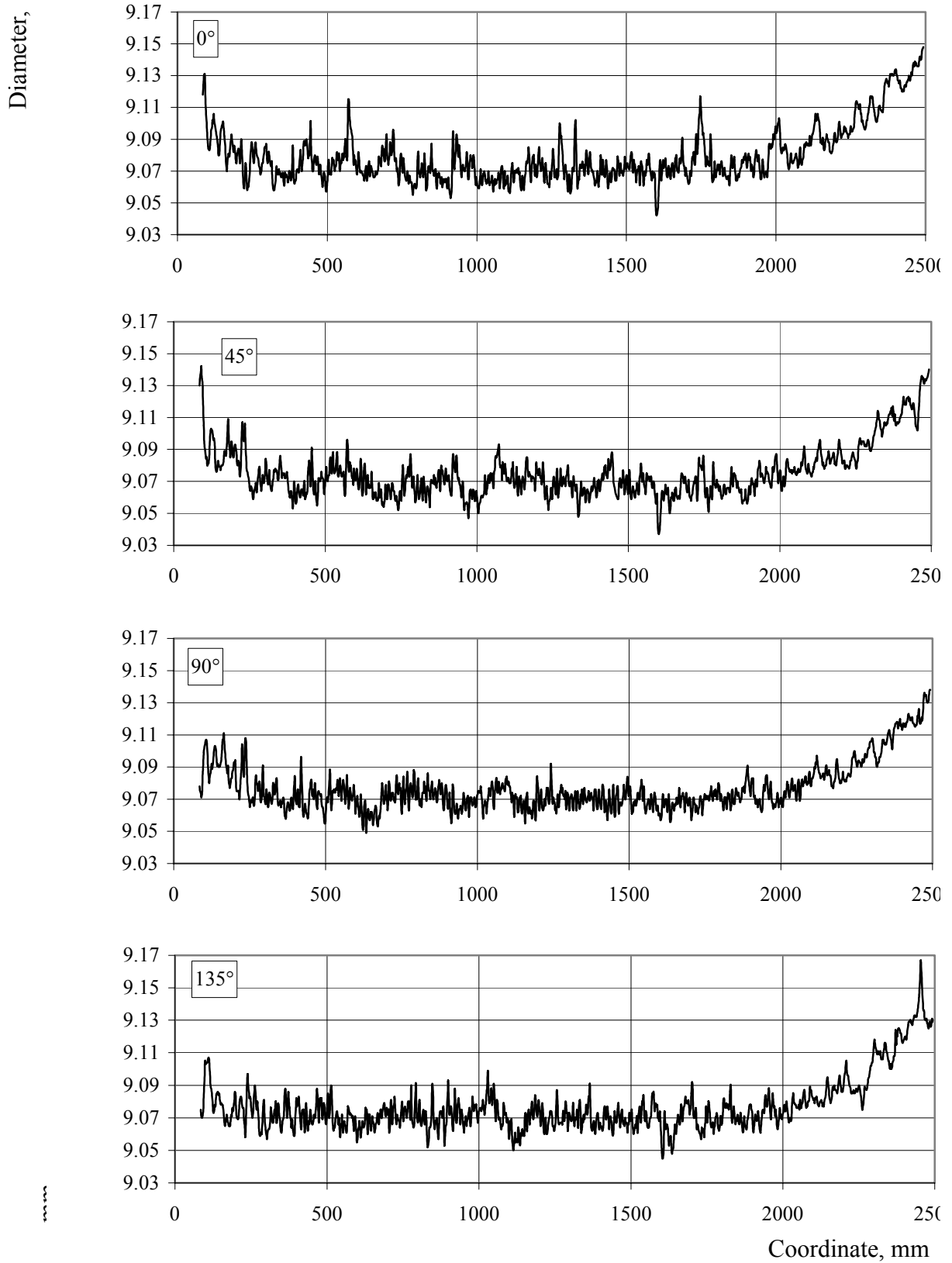
Fig. 11. The cladding profile for fuel rod No. 78 in four orientations.
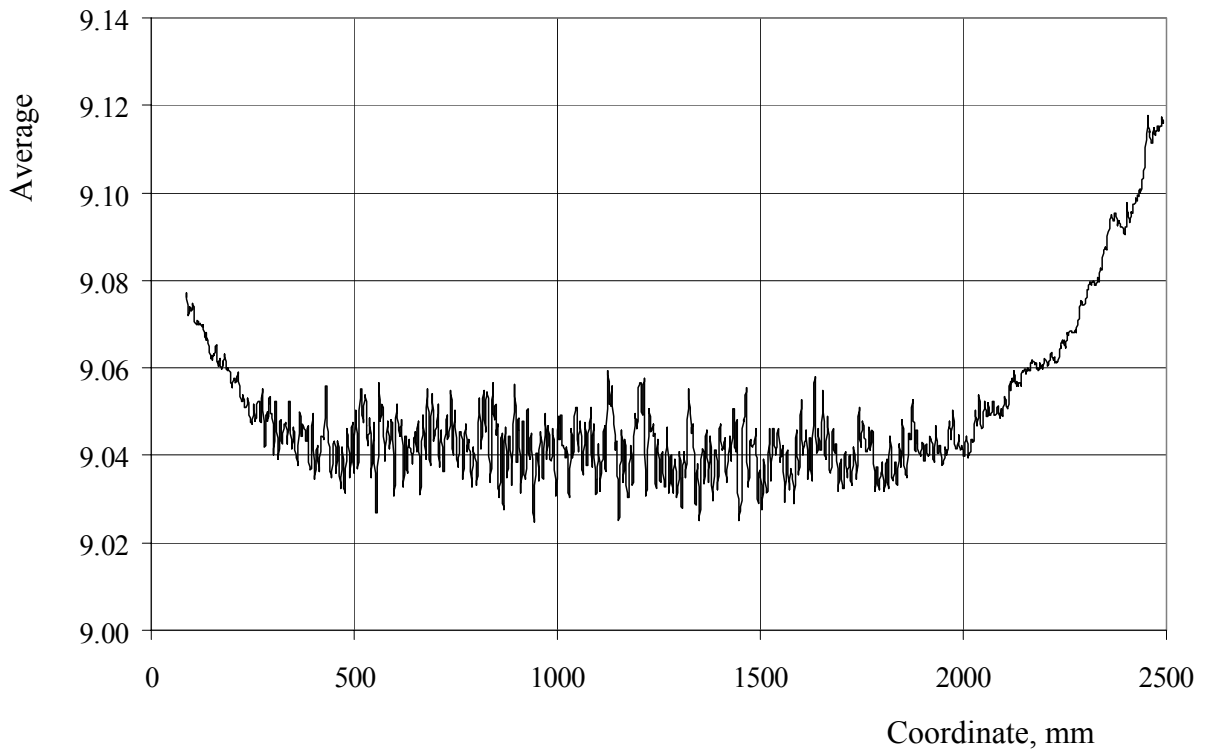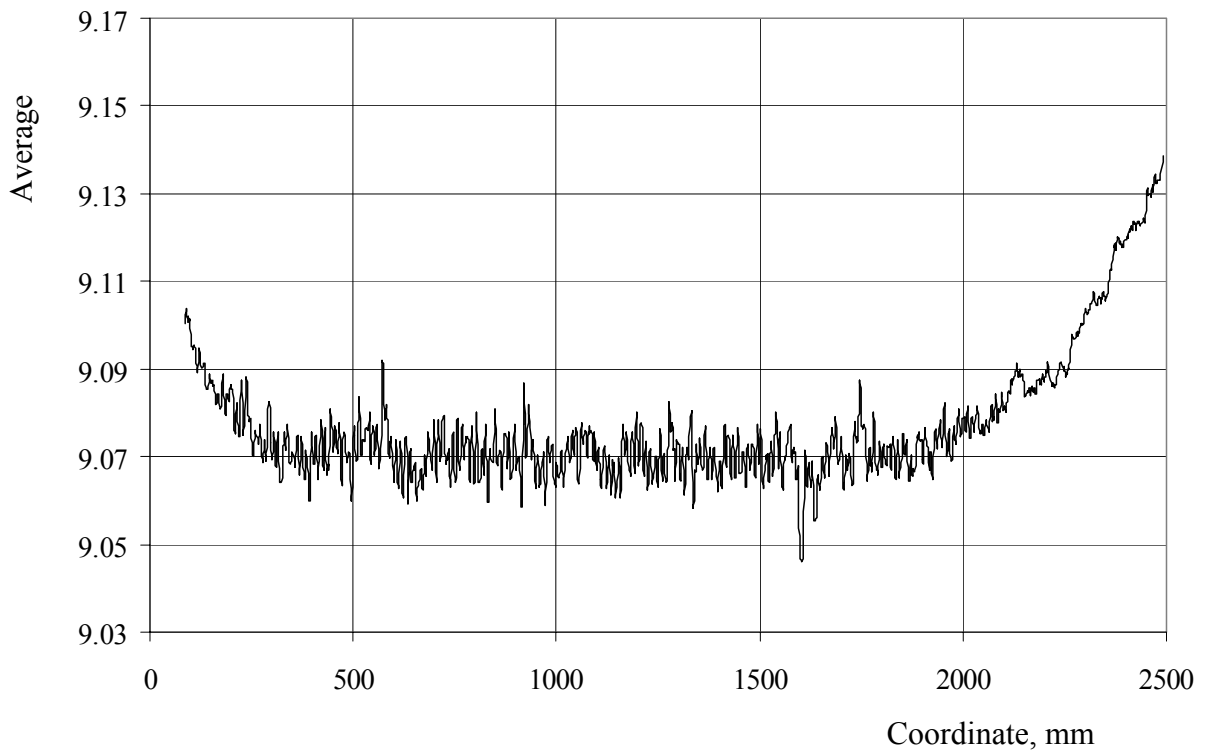
Fig. 12. Average diameter distribution along the cladding of fuel rods No. 64 (a) and No. 78 (b).

2.3.4. Eddy-current testing

Eddy-current testing of FR claddings was carried out on two frequencies of 150 and 400kHz using a flow- through sensor. The through hole is 9.8 mm in diameter. The flaw detector was calibrated using an artificial flaw.

Frequencies of 150 and 400 kHz were chosen based on the maximum sensitivity of the flow detector to the defects located on the inner and outer surfaces of the cladding as well as based on the maximum sensitivity of both frequencies to through defects.

Figure 13 shows test results of claddings for fuel rod No. 64 and No. 78. It is possible to separate three regions on the cladding for fuel rod No. 64, which differ in the fluctuation of the response signal as related to the average value. This is the lower part of the fuel rod with coordinates from 0 to 250 mm, middle part with coordinates 250–2100 mm and the upper part with coordinates from 2100 mm up to the fuel column notch location with a coordinate of ~2450 mm.

An increase of the response signal amplitude fluctuation over the region from 250 to 2100 mm as compared with the lower and upper parts of fuel rods are caused by local changes of the cladding diameter because of its interaction with the fuel pellets. Coordinates of the region opening and closing agree with coordinates of the cladding region where the increase in signal amplitude fluctuation was noticed from the eddy current probe (Fig.1.13a). There was no signal increase over the general background at the place of spacer grid location. Eddy-current test results show that surface, internal and through defects are absent.

The graph of eddy-current results for fuel rod No. 78 does not differ much from that for fuel rod No. 64. It is possible to separate three regions, which correspond to the lower, middle and upper parts of the fuel rod. A distinctive feature for fuel rod No. 78 is the presence of several signals with amplitudes in excess of the background value.

The occurrence of such signals is caused by the local increase (by 0.02÷0.04 mm as compared with the average value) of the cladding diameter at point of ~250, 600 and 900 mm (location of 4 spacer grids, Fig. 11). The analysis revealed that the surface, internal and through defects are absent in the cladding of fuel rod No. 78.

2.3.5. Oxide film thickness

The thickness of the oxide film on the outer surface of the cladding was measured along two azimuthal orientations, which make an angle of 90°. Measurements were carried out using eddy-current thickness gauge Fischerscope MMS-D09A and ET3.3-D09A probe.
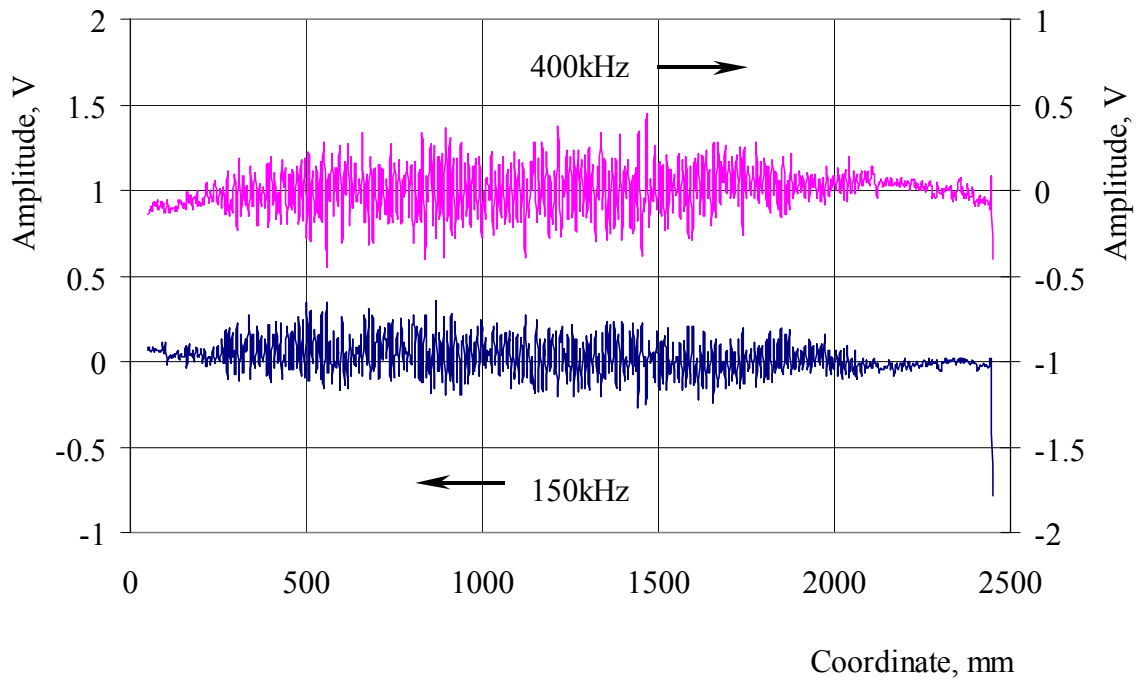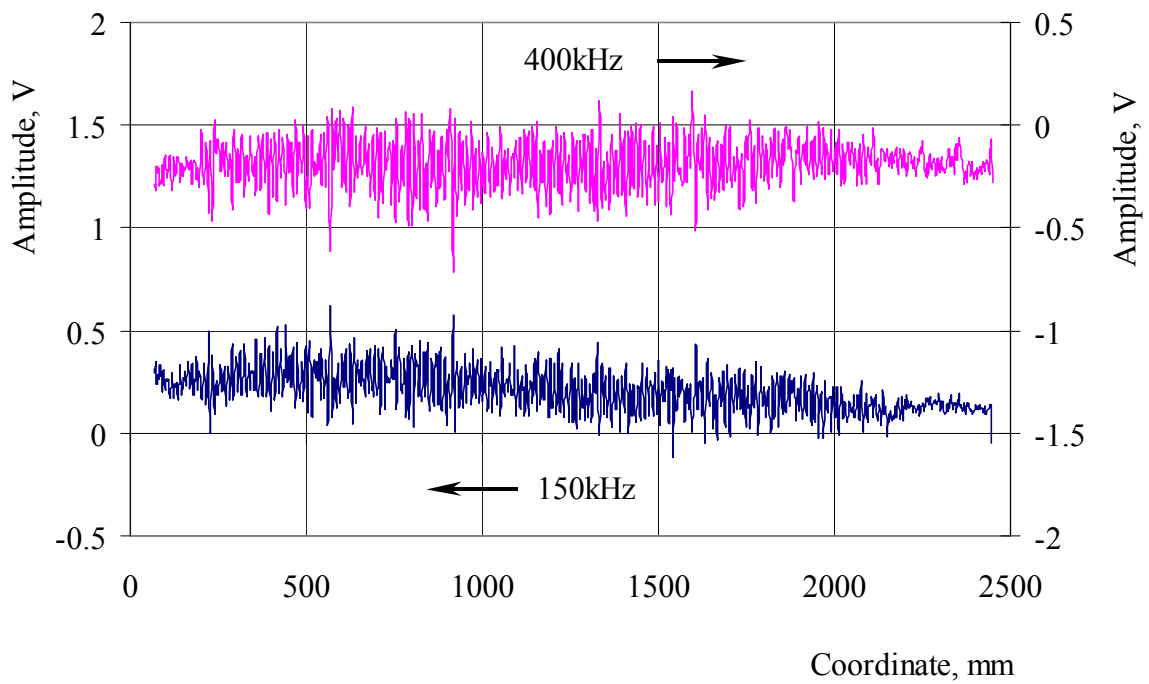
Fig. 13. Eddy-current testing of cladding for fuel rods No. 64 (a) and No. 78 (b).

Figures 14 and 15 demonstrate the results of the oxide film measurement on the outer cladding surface of fuel rods No. 64 and 78, which are made in two orientations (through 90°) as well as result of their averaging. The oxide film thickness increases steadily from the lower to the upper part of fuel rod. The average value of the oxide film thickness varies within 2–4 µm in the lower part of fuel rods and up to 5–7 µm in the upper one. The results of measurement demonstrate that the oxide film overlaps the cladding surface uniformly without any noticeable increases of thickness at the places of spacer grid locations.
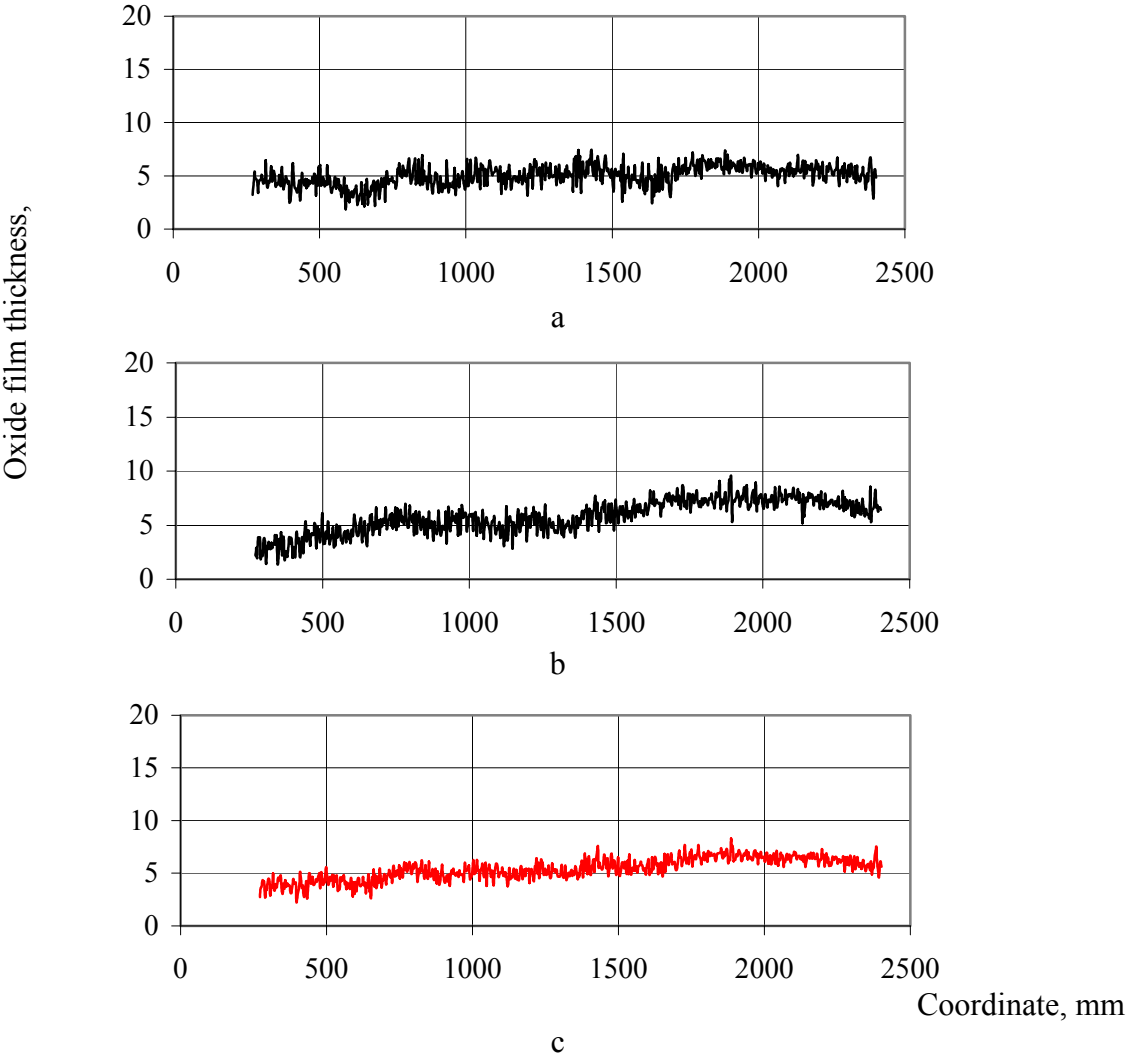
Fig. 14. Oxide film thickness on the outer cladding surface of fuel rod No.64 in two orientations through 90° (a, b) and average value (c).
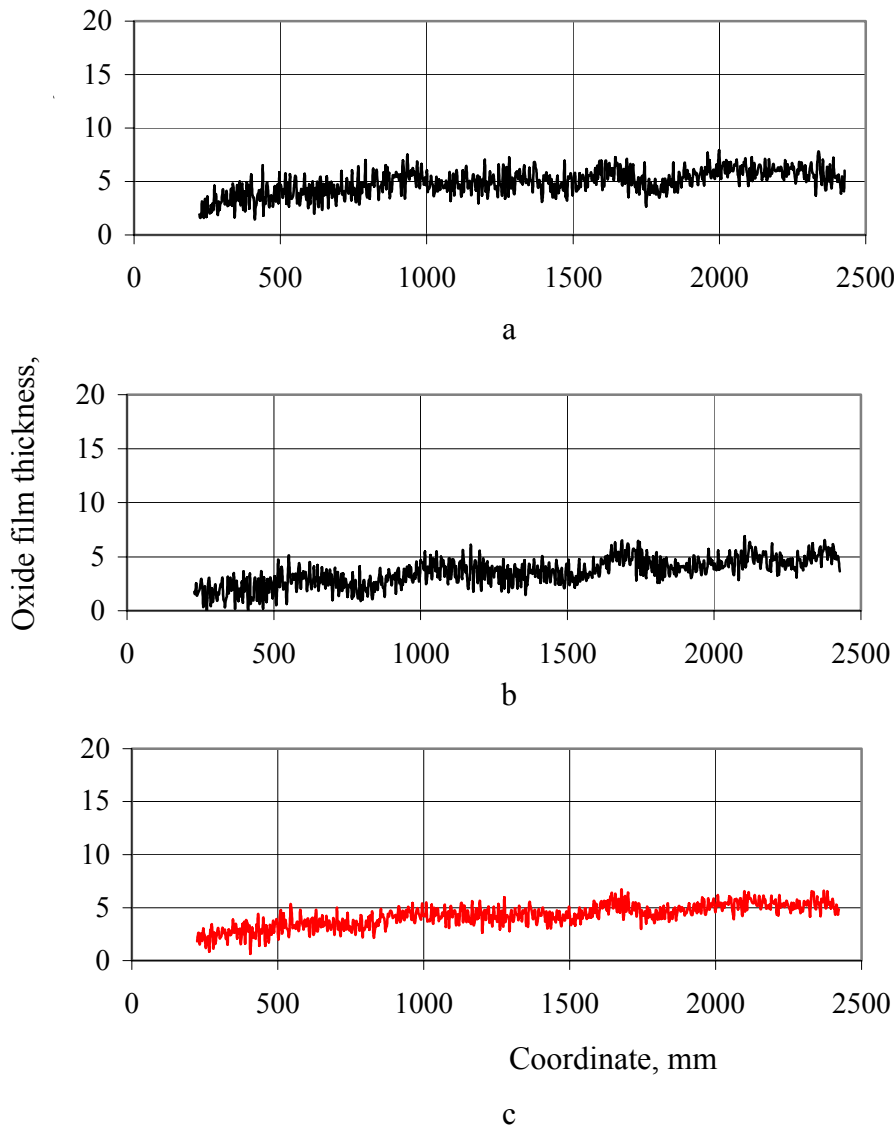
Fig. 15. Oxide film thickness on the outer cladding surface of fuel rod No. 78 in two orientations through 90° (a, b) and average value (c).

2.3.6. Gamma spectrometry

Gamma scanning of the fuel rods was performed with the scanning pitch of 10 mm. The slit collimator was 3.0 mm in height. Profiles of count rate for Cs^{137} gamma quanta are given in Fig. 16. Periodic minimums of Cs^{137} concentration are noticeable at the place of spacer grid location. They are caused by absorption of neutrons with the spacer grid material. Fuel burnup in these fuel rods was calculated based on the comparison method of Cs^{137} gamma-line count rate (with allowance for decay correction during the cooling period after irradiation and operation time) in the fuel rod under examination and in the standard specimen.

The maximum and average fuel burnups in fuel rod No. 64 constituted 53.6 and 46.2MW·d/kgU, respectively. The axial irregularity coefficient for Cs^{137} accumulation comprised 16. The same values for fuel rod No. 78 made up 53.3; 45.9MW·d/kgU and 16, respectively.
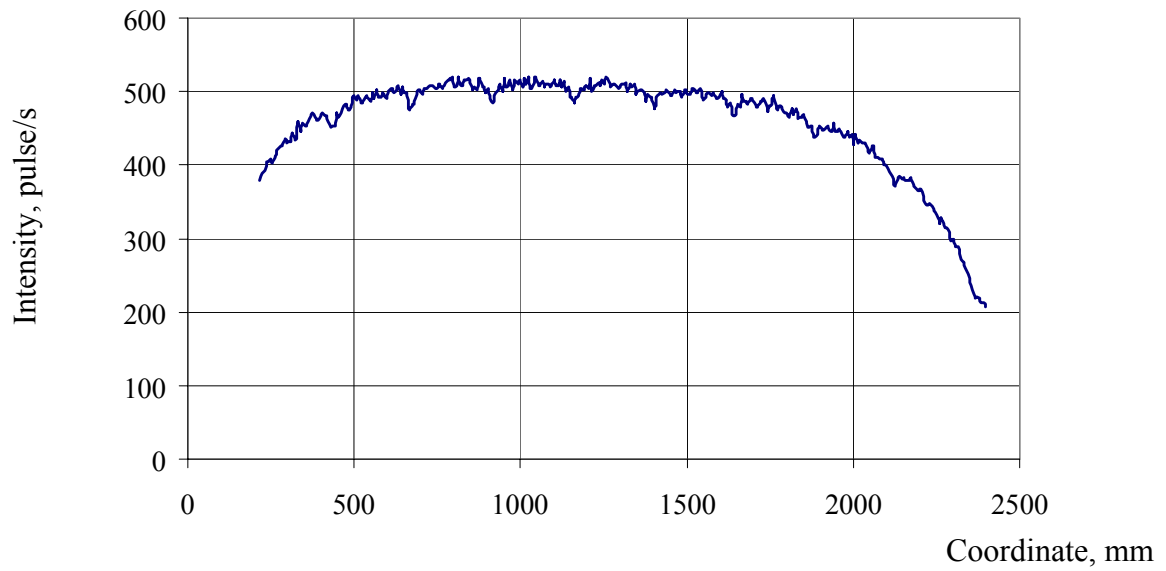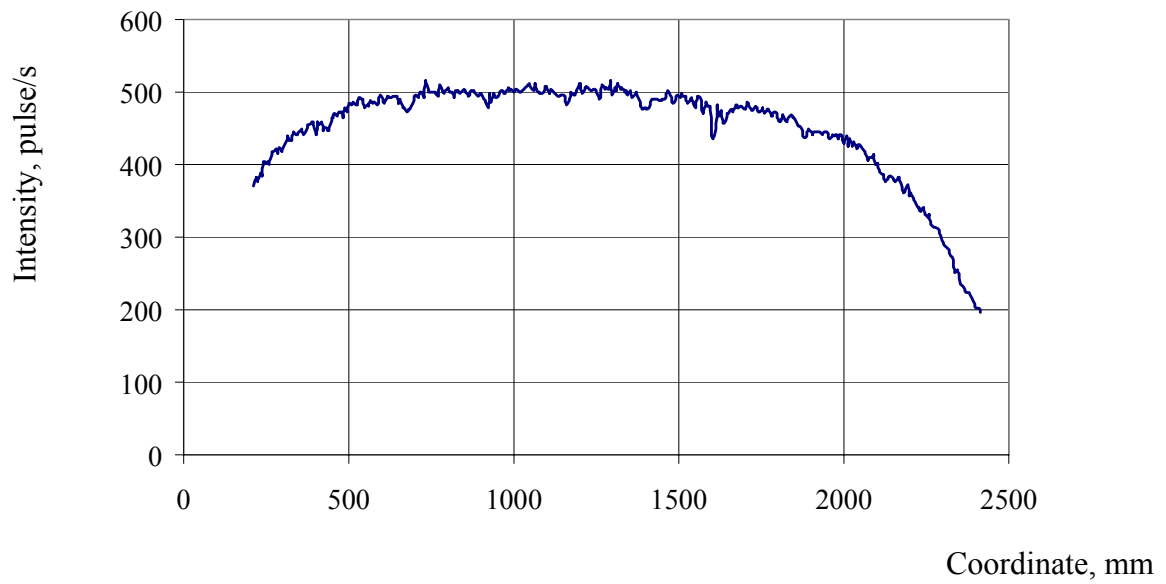
Fig. 16. Profiles of Cs137 gamma-quanta count rate for fuel rod No.64 (a) and No.78 (b).

2.4. DESTRUCTIVE EXAMINATIONS OF "EQUIVALENT FUEL RODS"

Fuel rods No. 52 and 65 (for fuel rod No. 64) as well as No. 65 and 79 (for fuel rod No. 78, Fig. 3) reached the average burnup of 46.2, 45.6 and 46.2 MW·d/kgU, respectively were chosen as "equivalent" neighbouring fuel rods.

2.4.1. Gas pressure and composition under the fuel rod cladding

Parameters of gases under the FR cladding were determined using a laser puncture device (refer to Appendix 1). Results of measurements are given in Table VII.

Table VII. Quantity and composition of gases under FR cladding in fuel assembly No.222

Fuel rod No.	Gas plenum of FR, cm³	Gas volume under normal conditions, cm³	Gas pressure in FR, MPa	He	N₂	CO₂	Ar	O₂	Kr	Xe	Fuel gas release, %
52	10.6	107	1.01	8.95	0.12	0.03	0.0007	0.0001	0.34	0.6	0.99
79	10.7	101.7	0.96	3.00	<0.12	<0.045	<0.015	<0.010	0.68	5.12	1.46

2.4.2. Mechanical properties of FR claddings

Mechanical properties of fuel rod No.65 cladding were examined using circular specimens to be 3 mm in height. They were cut out from the cladding with specified coordinates 2506; 2156; 941 mm. Test were carried out at two temperatures of 20 and 350°C. Test data are shown in Table VIII.

Table VIII. Mechanical properties of fuel rod No. 65 cladding

Fuel rod No.	Coordinate, mm	20°C				350°C			
		R_m, MPa	$R_{p0.2}$, MPa	A_{un}, %	A_{tot}, %	R_m, MPa	$R_{p0.2}$, MPa	A_{un}, %	A_{tot}, %
65	2506	578	507	6.6	19.1	410	385	4.4	17.7
	2156	603	529	6.5	21.7	403	374	4.2	24.4
	941	610	546	6.4	20.2	408	375	5.5	22.0

2.5. ESTIMATION OF GAS PRESSURE UNDER THE CLADDING RODS AND FISSION GAS RELEASE UNDER THE CLADDING

Possible fission gas release (FGR) under the cladding of fuel rods No. 64, 78 as well as gas pressure in the fuel rod were estimated based on the experimental array data obtained in the course of examination of WWER-440 fuel rods operated during 4 and 5 fuel cycles. Figure 17 demonstrates fission gas yield versus burnup relationship [6].
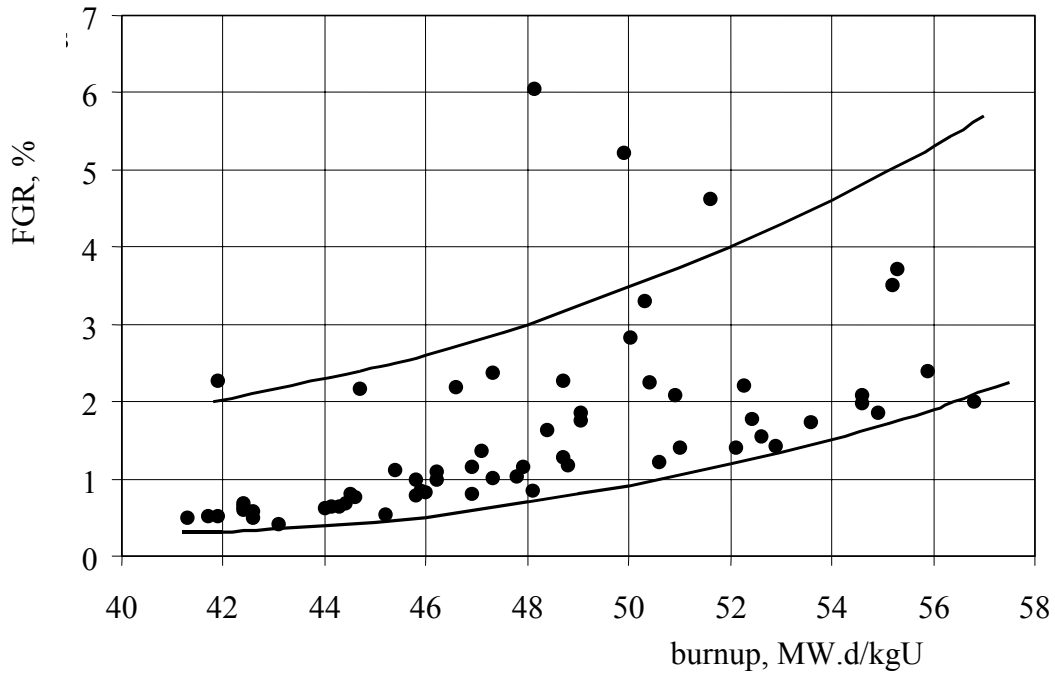
Fig. 17. Fission gas yield under WWER-440 FR cladding versus burnup.

Taking into consideration the experimental data scattering, it should be expected that fission gas release under claddings of fuel rods No. 64 and 78 could be in the range from 0.5% to 2.7% and from 0.5% to 2.6%, respectively.

Figure 18 shows the relationship between the gas pressure in WWER-440 fuel rods and burnup. Based on the experimental array data, it can be expected that gas pressure in fuel rods No. 64 and 78 be within the range from 0.9 to1.4 and from 0.9 to 1.3 MPa, respectively.
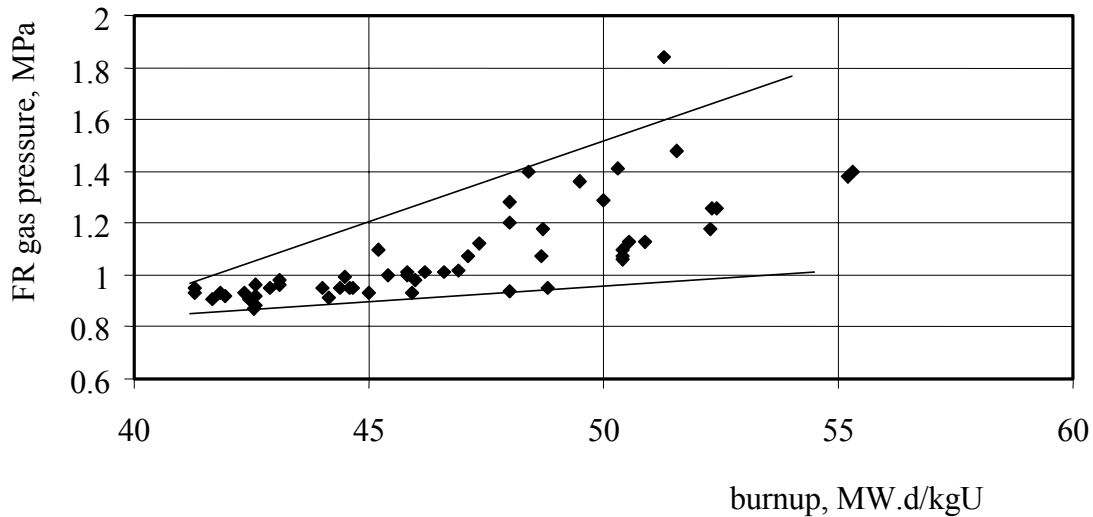
Fig. 18. Gas pressure in WWER-440 fuel rods versus burnup.

2.6. ESTIMATION OF FR CLADDING DEFORMATION DUE TO THERMAL TESTING

Deformation of WWER-440 FR claddings resulting from thermal testing was estimated using the phenomenological model of anisotropic thermal creep of cladding tubes (made of Zr-1%Nb alloy) that was published in [7–10]. The model describes the transient and steady state stages of thermal creep at temperatures from 250°C to 450°C and the steady state creep stage up to 800°C, when the stress is up to ~0.8 Rm and radiation damage doses are from 0 to 30dpa.

The test temperature curve is shown in Fig. 19. When the test temperature increases from 350°C up to 390°C the hoop strain ε_θ of FR cladding is calculated with allowance for hardening. In doing so, the initial time t_0 for a temperature of 390°C is taken so that the initial deformation for these conditions is equal to the finite deformation ε_K under the same test conditions (T=350°C).
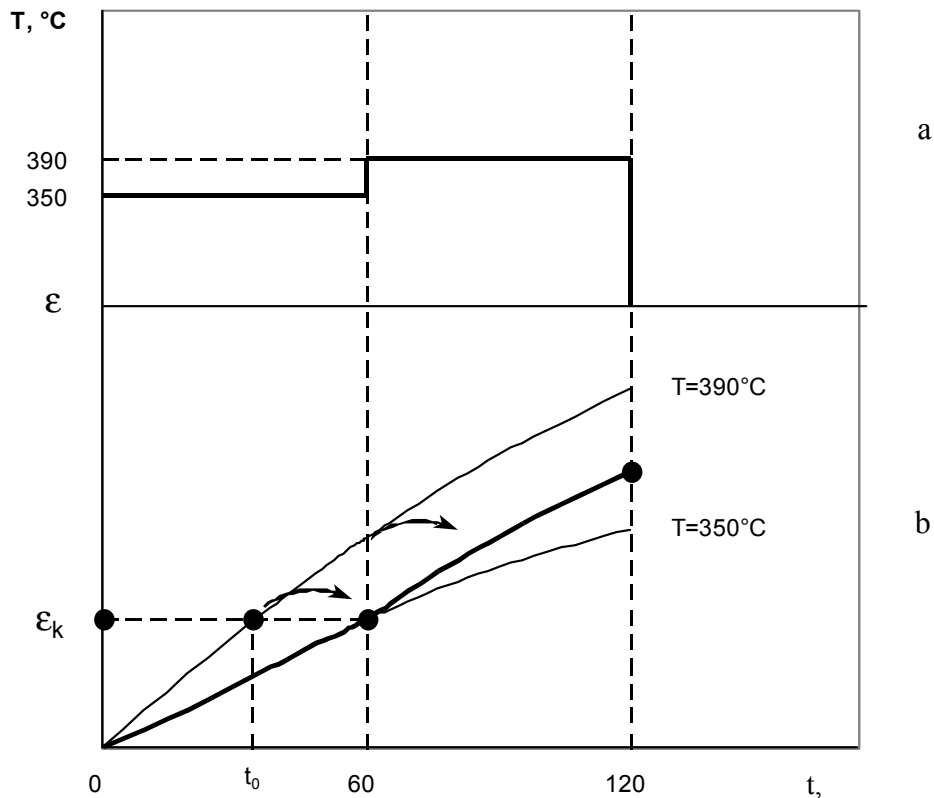
Fig. 19. Test temperature curve (a) and creep curve (b).

Stress-strained state of the cladding is defined by a complete system of equations for interrelation of $\dfrac{d\varepsilon_z}{dt}$, $\dfrac{d\varepsilon_\theta}{dt}$, $\dfrac{d\varepsilon_r}{dt}$ strain rate components and σ_z, σ_θ, σ_r stress components in the longitudinal z, tangential θ and radial directions **r**, their effective values $\dfrac{d\varepsilon_{eff}}{dt}$, σ_{eff} and G, H,

F anisotropy factors. Instead of the fast neutron (E>0.1MeV) fluence, the K_t radiation damage dose is used in calculations.

The system of equations is written in the following form for thin-wall claddings of WWER fuel rods:

$$\frac{d\varepsilon_z}{dt} = \frac{d\varepsilon_{eff}}{dt}\frac{\sigma_\theta}{\sigma_{eff}}(0.5 - G);$$

$$\frac{d\varepsilon_\theta}{dt} = \frac{d\varepsilon_{eff}}{dt}\frac{\sigma_\theta}{\sigma_{eff}}(F + \frac{G}{2});$$

$$\frac{d\varepsilon_r}{dt} = -\frac{d\varepsilon_{eff}}{dt}\frac{\sigma_\theta}{\sigma_{eff}}(F + \frac{H}{2});$$

$$\sigma_{eff} = (F + 0.25)^{\frac{1}{2}}\sigma_\theta, \quad G + H = 1. \tag{1}$$

Stress in the tangential direction is written in such a way:

$$\sigma_\theta = \frac{(D - \delta)(P - P_0)}{2\delta}, \tag{2}$$

where   D, δ - diameter and thickness of cladding wall;

P, P_0 – gas pressures under the cladding and from outside, respectively.

$$P = P_{n.c.}\frac{T}{T_{n.c.}}, \tag{3}$$

where $P_{n.c.}$ – gas pressure under the cladding under the normal conditions;

$T_{n.c.}$, T – temperatures under the normal conditions and in testing, respectively.

Effective rate of the steady state creep is defined in the following form:

$$\left(\frac{d\varepsilon_{eff}}{dt}\right)_{s-s} = \left(\frac{d\varepsilon}{dt}\right)_{H-X} + \left(\frac{d\varepsilon}{dt}\right)_{Ko} + \left(\frac{d\varepsilon}{dt}\right)_{C_1} + \left(\frac{d\varepsilon}{dt}\right)_{C_2}, \tag{4}$$

where $\left(\frac{d\varepsilon}{dt}\right)_{H-X} = 1.73\cdot10^{13}\frac{\sigma_{eff}}{T}e^{-\frac{30100}{T}}$ - Nabarro-Herring creep;

$$\left(\frac{d\varepsilon}{dt}\right)_{Ko} = 1.95\cdot10^6\frac{\sigma_{eff}}{T}e^{-\frac{18000}{T}}\text{ - Koble creep;}$$

$$\left(\frac{d\varepsilon}{dt}\right)_{C_1} = \frac{2.88\cdot10^{25}}{1 + 8.31\cdot10^{-9}\cdot(1 - e^{-3K_t})\cdot e^{\frac{13500}{T}}}\cdot\frac{\sigma_{eff}^5}{TG_r^4}e^{-\frac{30100}{T}};$$

$$\left(\frac{d\varepsilon}{dt}\right)_{C_2} = \frac{1.72\cdot10^{22}}{1 + 8.31\cdot10^{-9}\cdot(1 - e^{-3K_t})\cdot e^{\frac{13500}{T}}}\cdot\frac{\sigma_{eff}^7}{TG_r^6}e^{-\frac{18000}{T}}.$$

where G_r – rigidity modulus related to the temperature of empirical function:

$$G_c = 2.72\cdot10^4 - 21(T - 573) \tag{5}$$

For the first two members in equation (4) G=H=F=0.5, but G=0.61; H=0.39; F=0.28 for the third and the fourth members. K_t in equation (4) is a damage dose (in dpa) reached in irradiation of FR claddings in the WWER-440 reactor, [$K_t = 0.2068 B_T$, where B_T is burnup, MW·d/kgU].

The effective rate of the transient creep can be defined in the following way:

$$\frac{d\varepsilon_{eff}}{dt} = \sum_{i=1}^{2}\left[0.839 t^{-0.50}\left(\frac{d\varepsilon}{dt}\right)_{C_i}^{0.65} + \frac{7.23\cdot10^{-4} t^{-0.50}\left(\frac{d\varepsilon}{dt}\right)_{C_i}^{1.21}}{\left(\frac{d\varepsilon}{dt}\right)_C}\left(1-\exp\left(-\frac{4.5\sigma_{eff}}{Rp_{0.2}}\right)\right)\right]\cdot$$

$$\cdot\exp\left(-3.61\left(\frac{d\varepsilon}{dt}\right)_C^{0.21} t^{0.50}\right) + \left(\frac{d\varepsilon_{eff}}{dt}\right)_{s-s}.$$

$$\text{(6)}$$

where $\left(\frac{d\varepsilon}{dt}\right)_C = \left(\frac{d\varepsilon}{dt}\right)_{C_1} + \left(\frac{d\varepsilon}{dt}\right)_{C_2}.$

The transient creep strain is written in the following way:

$$\varepsilon_{eff} = \sum_{i=1}^{2}\left[0.465\left(\frac{d\varepsilon}{dt}\right)_{C_i}^{0.44} + \frac{8.4\cdot10^{-4}\left(\frac{d\varepsilon}{dt}\right)_{C_i}}{\left(\frac{d\varepsilon}{dt}\right)_C}\left(1-\exp\left(-\frac{4.5\sigma_{eff}}{Rp_{0.2}}\right)\right)\right]\cdot$$

$$\left(1-\exp\left(-3.61\left(\frac{d\varepsilon}{dt}\right)_C^{0.21} t^{0.50}\right)\right) + \left(\frac{d\varepsilon_{eff}}{dt}\right)_{s-s} t.$$

$$\text{(7)}$$

where
σ_{eff} = effective stress in MPa;
ε_{eff} = effective strain in %;
t   = time in h

The conditional time t for transient creep was calculated based on:

$$1-\exp\left(-3.61\left(\frac{d\varepsilon}{dt}\right)_C^{0.21} t^{0.50}\right)=0.95. \qquad\text{(8)}$$

Figure 20 demonstrates the relationship between the time period of transient creep and effective rate.
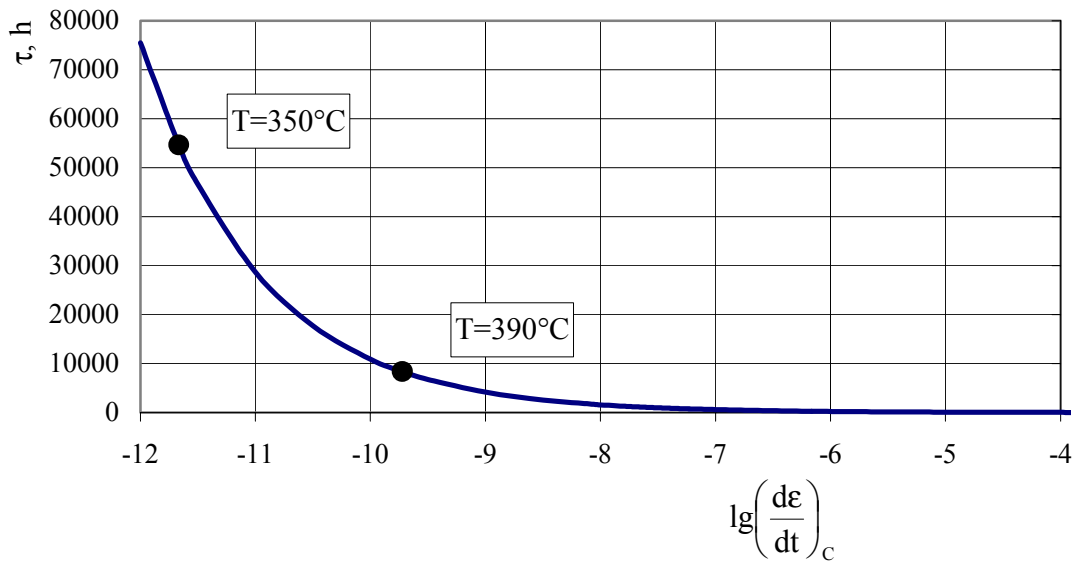
Fig. 20. Conditional time of the transient creep against effective rate $\left(\dfrac{d\varepsilon}{dt}\right)_C$.

Calculated force profiles of the effective rate for steady state thermal creep are shown in Fig. 21.
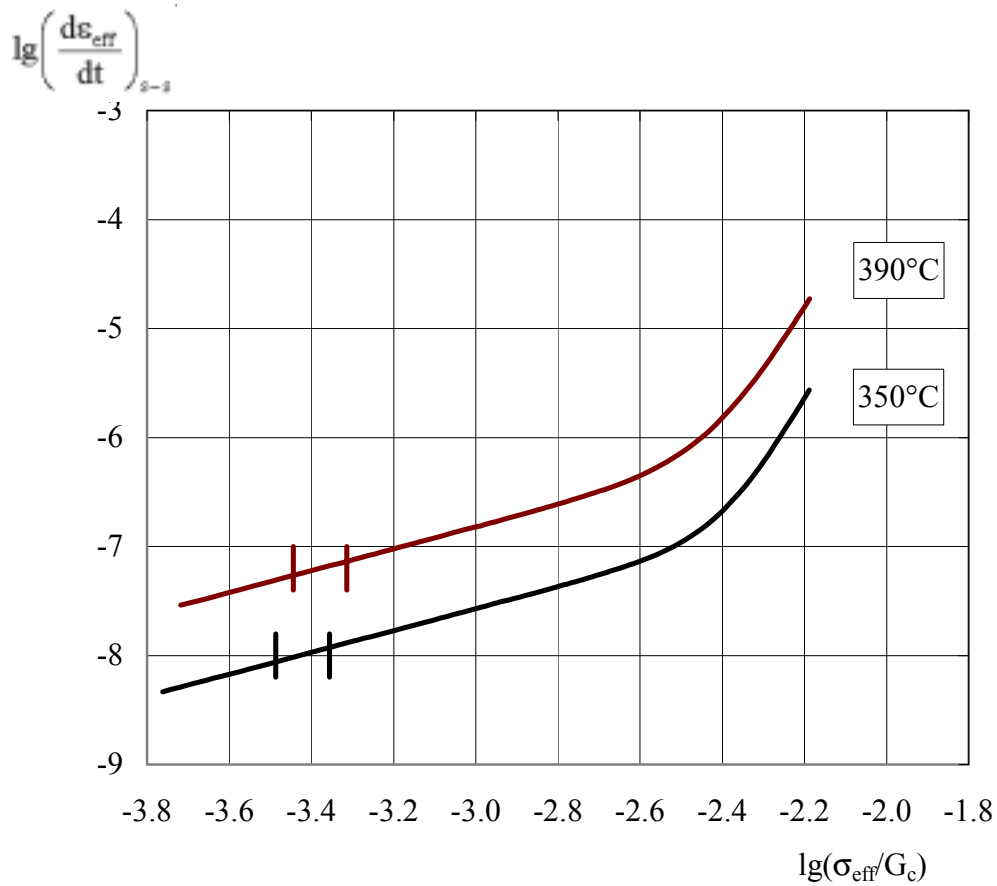
Fig. 21. Calculated force profiles of the effective rate for steady state thermal creep.

Table IX incorporates source data for calculation of cladding deformation for fuel rods No.64 and 78.

Table IX Source data for $\left(\dfrac{d\varepsilon}{dt}\right)$ calculation.

Fuel rod No.	D, mm	δ, mm	K_t, dpa	$P_{n.c.}$, MPa	$\sigma_{\theta,350°C}$, Mpa	$\sigma_{\theta,390°C}$, MPa
64	9.04	0.65	9.7	0.9–1.4	11.7–18.6	12.5–19.8
78	9.07	0.65	9.6	0.9–1.3	11.7–17.3	12.5–18.4

According to the calculation, the conditional time period of transient creep at test temperature of 350°C makes up ~55 000 hours and at 390°C it makes up ~9000 hours (refer to Fig. 20). So the cladding deformation during the whole testing of fuel rods is defined by equation (7) for the transient creep. Markings in the curve shown in Fig. 21 are used to show the range of possible values σ_{eff} for fuel rods under testing. The effective rate of the steady state creep makes up ~10^{-8}hours^{-1} for the first test condition, and it constitutes ~8×10^{-8}hours^{-1} for the second test condition (T=390°C). The calculated results for effective strain-test time relation are given in Fig. 22. According to these values it is possible to calculate ε_θ and ε_Z.
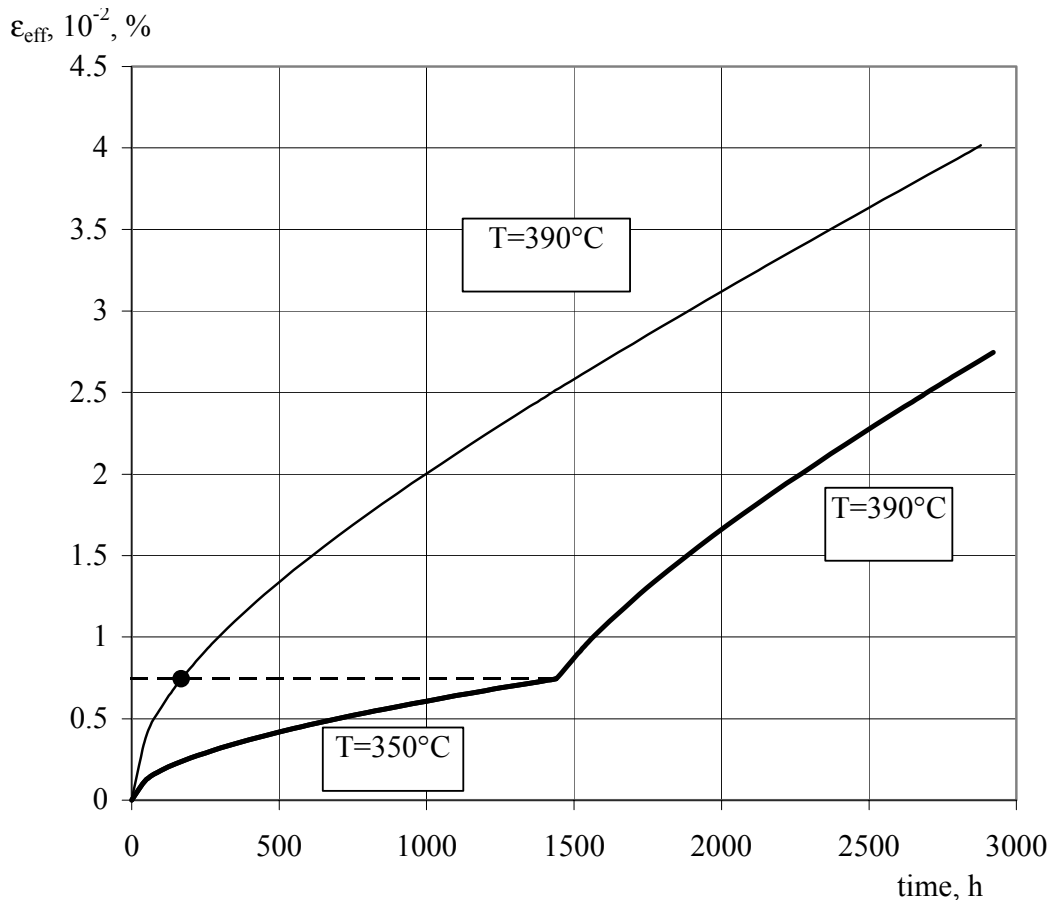
Fig. 22. Effective strain of FR claddings against the test time at 350 and 390°C.

The tangential deformation of FR cladding after the first and the second test conditions will equal 0.005 and 0.02%, respectively. The axial deformation of cladding will equal $5 \cdot 10^{-4}$% and $2 \cdot 10^{-3}$% after the first and the second test conditions, respectively.

So according to the calculated values of FR cladding deformation, it is evident that the maximum increase in diameter shouldn't be more than 2μm, and the maximum decrease of FR length shouldn't be more than 0.1 mm.

3. TEST STAND AND TEST CONDITIONS FOR FUEL RODS

A testing device was used for FR testing. Its major element is the electrically heated module located in the hot cell (Fig. 23). Fuel rods under testing are placed inside the sealed capsule filled with argon, which in turn is located into the electrically heated module. The electrically heated module comprises four heating units arranged along the full height. The heating units are operated independently from each other. Each heating unit is provided with a thermocouple to control the operating mode of the module and to provide the control over the temperature in the capsule. The capsule incorporates four additional thermocouples arranged along its axis. Co-ordinates of the thermocouples as related to the capsule bottom are equal 443; 1,513; 2,543 and 3,700 mm, respectively. Figure 23b demonstrates the FR location in the capsule.

The distribution of temperature along the capsule axis in the steady state operating mode is shown in Fig. 24. As seen in Fig. 24, the maximum value of temperature deviation from the predetermined one (350, 390°C) is no more than 6°C. The test stand control system allows for maintaining the temperature along the fuel rod in the steady state operating mode within ±2°C relative to the temperature distribution shown in Fig. 24. When the fuel rods were tested at 350 and 390°C, time required for bringing the electrically heated module to the steady state mode constituted 200 and 100 minutes, respectively. The control over the temperature inside the capsule was exercised according to the readings of the four thermocouples arranged along the capsule axis. Figure 25 demonstrates the temperature profiles plotted according to the readings of thermocouples at the moment of bringing the electrically heated module to the steady state mode.

The fuel rods were tested at 350°C continuously during 1440 hours after bringing the electrically heated module to the steady state operating mode. Then the module was switched off and after cooling (Fig. 26a) the fuel rods were withdrawn from the capsule and sent for non-destructive examinations.

The fuel rods were inserted again into the testing device after examination and continuously tested at 390°C, also for 1,440 hours. Temperature profiles plotted according to the thermocouple readings in the course of module cooling after testing are given in Fig. 26b. Fuel rods were withdrawn from the capsule and examined using the same non-destructive techniques as for a temperature of 350°C.
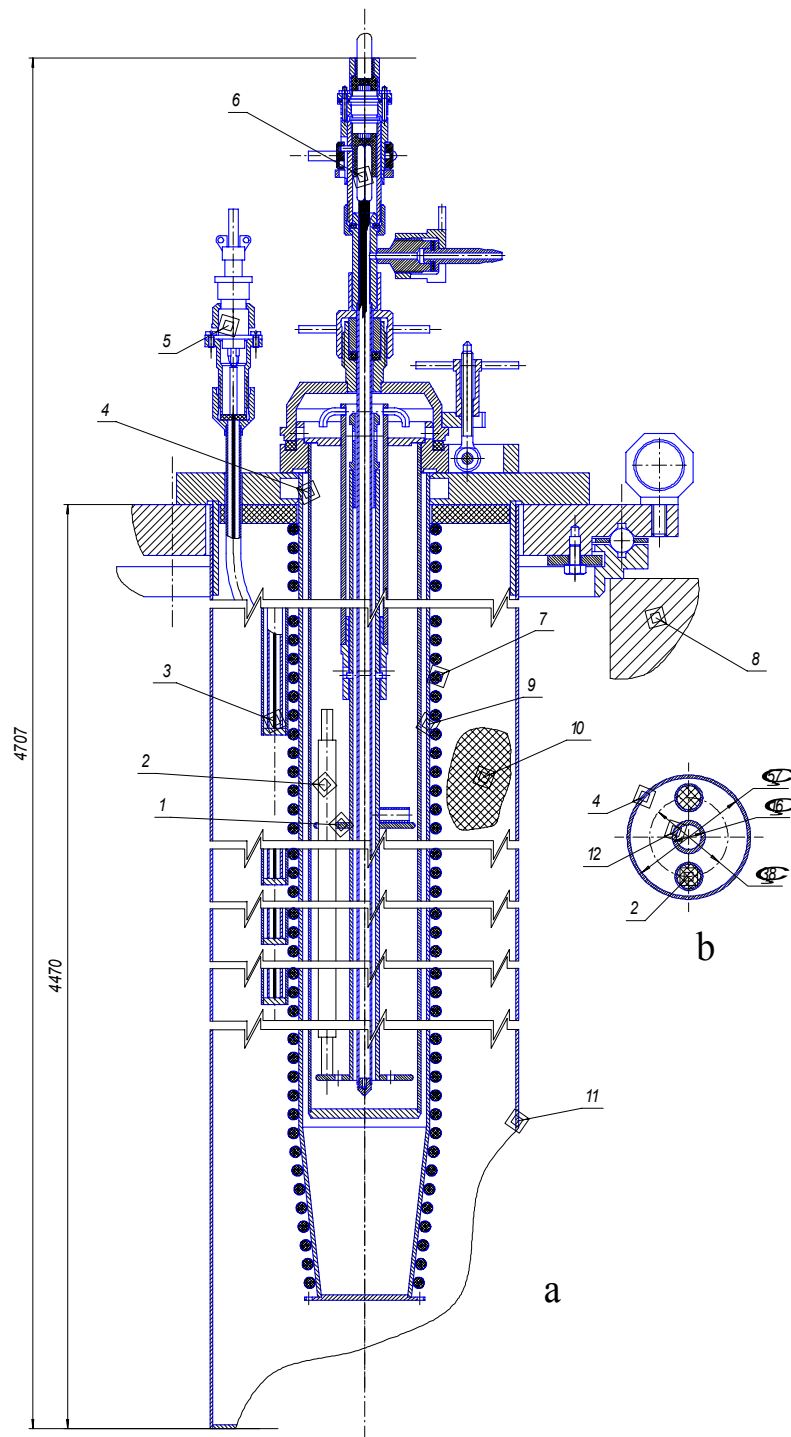
Legend: 1-case; 2-fuel rod; 3-thermocouple of the heating unit; 4-capsule; 5-joint; 6-thermocouples inside capsule; 7-heating unit; 8-hot cell well; 9-vessel; 10-insulation; 11-wrapper; 12-case channel.

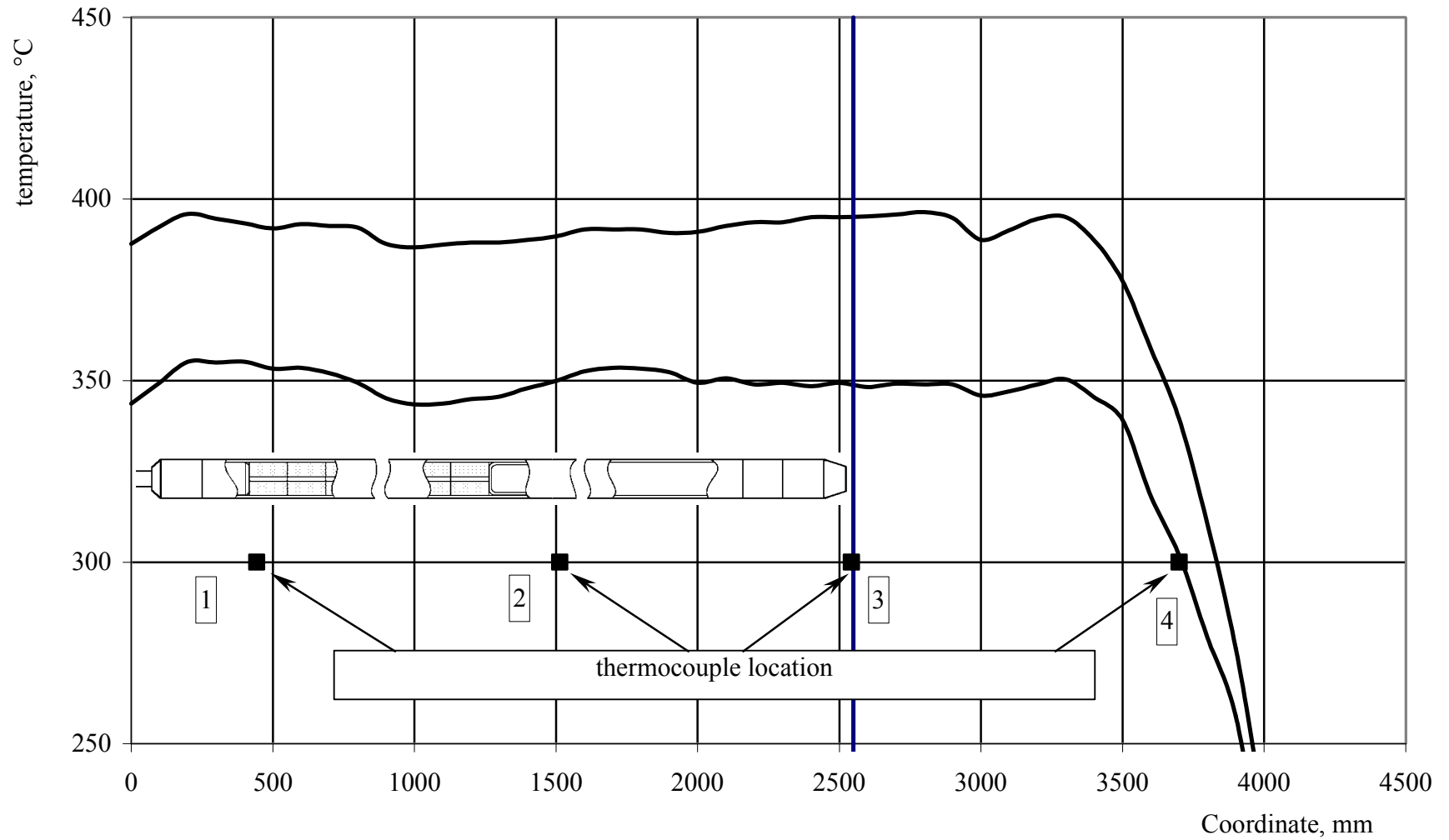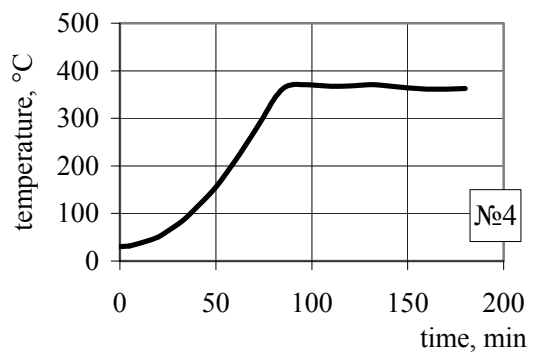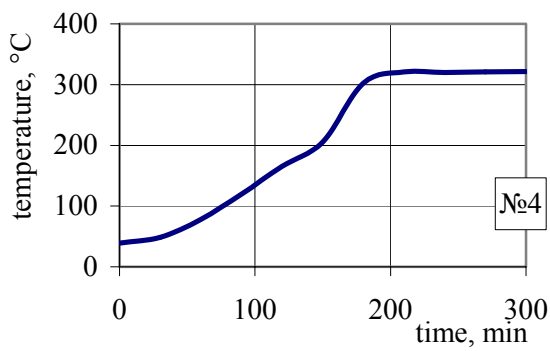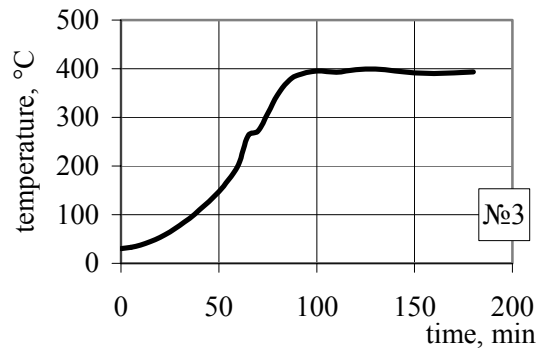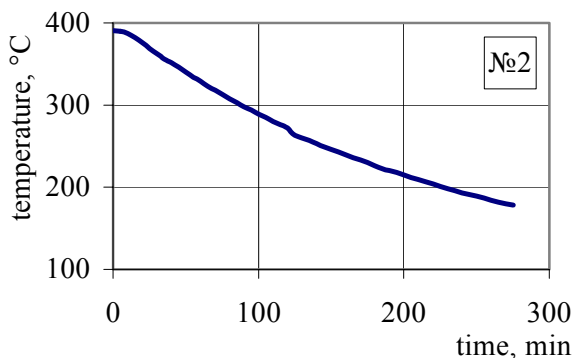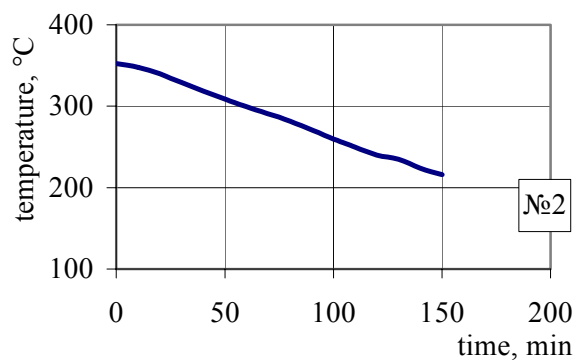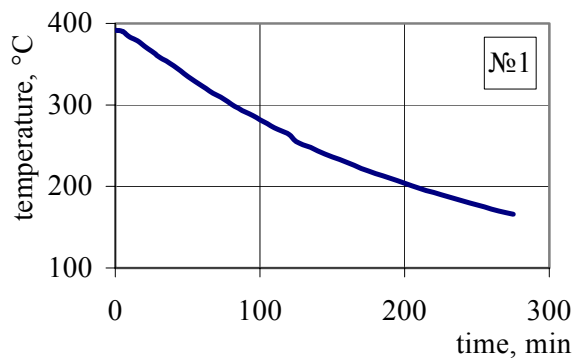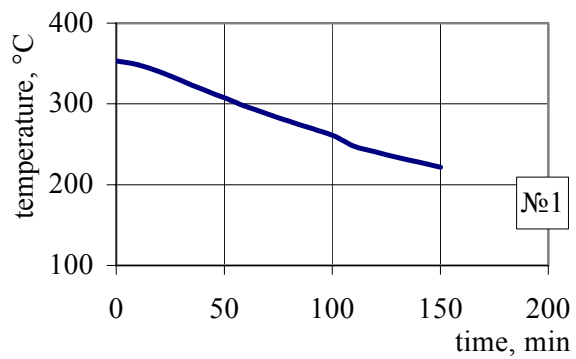*Fig. 23. Electrically heated module (a) and arrangement of FR in the capsule (b).*

Fig. 24. Temperature distribution along the fuel rod in the electrically heated module capsule under steady state conditions: 1, 2, 3, 4 – thermocouples numbers.
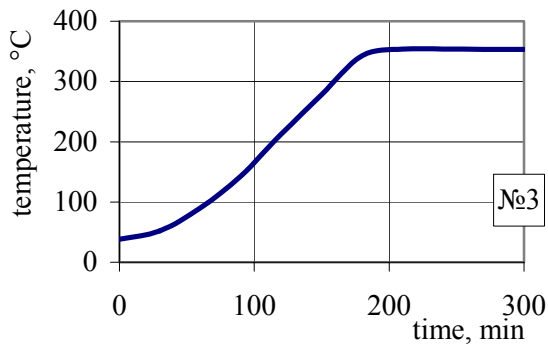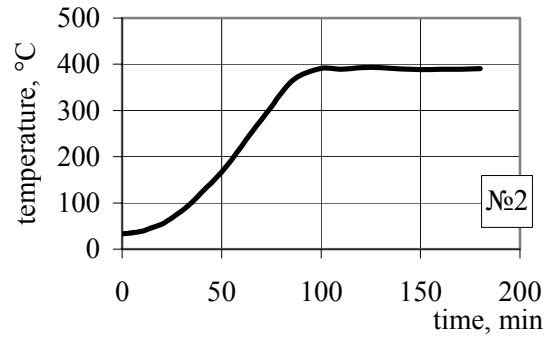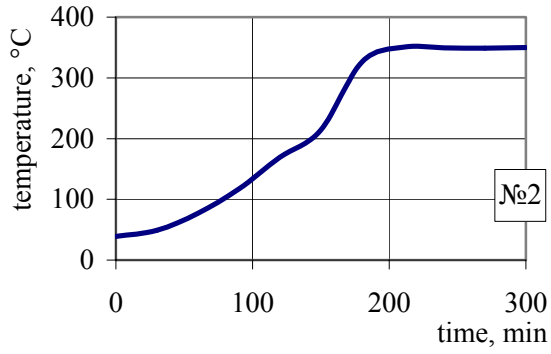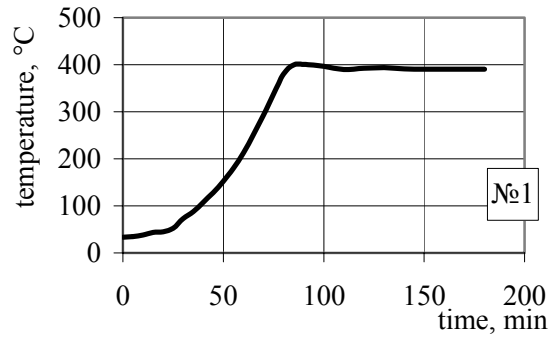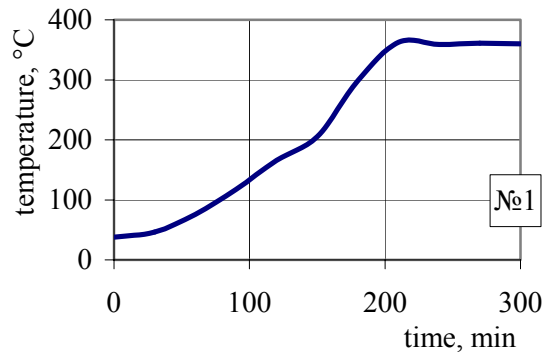
Fig. 25. Time profiles plotted according to readings of thermocouples No.1, 2, 3, 4 when the electrically heated module reached steady state at 350°C (a) and 390°C (b).
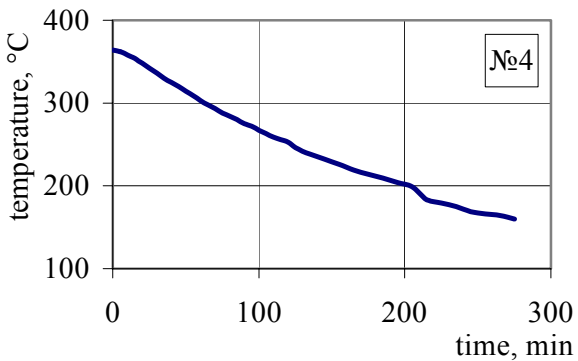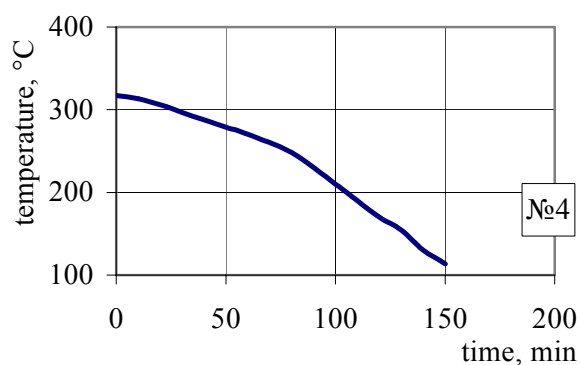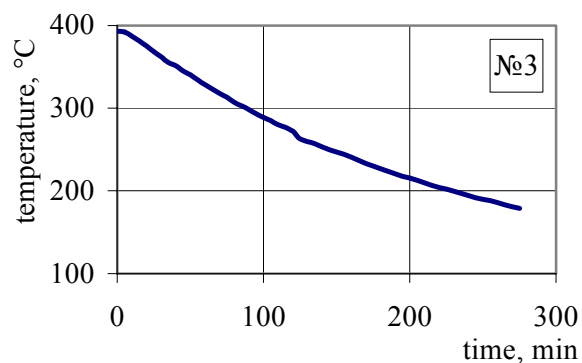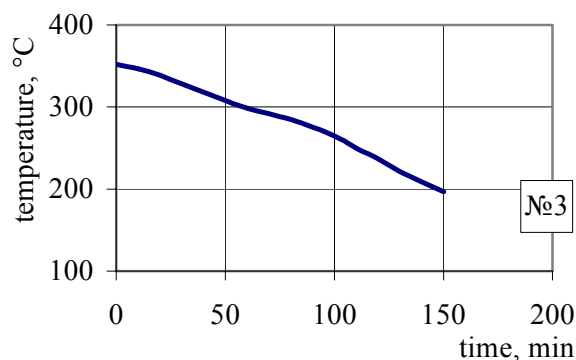
Fig. 26. Time profiles plotted according to readings of thermocouples No.1, 2, 3, 4 when the electrically heated module reached cooling after FR testing at 350 C (a) and 390°C (b).

4. COMPARISON ANALYSIS OF THE NONDESTRUCTIVE EXAMINATION RESULTS OF FUEL RODS BEFORE AND AFTER THERMAL TESTING AT 350°C AND 390°C

After thermal testing, the fuel rods were examined using the same NDT methods that had been applied during their certification:

- visual examination;
- leakage test;
- diameter measurements in 4 azimuthal orientations;
- length measurement;
- eddy-current flaw detection;
- measurement of oxide film;
- gamma-scanning.

The nondestructive examination results are presented in Appendix 2.

4.1. VISUAL INSPECTION OF THE FUEL ROD SURFACE

On comparison of the photos of the fuel rod cladding fragments (Figs 7 and 8) before and after thermal testing (Figs A2.1 and A2.2 of Appendix 2), it is seen that the external appearance of the fuel rod claddings did not change after testing at 350°C and 390°C. In several cladding areas, the oxide outlines are observed to remain the same after testing. As it was before testing, the surface of the lower cladding part has a dark-grey colour and on moving upwards the dark colour intensity weakens.

The unchanged appearance of the external cladding surface gives indirect evidence that no additional oxidation occurred as a result of thermal tests. [5].

4.2. GEOMETRICAL PARAMETERS OF FUEL RODS

After testing at 350°C and 390°C, the cladding profiles actually did not change in all 4 azimuthal orientations (Fig. 27).
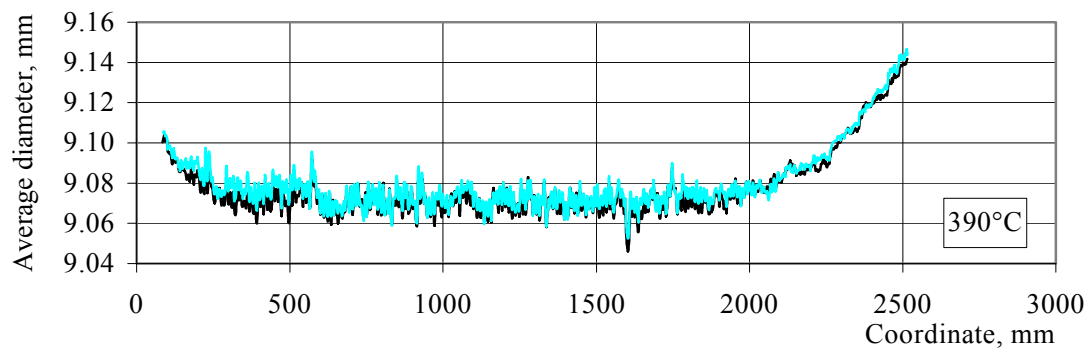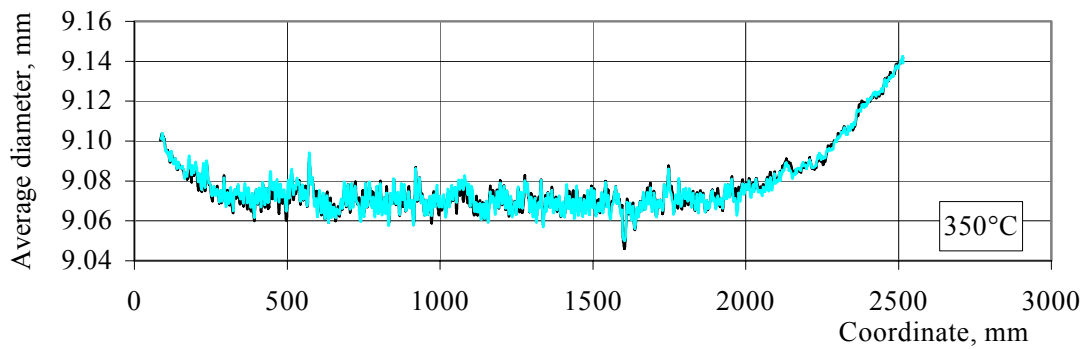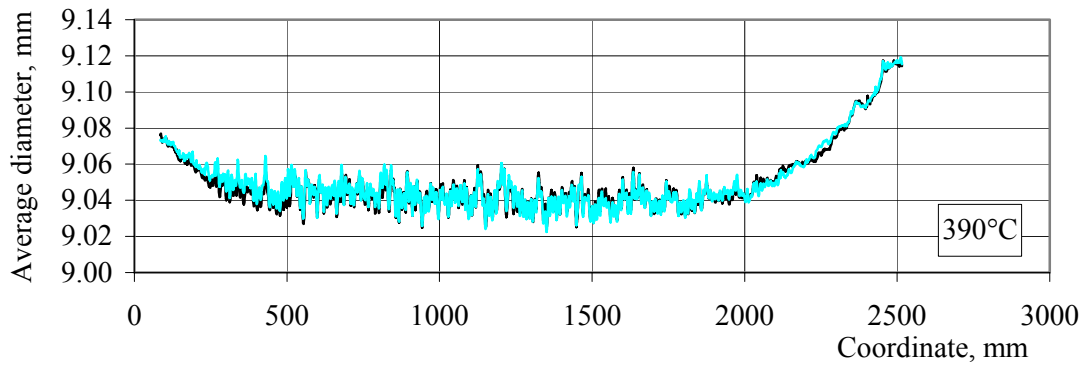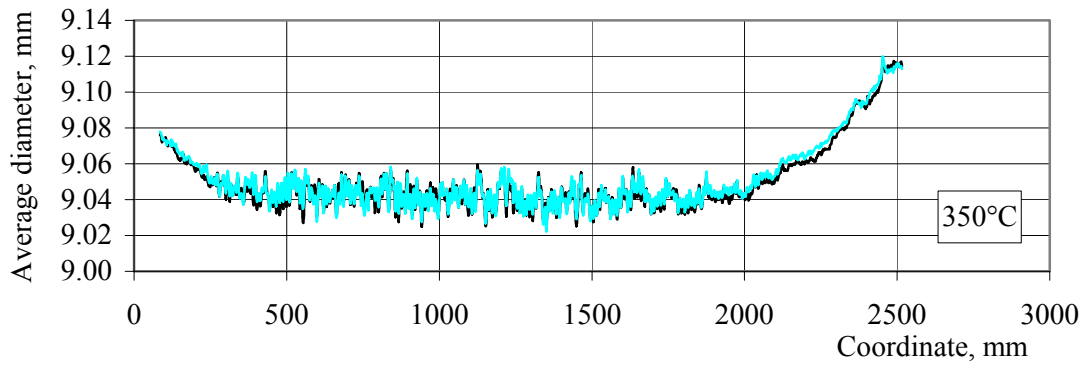
Fig. 27. The distribution of the average diameter along the claddings of fuel rods No.64 (a, b) and 78 (c, d) before and after thermal testing at 350°C and 390°C.

In order to estimate the cladding diameter changes as a result of thermal creep the cladding diameter change $\Delta d_i^{(k)}$ were calculated in each of cross-sections **i** of the fuel rod where the measurements were performed:

$$\Delta d_i^{(k)} = \frac{1}{4}\left[\sum_{j=1}^{4} d_{j,i}^{(k)} - \sum_{j=1}^{4} d_{j,i}^{(0)}\right],$$

where   j – number of azimuthal orientation of the cladding against the transducers on measuring the diameter;

   i – number of fuel rod cross-section where the diameter measurement were performed, **i**=1, 2…1215;

   $d_{j,i}^{(k)}$ – fuel rod diameter in cross-section **i** of azimuthal orientation **j** after testing stage **k**; **k**=1 –temperature is 350°C; **k**=2 – temperature is 390°C.

$d_{j,i}^{(0)}$ – initial value of the cladding diameter in cross-section **i** of azimuthal orientation **j**.

Values $\Delta d_i^{(k)}$ are statistically due to the fact that on repeated measurement of the cladding diameter after testing it is impossible for the transducer to hit ideally the same points on the cladding surface where the diameter was measured before testing and also because of an error of the diameter measurement.

In order to take account of the systematic error component, the cladding diameter measurements of the untested surveillance fuel rod were performed and corresponding corrections were introduced in to the measurement results.

Figures 28 and 29 present the distribution $P(x) = f\left(\Delta d_i^{(k)}\right)$ of values $\Delta d_i^{(k)}$ for both fuel rods after their testing at 350 and 390°C, correspondingly. On the basis of this distribution, an average value of the diameter changes $\Delta d^{(k)}$ was defined along the whole fuel rod length

$\Delta d^{(k)} = \dfrac{1}{1215}\displaystyle\sum_{i}^{1215}\Delta d_i^{(k)}$ as well as dispersion $\sigma = \sigma\left(\Delta d_i^{(k)}\right)$.

After the first stage of thermal testing at 350°C the diameter increment $\overline{\Delta d_i^{(1)}}$ of fuel rod cladding No.64 is within the range 1.0±6.0µm (with confidence probability 0.95) (Fig. 28a), and for fuel rod No.78 - 0±4.0µm (Fig.3.2b). After the second testing stage, the value $\overline{\Delta d_i^{(2)}}$ is within the range 0.7±6.0µm and 2.6±6.0µm for fuel rods No.64 and 78, correspondingly (Fig. 29).
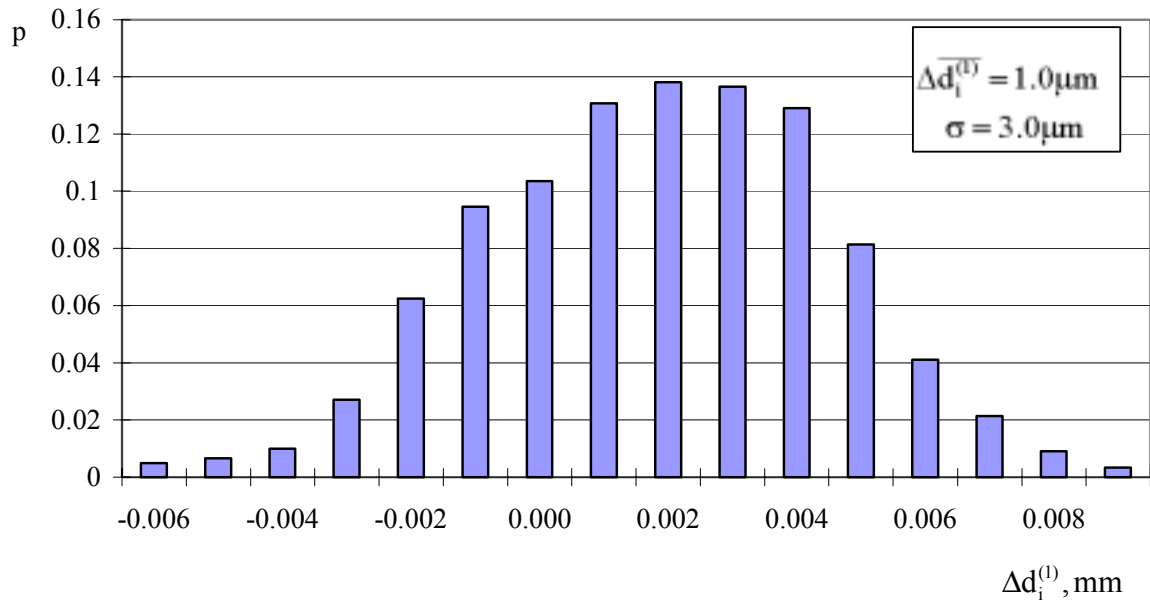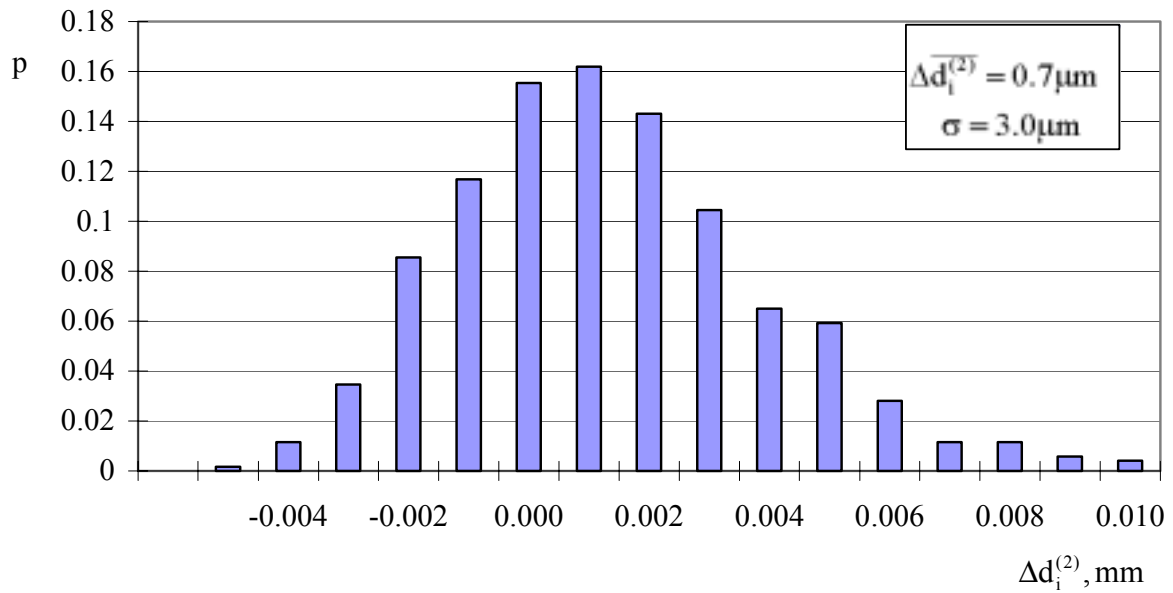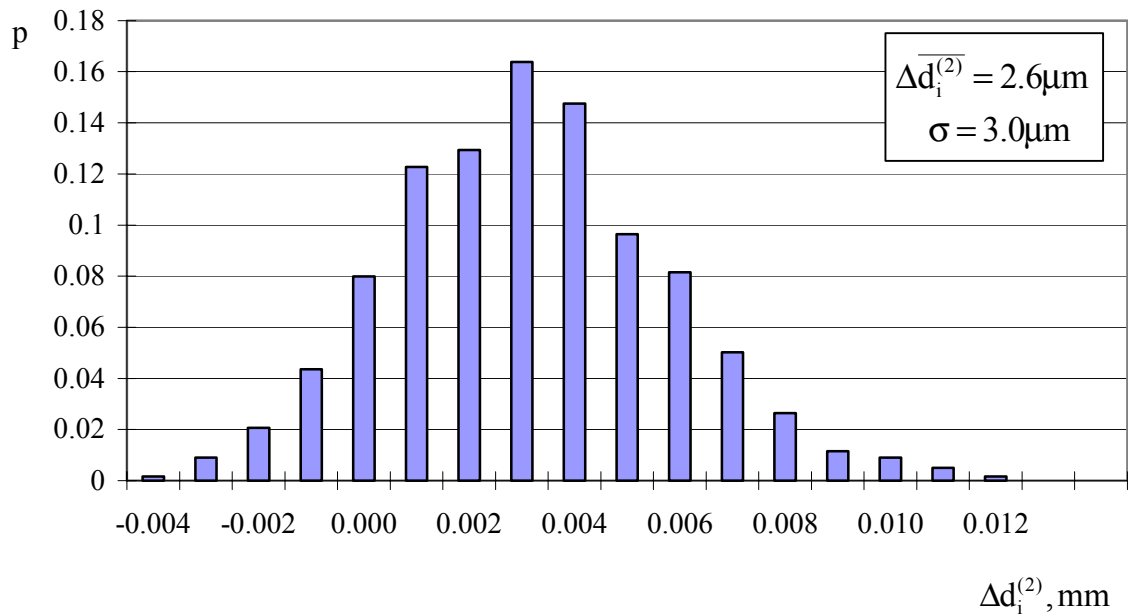
a
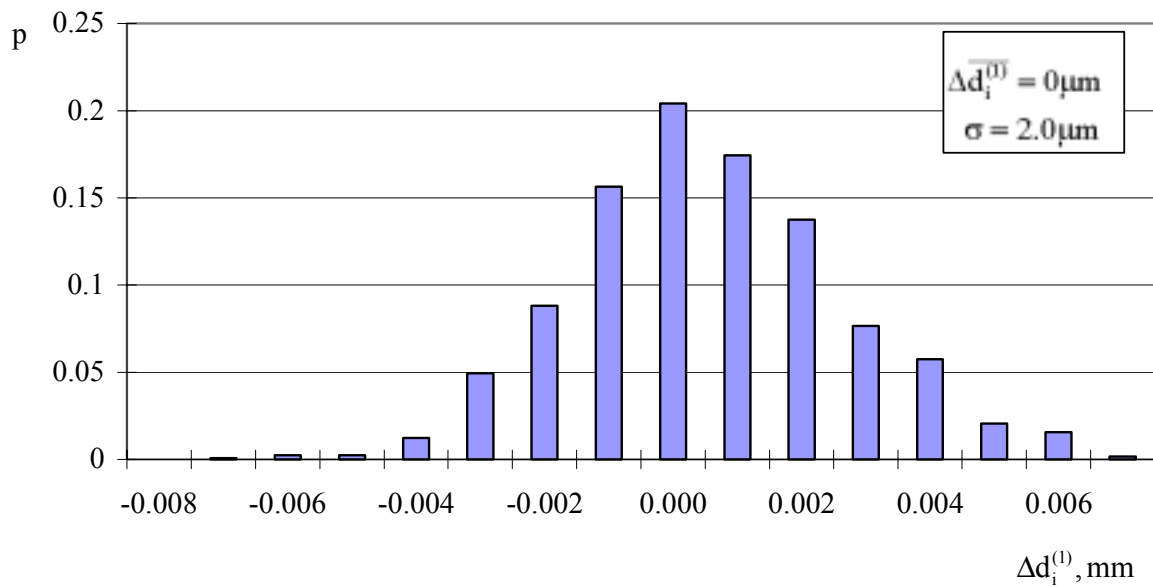
b

Fig. 28. The distribution of Δd_i after thermal testing at 350°C, No.64 (a) and No.78 (b).

a

b

Fig. 29. The distribution of Δd_i after thermal testing at 390 °C, No.64 (a) and No.78 (b).

The analysis results (Table A2.I Appendix 2) on the fuel rod length measurement before and after thermal testing indicate that, taking account of the measurement error equal to ±0.3mm, no length changes of fuel rods No. 64 and 78 were revealed.

4.3. FUEL ROD CLADDING STATE BASED ON THE RESULTS OF EDDY-CURRENT FLAW DETECTION

After thermal testing, the results of eddy-current testing (Figs A2.9–A2.10, Appendix 2) indicated no change compared to the initial test (Fig. 13). This indicates that during the tests no noticeable deformation of the fuel rod cladding occurred, and that no cladding defects could be detected with the eddy-current flaw detector.

4.4. OXIDE FILM THICKNESS ON THE OUTER CLADDING SURFACE

In comparing the measurement results of the oxide film thickness on the outer fuel rod cladding surface before (Figs 14–15) and after (Figs A2.11–A2.14, Appendix 2) thermal testing, it became obvious that the average thickness of the oxide film achieved ~5μm, and in the course of thermal testing it did not change. The oxide film covered the fuel rod cladding surface uniformly, and its thickness increased insignificantly by about 1–2μm from the fuel rods bottom to its top.

The absence of additional oxidation of the outer surface of the claddings in the course of tests was expected, since the tests were performed in an inert gas (argon) medium.

4.5. GAMMA-SPECTROMETRY RESULTS

A comparison of the gamma-spectrometry results of the fuel rods before (Fig. 16) and after their testing (Figs A2.15–A2.16, Appendix 2) showed that on heating the fuel rods up to 350°C and 390°C there is no fission products migration, in particular with respect to ^{137}Cs. The distribution manner of ^{137}Cs remained the same in fuel rods No. 64 and 78 after their testing.

5. DISCUSSION

Two WWER-440 fuel rods with cladding made of Zr-1%Nb alloy were chosen and certified for thermal testing after their operation as part of a fuel assembly with an average burnup of ~46MW·d/kgU during 5 fuel cycles in unit 3 of Kola NPP. For 2.5 years, these fuel rods have been cooled inside the fuel assembly in the spent fuel pool, and then after fuel assembly dismantling at the SSC RF RIAR, they have been stored in air at a temperature below 80°C for 7 more years.

As a result of the seven-year storage in air, the main fuel rod parameters such as cladding diameter, oxide layer thickness, distribution of long lived fission products in fuel did not change.

On the basis of the destructive examination results of "equivalent" fuel rods neighbouring the chosen ones in the fuel assembly an estimation was made of pressure and gas composition under the cladding and also of mechanical properties of the fuel rod cladding materials.

The fuel rods chosen for testing are typical WWER-440 fuel rods. They reached a burnup of 40–50MW·d/kgU and are representative for investigation of the WWER-440 spent nuclear fuel (SNF) behaviour under dry storage conditions.

According to the experimental conditions, the fuel rods were tested at two temperatures 350 C and 390°C. 350°C is postulated as the maximum permissible temperature of the fuel rod cladding under standard storage conditions. 390°C is an intermediate temperature between that of standard storage conditions and the maximum permissible temperature under transient and emergency storage conditions.

According to the experimental conditions, the thermal testing duration of the fuel rods was restricted to 2 months at each temperature, comprising 1/300 part of the design storage period for SNF. Thus, because of the small testing period, one of the main processes that could lead

to any marked change in the fuel rod parameters (i.e. fuel rod cladding deformation as a result of thermal creep) was considered.

The calculated estimation of the cladding deformation value was performed using a phenomenological model of anisotropic thermal creep of cladding tubes made of Zr-1%Nb alloy. The phenomenological model of anisotropic thermal creep [7–10] was developed on the basis of a great experimental data array that had been obtained with irradiated and unirradiated specimens.

It should be noted that there are no experimental data on thermal creep of irradiated claddings made of Zr-1%Nb alloy in the temperature range and hoop stresses σ_θ characteristic of the WWER-440 SNF dry storage. Creep testing was performed either at high temperatures (500–800°C) or at high hoop stress values δ_θ>50Mpa [typical hoop stresses of the WWER-440 fuel rods at 350°C are within the range 10–20Mpa].

Figure 30 presents the calculation results of the dependence of the cladding effective strain on the long term storage at 350°C and 390°C, for gas pressure inside the cladding equal to 1.4MPa (20°C). In 50 years of dry storage at 350°C, the cladding hoop deformation ε_θ<ε_{eff} will achieve ~0.5%, which satisfies the safe storage criterion stated in the Introduction. This calculation can be considered conservative, since the cladding storage temperature will decrease overtime in storage. Small or negligible temperature decrease can occur if a dry storage container is filled with SNF after a very long pre-cooling time (to the limits of its decay heat release). This situation may result in two consequences:

1. the temperature in the container is relatively high within the limits of licensing parameters;
2. the temperature stays nearly constant since the decay heat decrease is small after a long pre-cooling time.

The calculated dependence of the cladding effective hoop strain shown in Fig. 30 exhibits the forecast for the behaviour of the SNF under the above conditions.
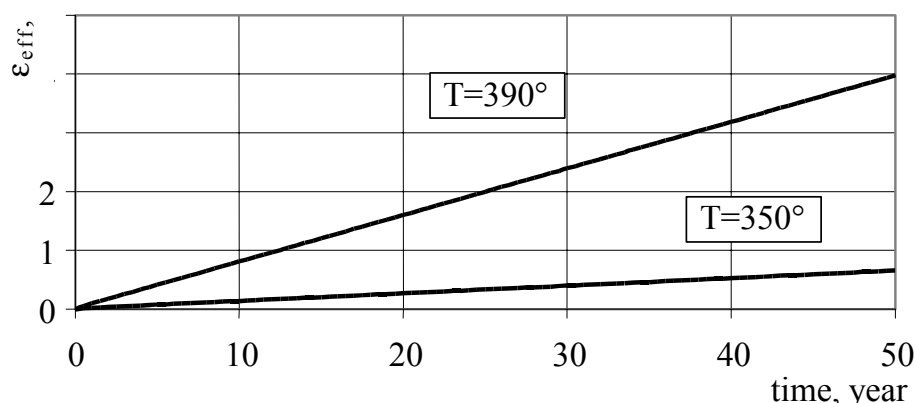

Fig. 30. The calculated dependence of the cladding effective deformation on the dry storage duration.

However in many cases, it is intended to store the fuel after a relatively short pre-cooling time, e.g. 5 years. In such a case the container will be loaded also to its limits of decay heat release capacity defined in the license. However after 5 years pre-cooling time the decay heat of the spent fuel will still decrease considerably. As a consequence, the SNF temperatures in the cask will drop considerably with time. Figure 31 exhibits the temperature drop of WWER SNF in CASTOR 440/84 cask [11, 12]. The hot spot temperature in the cask drops in less than 15 years by about 100°C. For that temperature characteristic the hoop strain for the fuel rod segment with the highest temperature was calculated with the same assumption used for the hoop strain calculations presented in Fig. 30. The temperature was kept constant, as after 15 years of storage since the temperature relationship given in [11, 12] is only valid for t<15 years. In the case considered, the hoop strain is practically frozen after 15 years of storage since the creep of the Zr-1Nb alloy is strongly dependant from the temperature. The calculations performed and shown in Fig. 31 shows that WWER-440 SNF can be easily stored in a CASTOR 440/84. The hoop strain, which is considered to be the limiting criteria in the licensing to avoid fuel defection, is with 0.025% nicely below the total hoop strain limit of 1%. Similar results for WWER-440 SNF in dry storage were reported from Czech investigators [12]. The decrease of the hoop strain with temperature was also reported in [13] for LWR SNF using Zircaloy-4 as cladding material with an higher average FA bundle burnup of 55 MW·d/kg of fissile material.
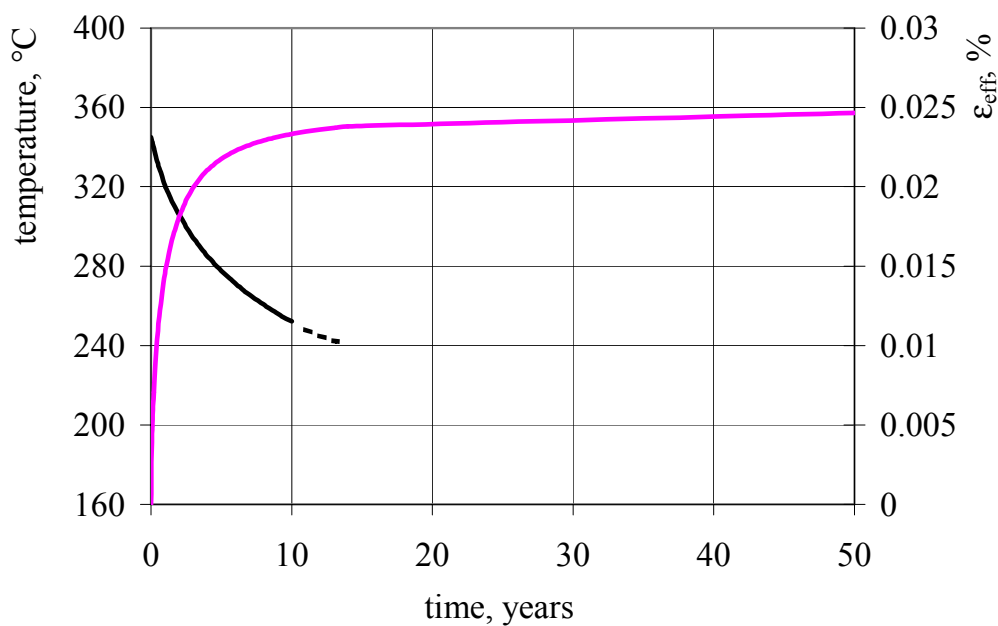

Fig. 31. Spent fuel storage performance prediction of a WWER-440 fuel rod.

The calculated estimation of the cladding deformation value presented in Fig. 30 showed that as a result of thermal testing, the cladding diameter will increase by about 0.5μm after the first testing stage at 350°C, and after the second testing stage at 390°C it will increase by 1.8μm.

The measurement results of the fuel rod cladding diameter showed that after thermal testing for 2 months at 350°C (followed by two-month tests at 390°C), the diameters of fuel rods No. 64 and 78 actually did not exceed the detection limit. After completing two test stages, the average value ($\Delta \bar{d}$) (averaged along the total fuel rod length) of the diameter increase of fuel rods No. 64 and 78 achieved ~1.0 and 2.6μm, respectively, at dispersion $\sigma(\Delta d_i)$ equal to 2.0–3.0μm.

Hence, the obtained experimental data on the cladding diameter change coincide with the calculated estimation performed. However, such small cladding deformations do not allow a correct estimation of the thermal creep rate value of the fuel rod cladding material. For such estimation, a longer testing period is required as compared to that of the experiment.

Other fuel rod parameters tested during fuel rod certification (external appearance of the cladding surface, oxide film thickness on the outer cladding surface, distribution of fuel fission products) did not change as a result of thermal testing.

To obtain a correct determination of the thermal creep rate for the WWER-440 cladding material under dry storage conditions it would be advisable to continue testing of these fuel rods during a period that would lead to an increase of the cladding diameter by 5–10μm. Figure 32 presents the calculation of the WWER-440 fuel rod cladding deformation, gas pressure (1.4MPa, (20°C)) under the cladding, for several scenarios of the fuel rod test continuation.
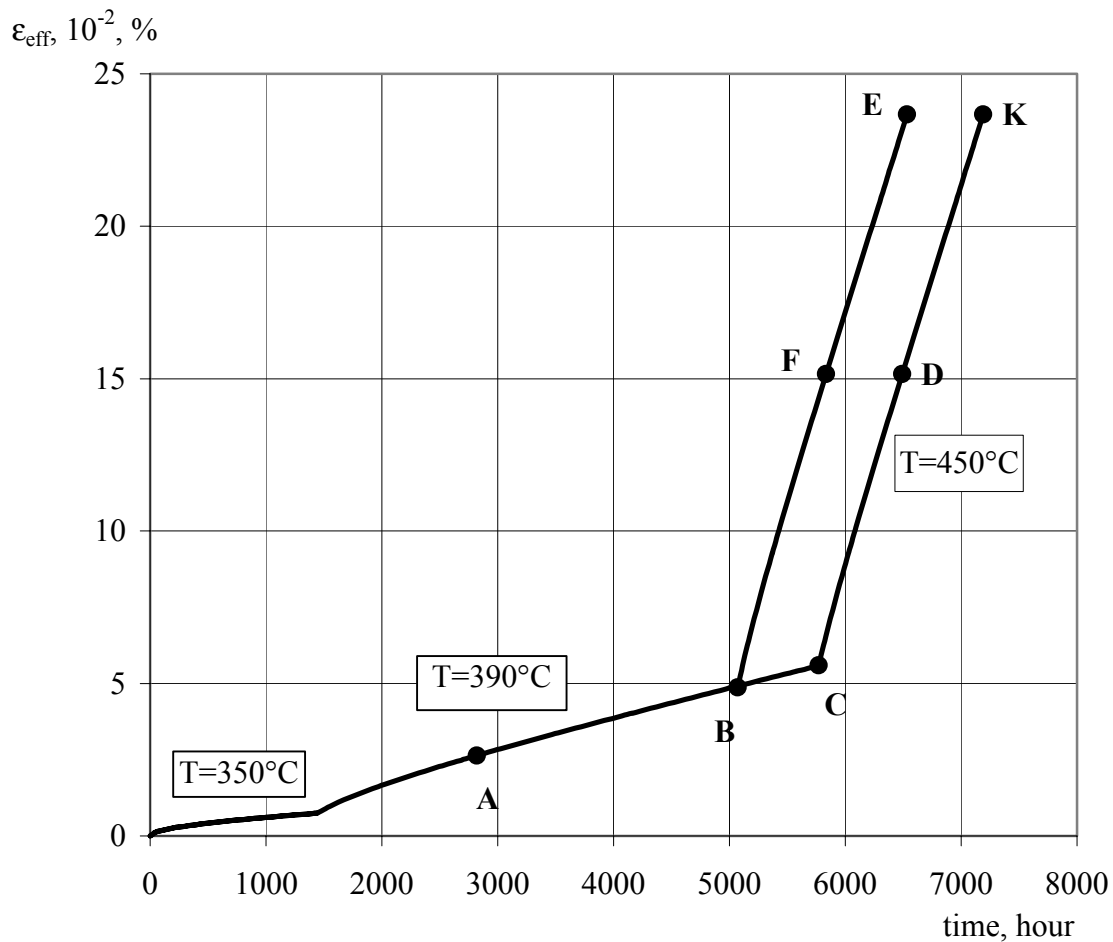
Fig. 32. The calculation results of the effective cladding deformation for different scenarios of the fuel rod test continuation.

Point A in Fig. 32 is the moment of the experiment completion. The fuel rod thermal test being continued at 390°C during 4 or 5 months (points B and C), the calculated estimation of the effective cladding deformation value achieves 0.06 and 0.07%, respectively, i.e. in terms of diameter increase makes up ~4 and 5μm, respectively. These cladding deformation values allow the estimation of the creep rate at 390°C.

In order to estimate the fuel rod behaviour under emergency and transient conditions at 450°C, testing of the same fuel rods can be continued during one (points F and D) or two (points E and K) months.

The calculated estimation of the effective cladding deformation value equals approximately 0.15–0.16 and 0.24–0.25% or about 10 and 18μm in terms of cladding diameter increase after one and two months of testing, respectively. Thus the considered scenarios of the fuel rod thermal testing continuation allow the estimation of the creep rate for the WWER-440 fuel rod claddings under dry storage conditions. The continuation of the fuel rod testing (the total test period will make up 10–11 months) would aid safety validations by checking the assumption stated in some papers [3] about possible fuel degradation in the course of dry storage with additional release of gaseous fission products under the cladding (that correspondingly leads to an increase of hoop stresses in the cladding material).

6. CONCLUSIONS

The test fuel rods were all taken from a WWER 440 FA operated in the Kola NPP (in fuel cycles 5 through 9). The FA had been in the reactor from 24 September 1986 until 15 October 1991. After five reactor cycles, it reached a burnup of 48.18 MW.d/kgU. Two fuel rods had been selected for dry storage tests and three additional fuel rods had been chosen from the neighbourhood for destructive testing. The nondestructive examinations of the test fuel rods involved visual inspection, leak testing, and diameter measurement in four azimuthal projections, length measurement, eddy-current testing, measurement of the oxide film thickness and gamma-scanning. In parallel three rods taken from the neighbourhood of the tested rods were inspected by destructive methods to obtain the fission gas content in the SNF, the void volume and mechanical test data of fuel rods with practically identical operation performance. These data are used to calculate the pressure in the test rods and the stresses in the cladding. From the test results, it can be concluded that:

(1) After thermal testing in argon environment at 350°C for two months and then at 390°C for another two months, the technical state of the fuel rods did not show any detectable changes. The external appearance of the fuel rod cladding surface, oxide film thickness, fuel rod length and distribution of fuel fission products remained the same after testing. A statistical assessment of all measured diameter changes resulted in a diameter change of 2.6 μm;
(2) Dry storage (with a small or negligible temperature decrease) results in a calculated constant hoop strain rate of the cladding. However, the cumulative strain does not exceed 1% in 50 years (secondary creep rate);
(3) A predictive calculation of the cumulative cladding hoop strain under a decreasing temperature condition indicates that the cladding creep is saturated after 10 years of dry storage. The predicted hoop strain (approximately 0.02%) is too low to cause safety concerns;
(4) The results of the test programme performed indicate that dry inert storage of WWER 440 SNF is feasible and safe within the investigated temperature range.

Appendix 1

Table I. List of the methods and their main characteristics used for investigation of the WWER-440 fuel rods before and after their tests under conditions simulating dry storage

No.	Operation	Technical characteristics	Registration No. of methods in the SSC RIAR Register
1 1.1	Visual inspection of fuel rods Taking pictures (1:1)	Periscope visual optical system with magnification $1^x \div 5^x$. Photos are made on the reel film with photocamera "Olympyc OM-2".	Methods «visual-optical inspection of spent FA and their elements in the hot cells", registration No.20.
1.2	Description	Recording of the observed peculiar features in the operator log with indication of an axial coordinate on the photographed picture of the fuel rod. Identification of the state observed in accordance with atlas of defects.	
2 2.1	Leakage test Registration of Kr^{85}	Method is based on Kr85 definition in the gas plenum area. Registration is performed by the gamma-spectrometry method.	«Leakage test methods of the WWER fuel rods by measuring Kr^{85} in gas plenum by the gamma-spectrometry method", registration No. 19.
3 3.1	Measurement of fuel rod geometry parameters Diameter measurement	Measurements of the fuel rod diameter are performed with a profilometers equipped with contact sensors (probes) of the "Magnetic ruler" type DG810, SONY (Japan). A carriage with two probes oriented in the opposite direction moves discretely along the specified length in generatrix along the fuel rod axis. Readings of each sensor are recorded with PC. Measurements are performed with a specified orientation number (from 2 to 16). The current value of the average diameter (ovality) is defined. Measurement error does not exceed $\pm 10 \mu m$.	Method «Measurement of the external cladding diameter of irradiated fuel rods with cylindrical profile", register No.21-1 (M-17031 OIT)

No.	Operation	Technical characteristics	Registration No. of methods in the SSC RIAR Register
3.2.	Length measurement	Measurement of the fuel rod length is performed by means of a measuring device that defines the position of the free fuel rod end against the other end, count starting point being «0». The device is calibrated against the length standard. Measurements of the position of the fuel rod end against the basic mark of the length standard are performed both contact-free (using an optical cathetometer) or by means of contact sensors with an accuracy of ±0.3mm.	Methods for measuring the fuel rod length, registration No.74-96, register No.57.
4	Eddy-current flaw detection		
4.1	Detection of cladding defects	Eddy-current flaw detection method using harmonic excitation of the through-flow coils connected according to the differential or absolute variant. Simultaneously two excitation frequencies are used with recording of actual and imaginary components of the response signal. In addition to the axial location of a defect (abnormalities in the cladding) it is possible to obtain qualitative and quantitative estimation of its type (external, internal, throughout) by comparing it with a standard incorporating the known artificial defects.	Register No.26-1.
		Eddy-current flaw detection method with pulse excitation of the through flow soils connected differentially. Somewhat better sensitivity to the defect size (<5% of the cladding wall thickness) through noise signals. Quantitative estimation of the defect (abnormality) type: internal, external or throughout.	Eddy-current flaw detection method of the irradiated WWER fuel rod claddings, register No. 26-7, (M-17010 OIT)

No.	Operation	Technical characteristics	Registration No. of methods in the SSC RIAR Register
4.2	Measurement of oxide film thickness	Eddy-current thickness measurements of the outer nonconductive film ZrO_2 is performed on the fuel rod cladding using high frequency system FISCHERSCOPE MMS-D09A with sensor ET3.3-D09A. The method is calibrated with oxidized specimens cut out from the standard cladding tube made of Zr+1%Nb alloy with the known values of its thickness or with polymeric films on the non-oxidized standard cladding. Measurement error is ±4μm.	Register No.565
5	Gamma-scanning	Axial gamma-scanning of fuel rods in the gamma-line spectrometry of fission products is performed using a standard device in the hot cell by moving the fuel rod discretely against the immovable split-like collimator. The split width is adjustable in order to direct a gamma-radiation beam onto the germanium detector. Relative gamma-activity of individual fission product isotopes is recorded. When additional measurements are performed in the same geometry of the standard fuel rod with preliminary certified values of absolute fission product concentration, the relative distributions can be converted to absolute ones. Thus, monitoring of Kr^{85} release in the fuel rod plenum is possible if the measurement error does not exceed 10÷20%.	Register No.22

No.	Operation	Technical characteristics	Registration No. of methods in the SSC RIAR Register
6	Definition of characteristics of the equivalent fuel rod in the FA (located near the tested one)		
6.1	Definition of gas pressure and free volume in the fuel rod	Puncturing of the fuel rod cladding is applied at the final investigation stage of the state of a fuel rod or neighboring surveillance specimens. The fuel rod cladding is burnt through with a laser beam; pressure measurements of gas released into the sealed vessel with calibrated volume are conducted. The released gas volume is calculated from the known volume of the calibrated vessel and gas pressure measured. Free volume of hollows in the fuel rod is defined by bleeding the known helium quantity into the punctures and preliminary evacuated fuel rod. The measurement error of gas volume achieves $2.7 cm^3$ in the range $30–150 cm^3$ and $6.8 cm^3$ in the range $150–1150 cm^3$.	Method «Gas pressure measurement in irradiated fuel rods in the laser puncture device", Register No.17
		Some part of gas is sampled to determine its composition by the mass-spectrometry method.	Mass-spectrometry analysis of the gas composition in fuel rods, Register No.54
6.2	Mechanical properties of the cladding material: ultimate strength and yield stress	Mechanical properties of the cladding material are defined on the basis of results of mechanical testing of annular specimens. Measurement accuracy: $\sigma_{0.2}$ - ±3-7%; σ_B - ±4-9%; δ_P - ±2-12%; δ_0 - ±5-14%.	Methods for tensile measurements of annular specimens cut out from thin-wall tubes made of zirconium alloys. STP 086-373-99

1. NONDESTRUCTIVE EXAMINATION RESULTS OF FUEL ELEMENTS No. 64 AND 78 AFTER THEIR THERMAL TESTS AT 350 AND 390°C.

1. VISUAL INSPECTION RESULTS.
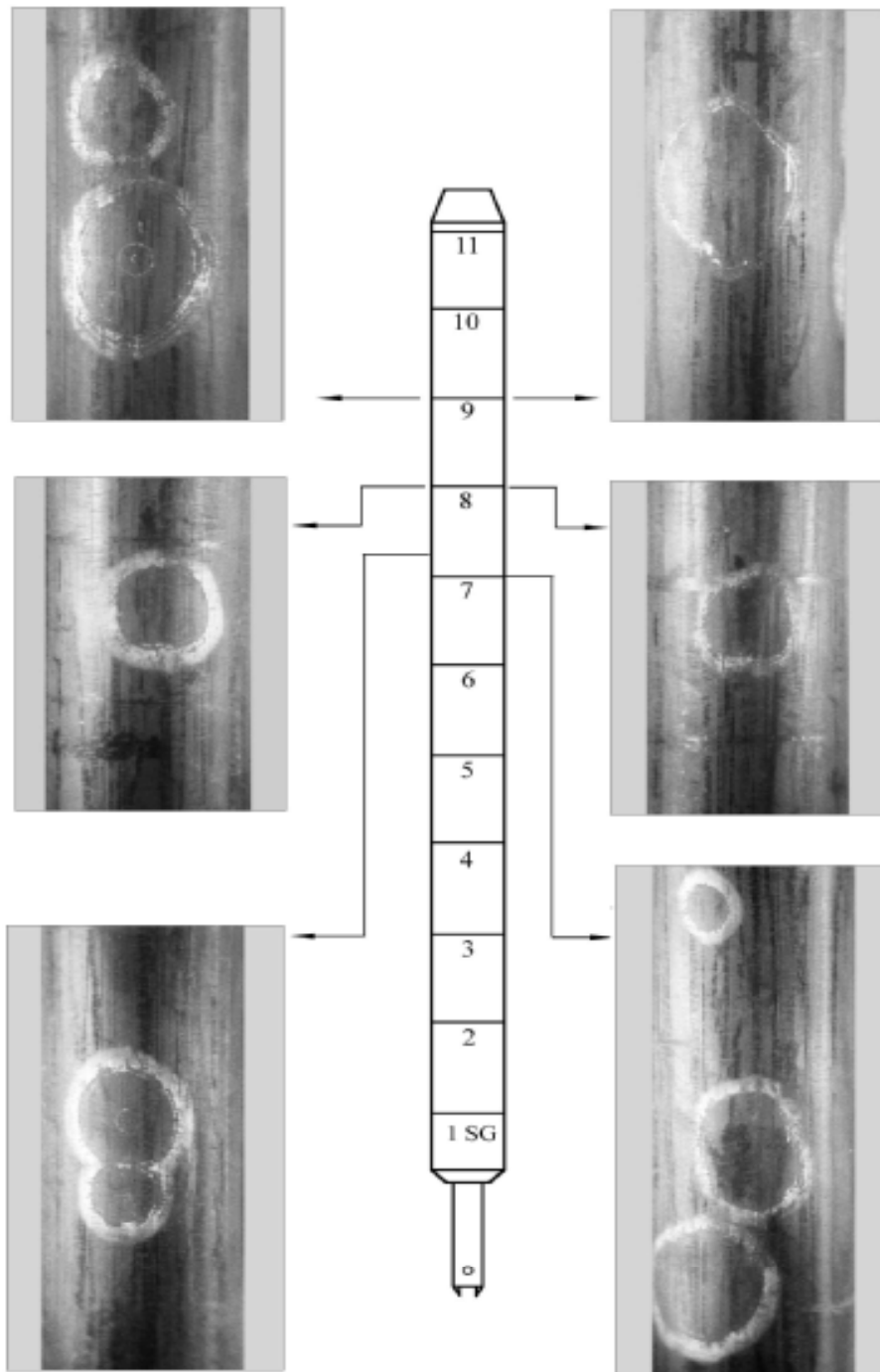
Fig. A2. 1. The cladding fragments of fuel rod No. 64 after thermal testing at 350 ℃.
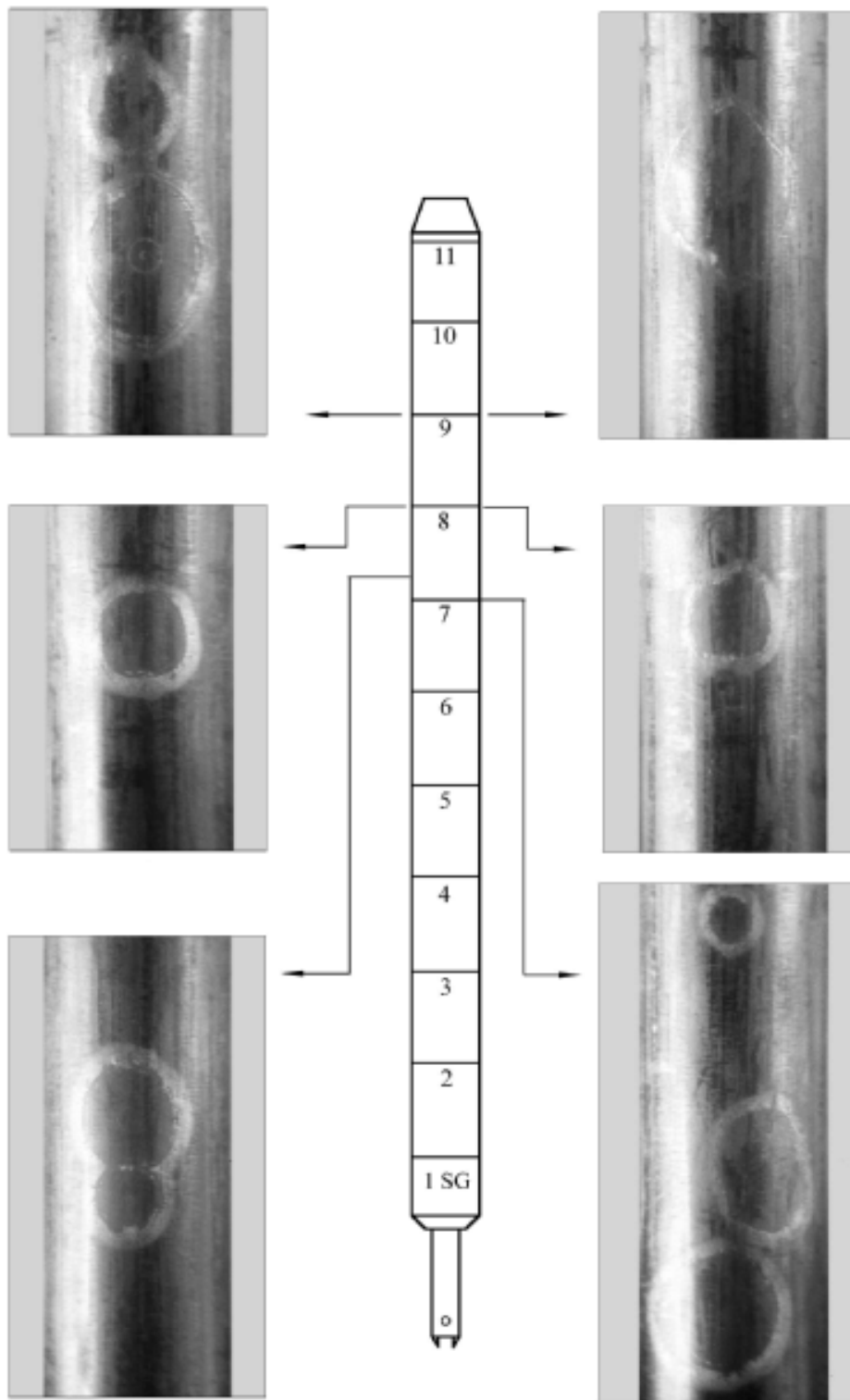
Fig. A2.2. The cladding fragments of fuel rod No. 64 after thermal testing at 390℃.
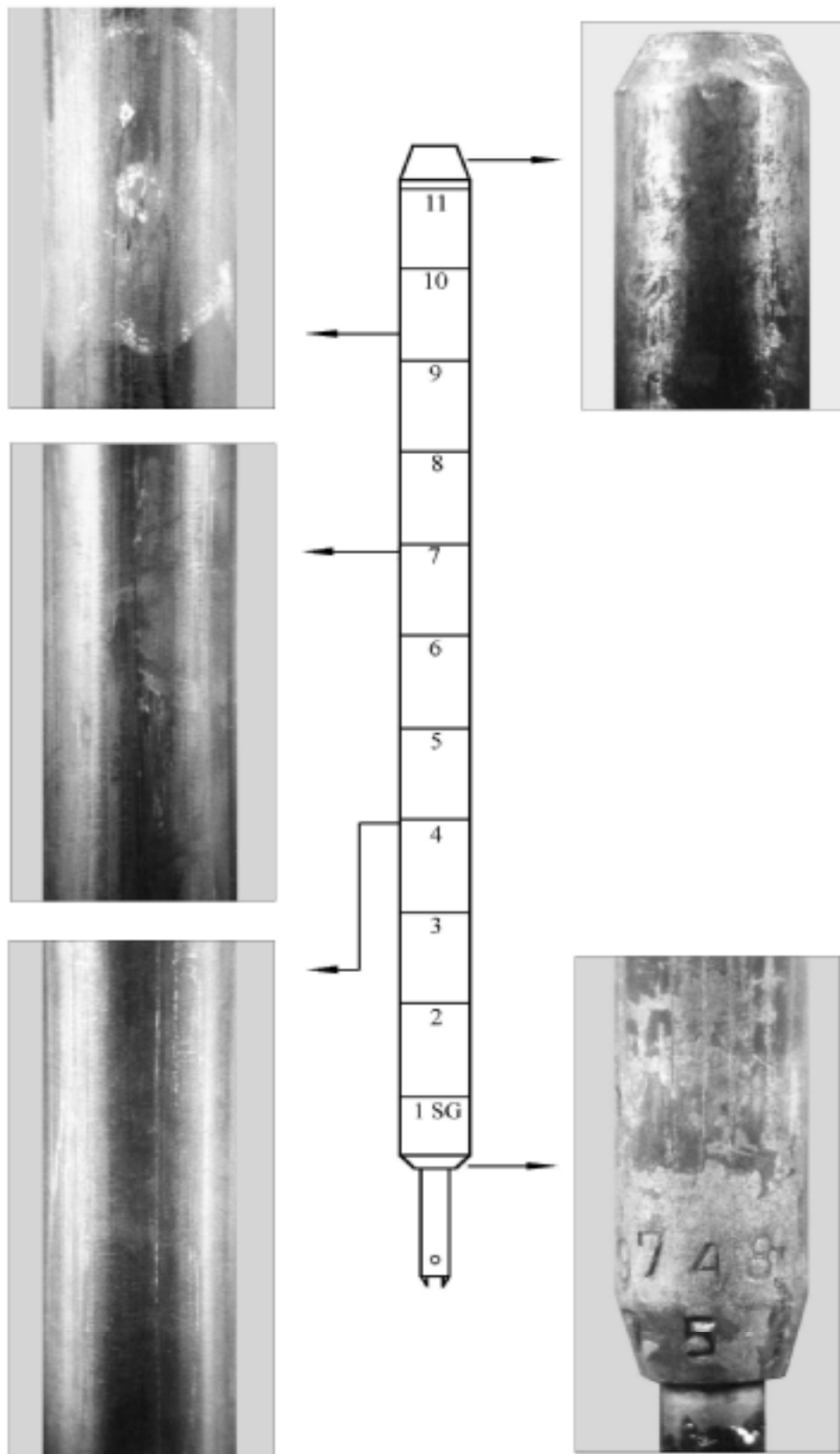
Fig. A2.3. The cladding fragments of fuel rod No. 78 after thermal testing at 350 ℃.
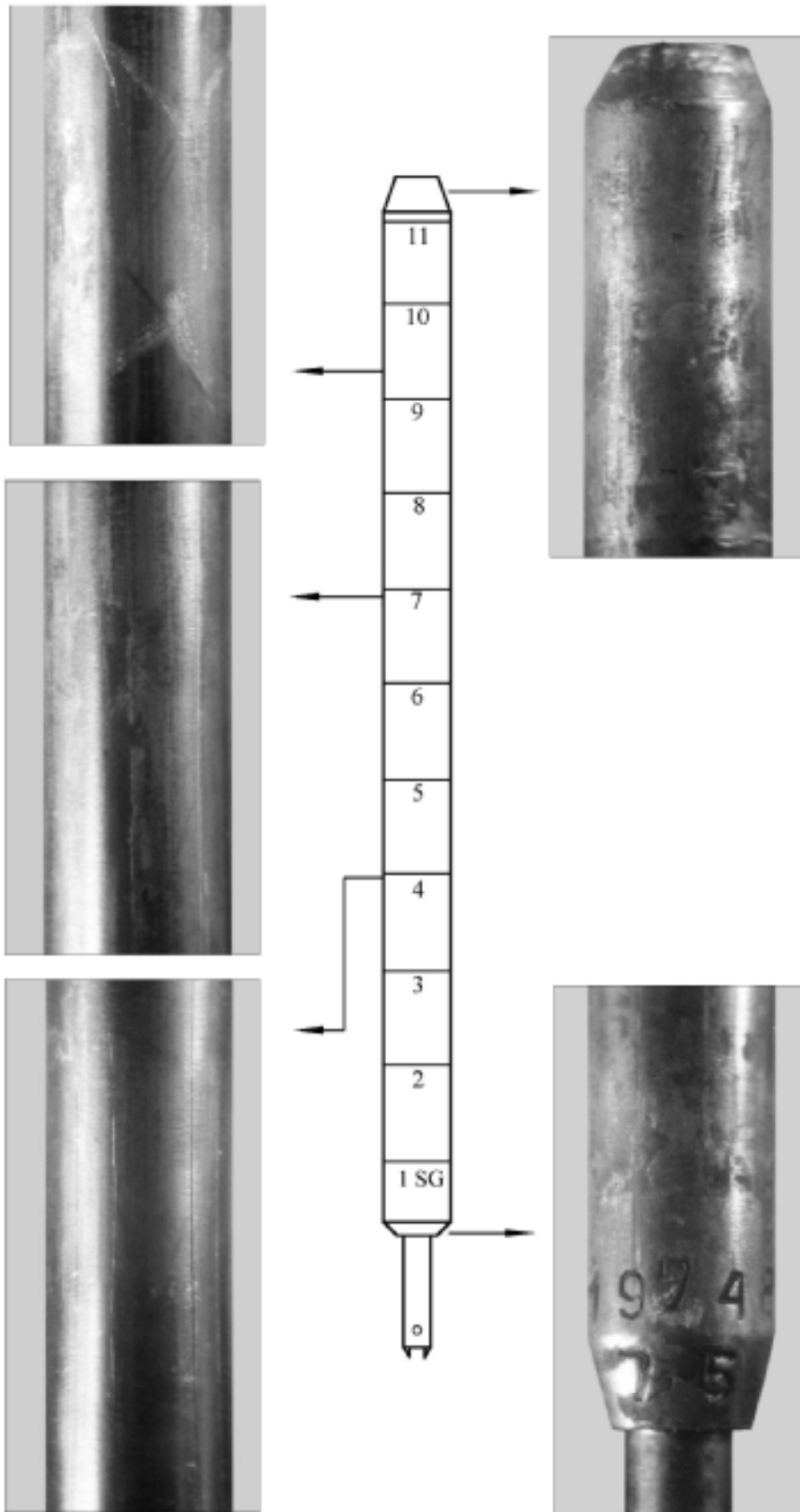
Fig. A2.4. The cladding fragments of fuel rod No. 78 after thermal testing at 390 ℃.

2. MEASUREMENT RESULTS OF THE FUEL ELEMENT GEOMETRY PARAMETERS
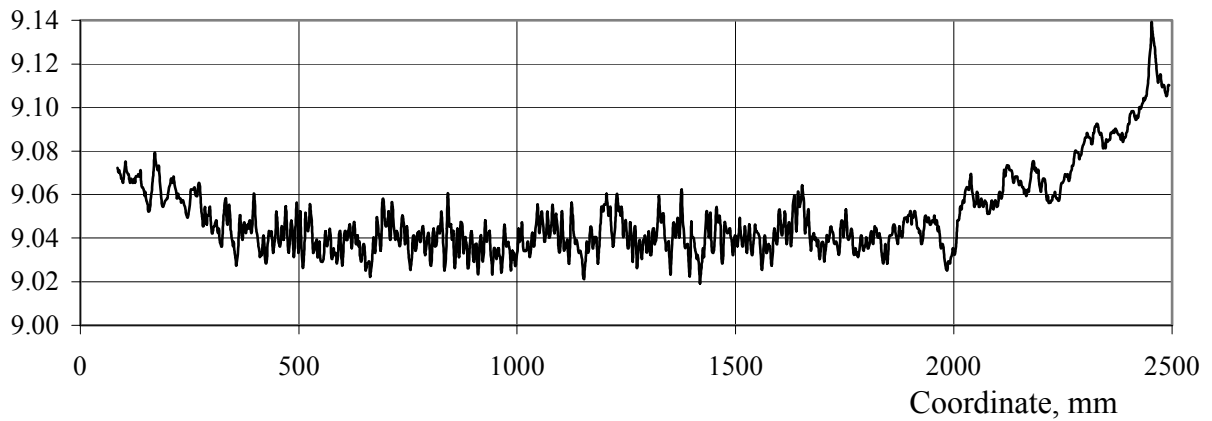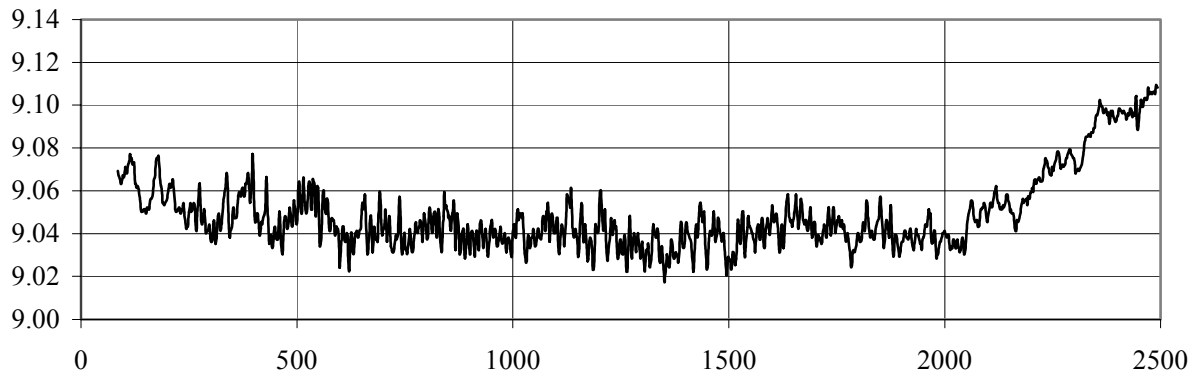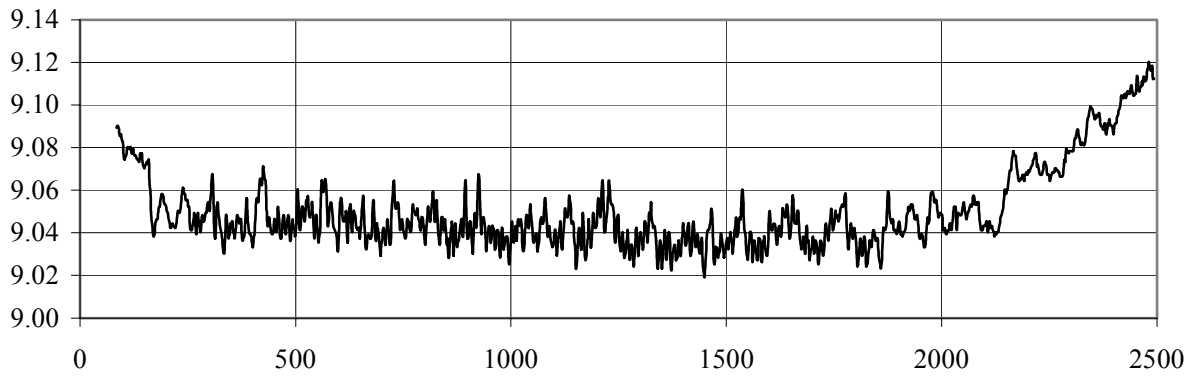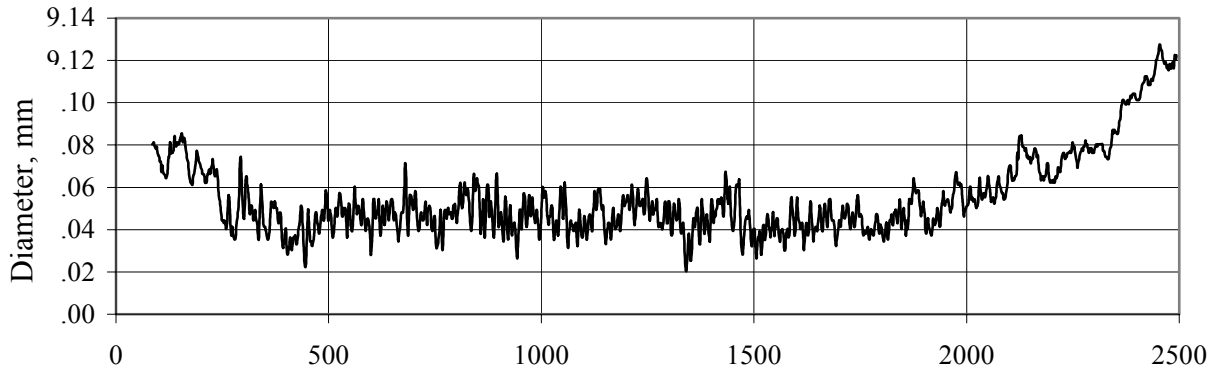
a
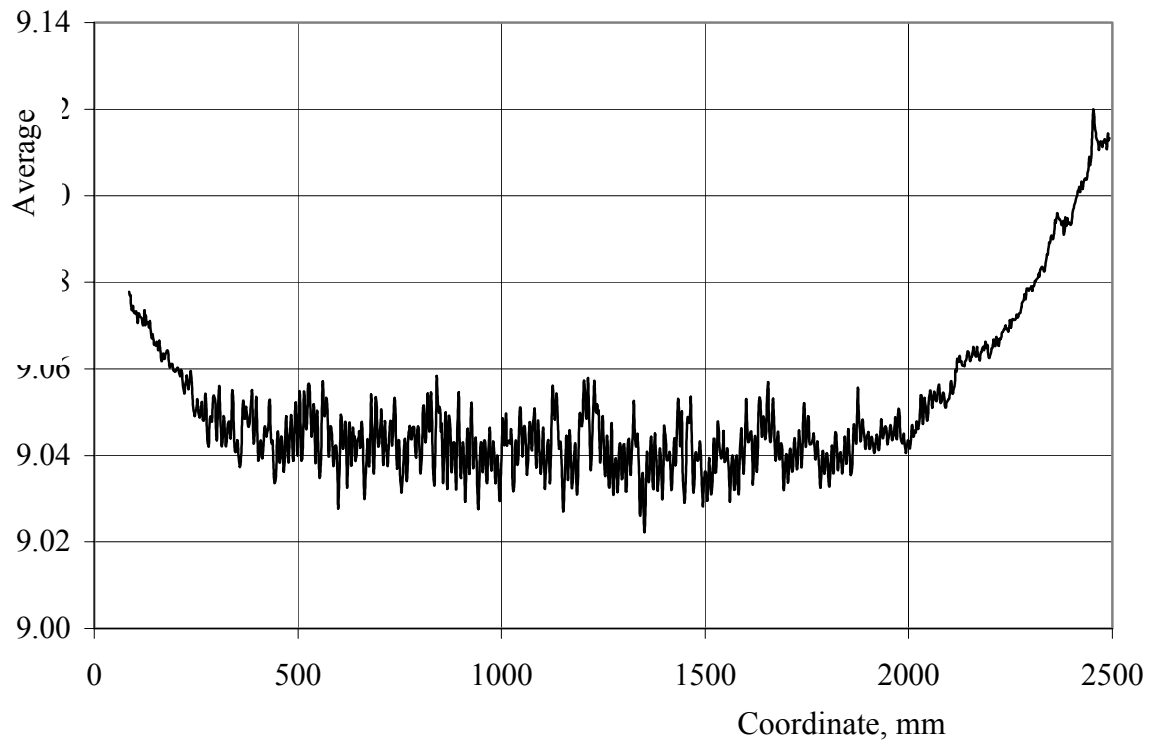
b

Fig. A2.5. The cladding profilometry results of fuel element No.64 in four orientations (a) and distribution of the cladding average diameter along the fuel element (b) after thermal test at 350°C.
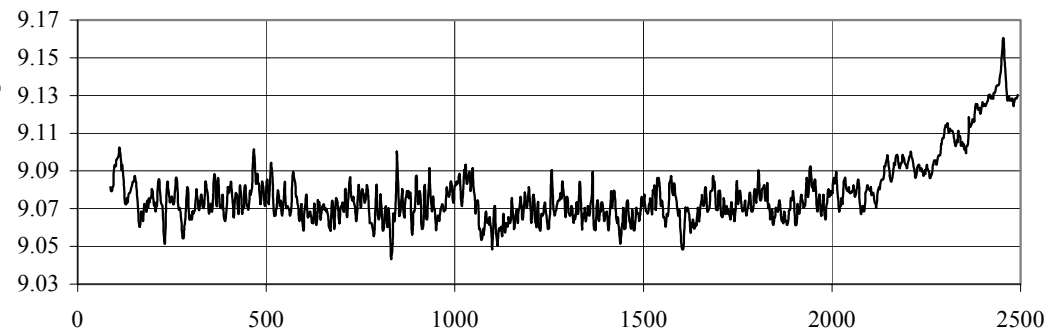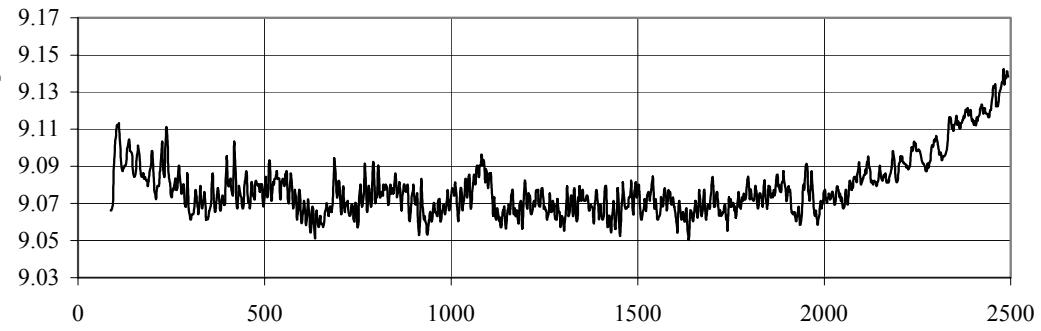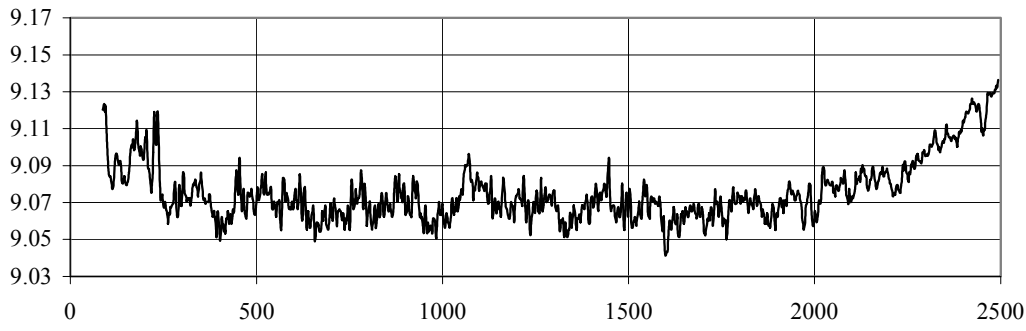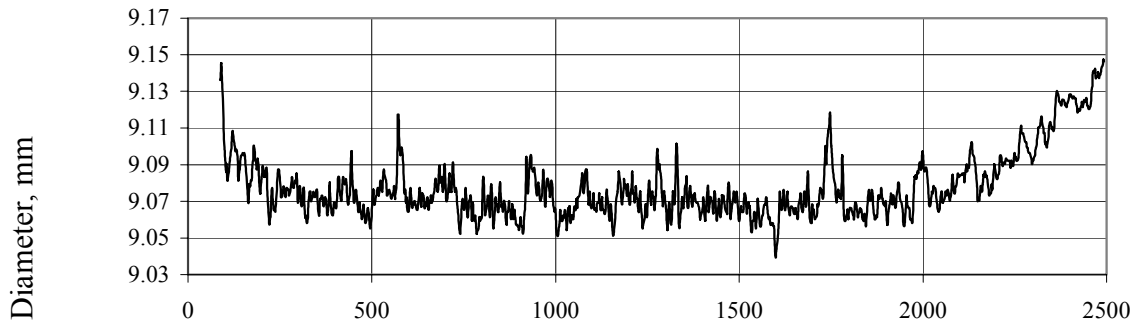
a
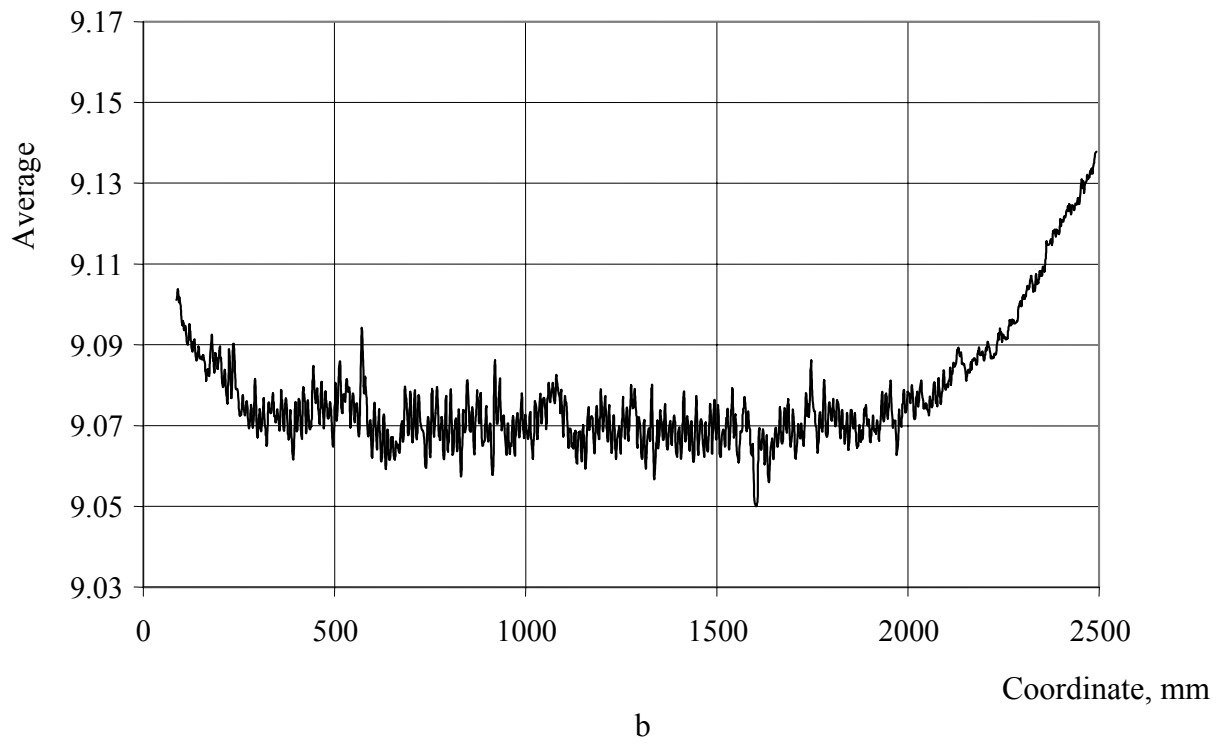
Fig. A2.6. The cladding profilometry results of fuel element No.78 in four orientations (a) and distribution of the cladding average diameter along the fuel element (b) after thermal test at 350°C.
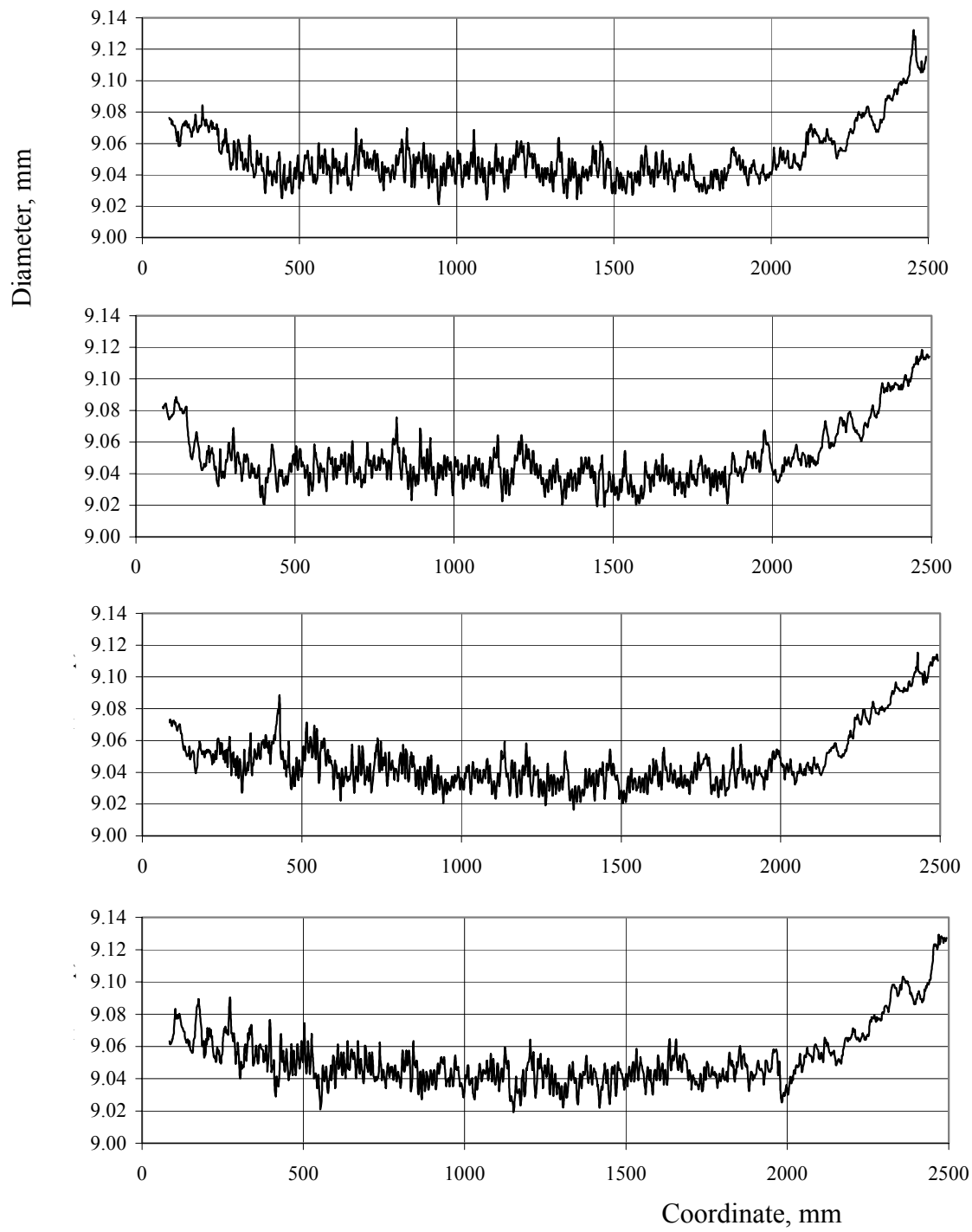
a
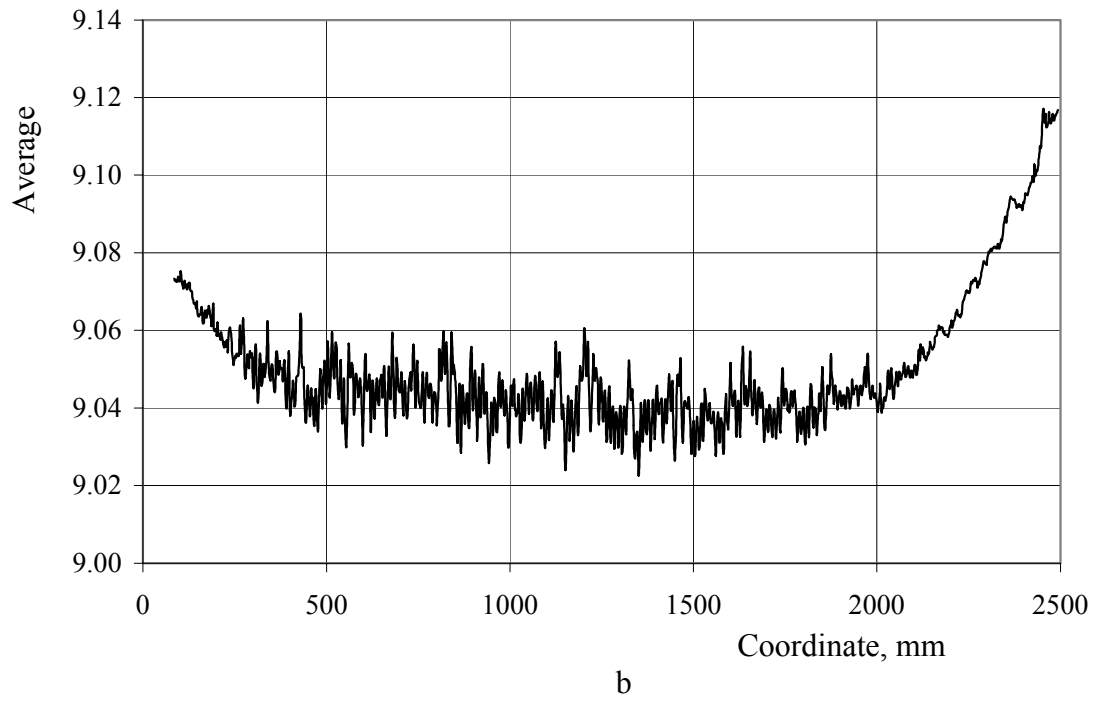
Fig. A2.7. The cladding profilometry results of fuel element No.64 in four orientations (a) and distribution of the cladding average diameter along the fuel element (b) after thermal test at 390 °C.

a

B
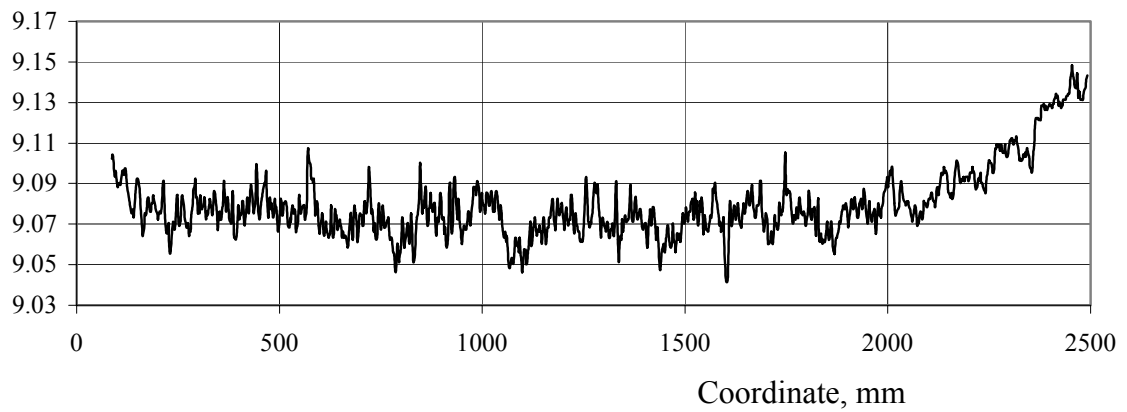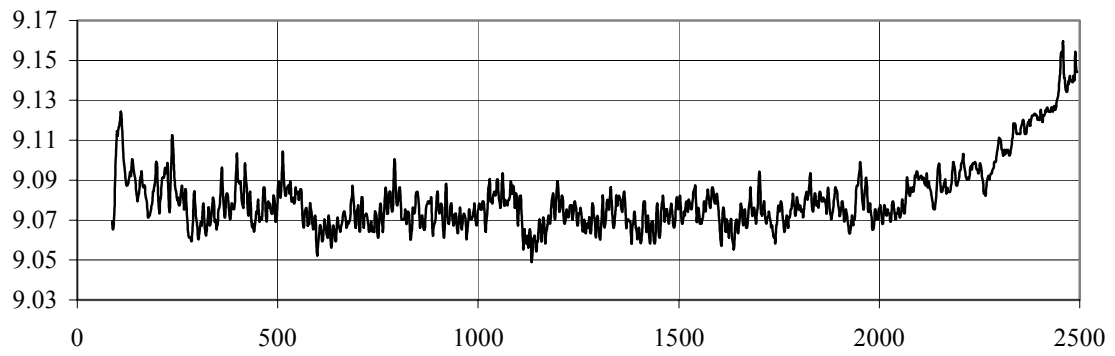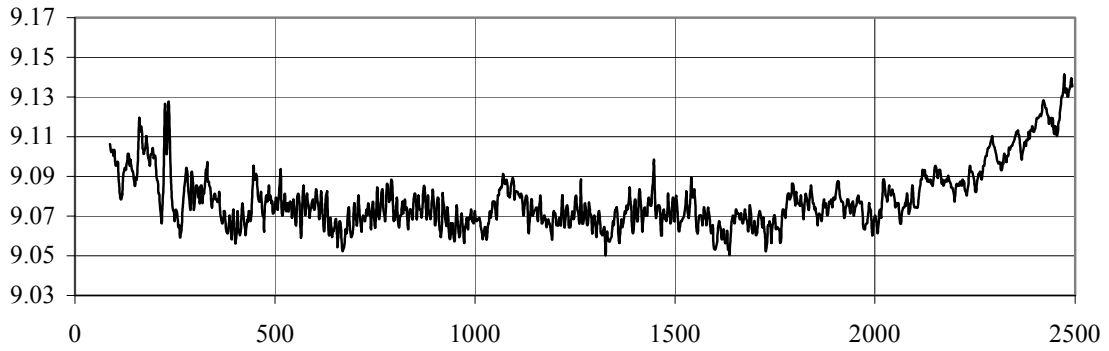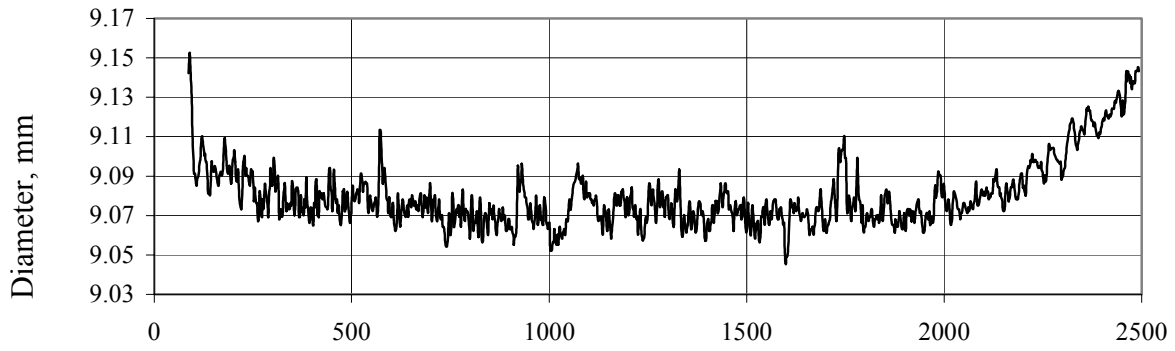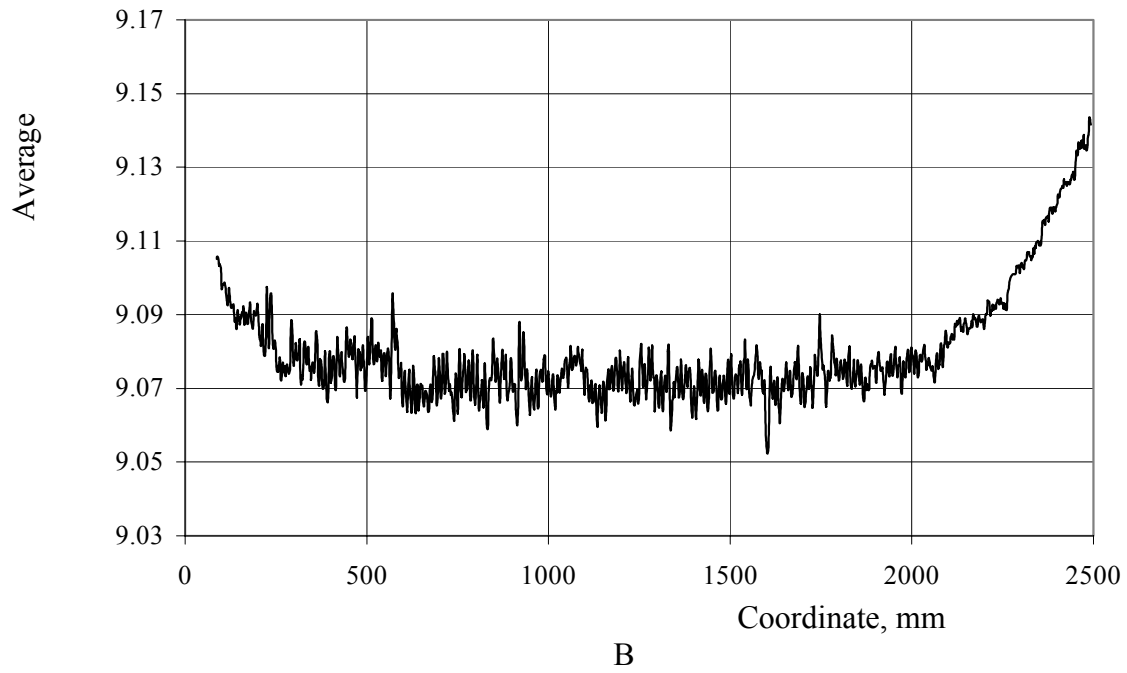
Fig. A2. 8. The cladding profilometry results of fuel element No.78 in four orientations (a) and distribution of the cladding average diameter along the fuel element (b) after thermal test at 390 °C.

Table A2.I. Measurement results of the fuel element length after thermal tests

T, °C	350	390
Fuel element No.64	2558.0±0.3mm	2558.4±0.3mm
Fuel element No.78	2558.4±0.3mm	2558.8±0.3mm

3. EDDY-CURRENT FLAW DETECTION RESULT

a

b
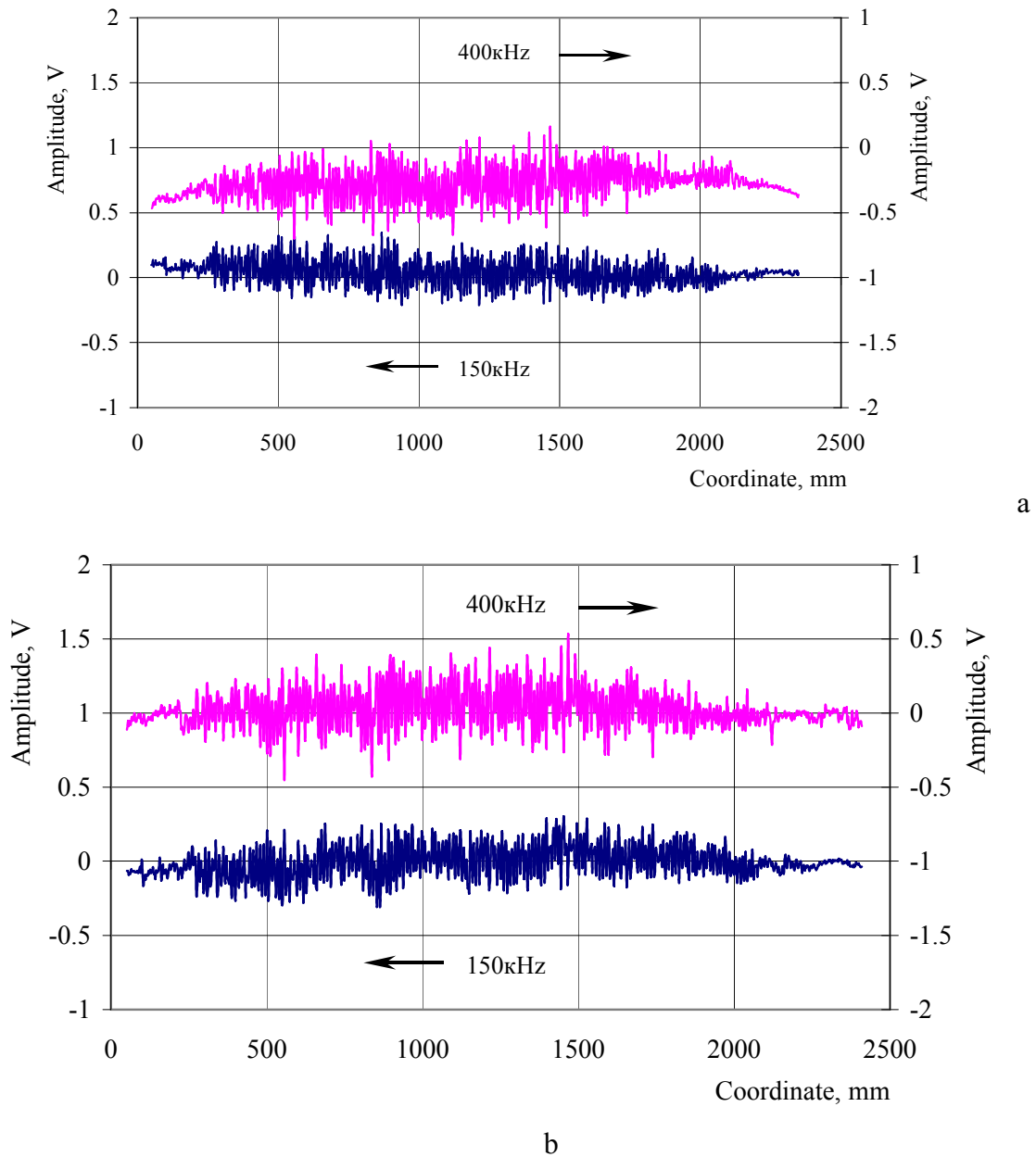
Fig. A2.9. Eddy-current test of cladding for fuel rod No .64 after thermal tests at 350°C (a) and 390°C (b).
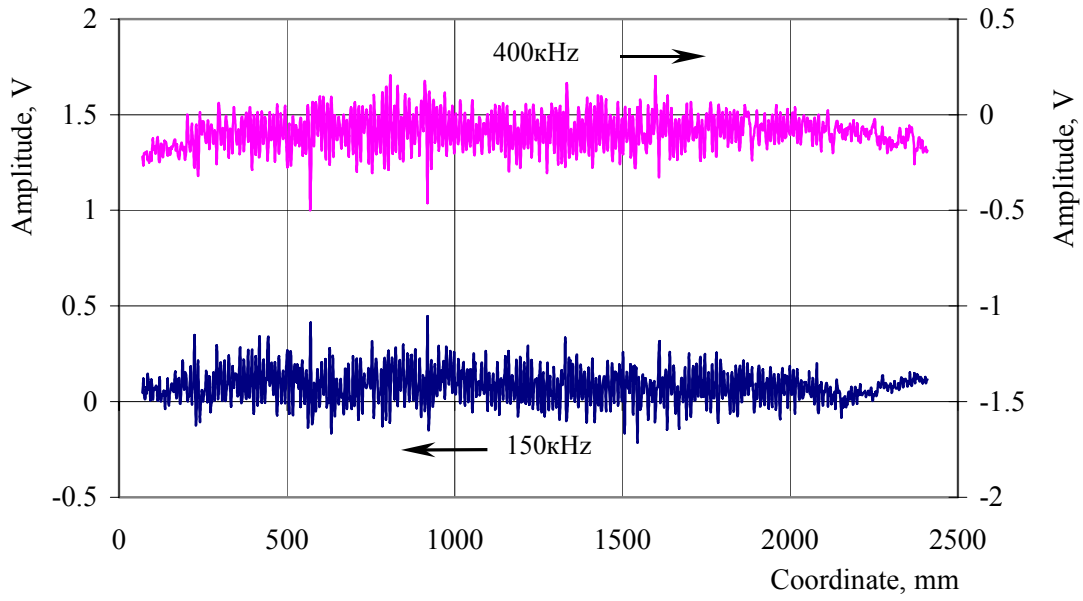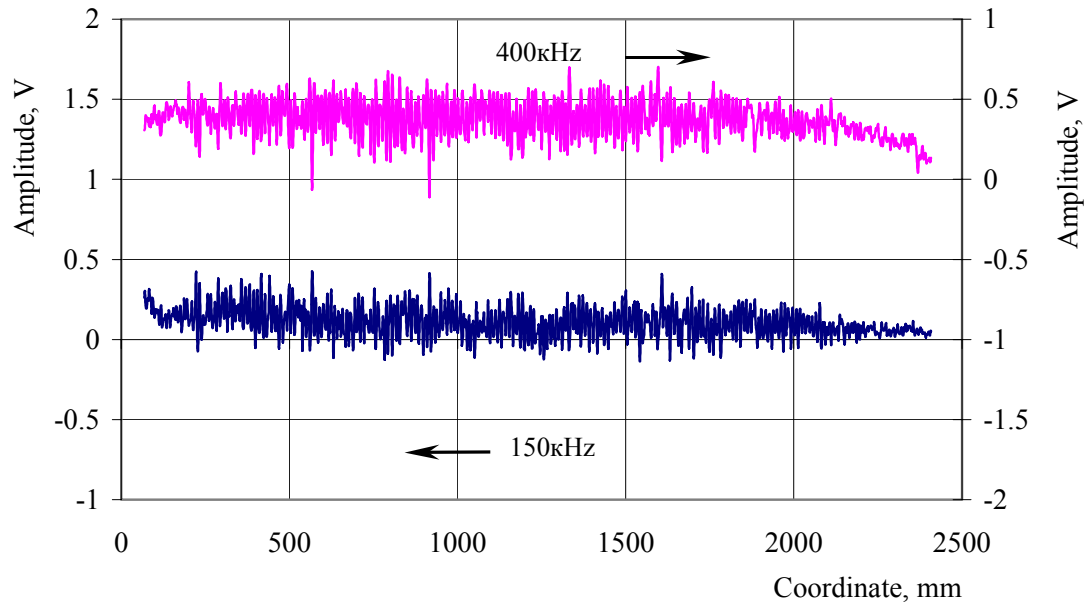
Fig. A2.10. Eddy-current test of cladding for fuel rod No. 78 after thermal tests at 350℃ (a) and 390℃ (b).

4. THICKNESS MEASUREMENT RESULTS OF THE OXIDE FILM ON THE OUTER
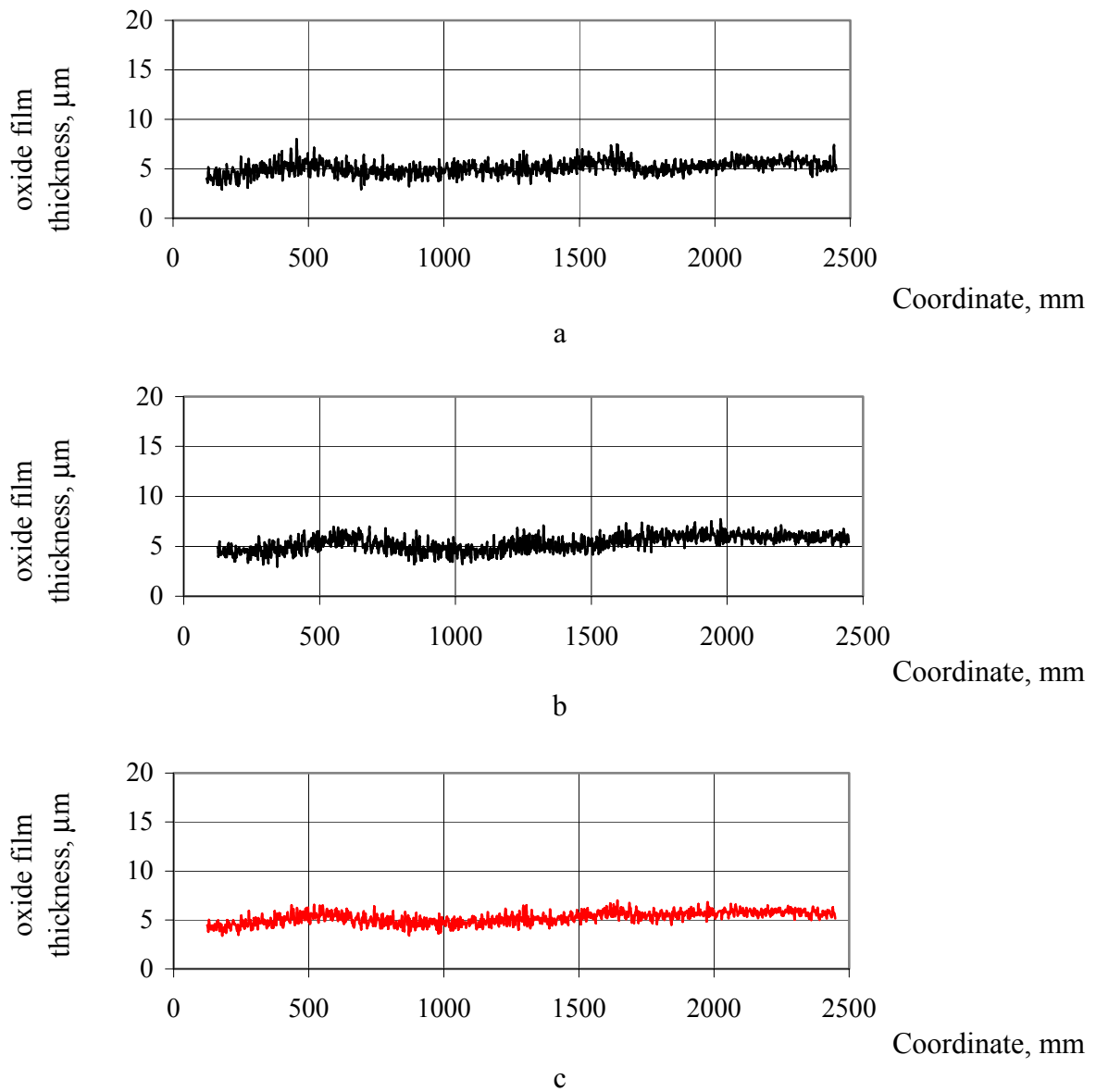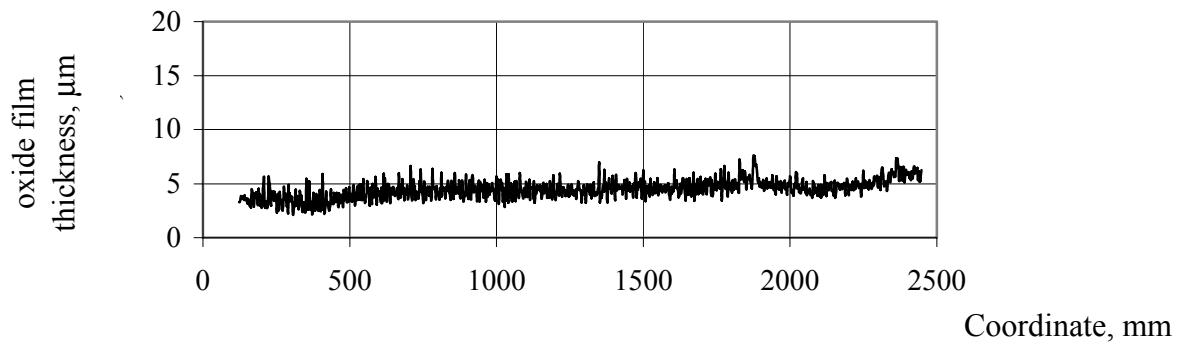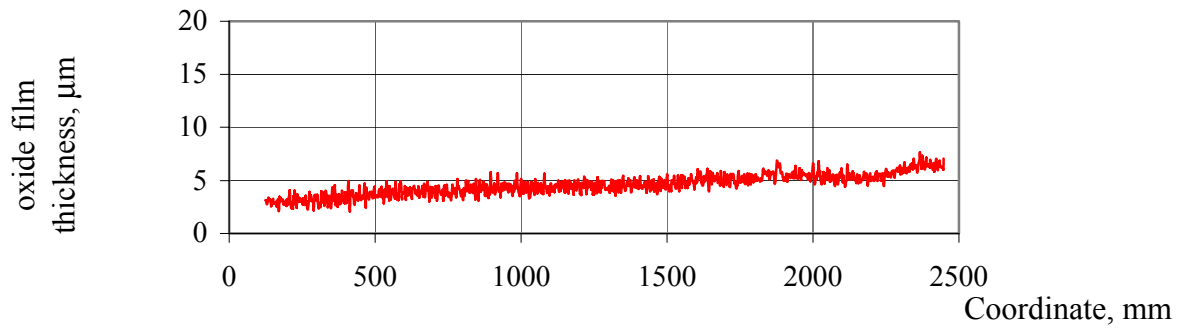   SURFACE OF THE FUEL ELEMENT CLADDING
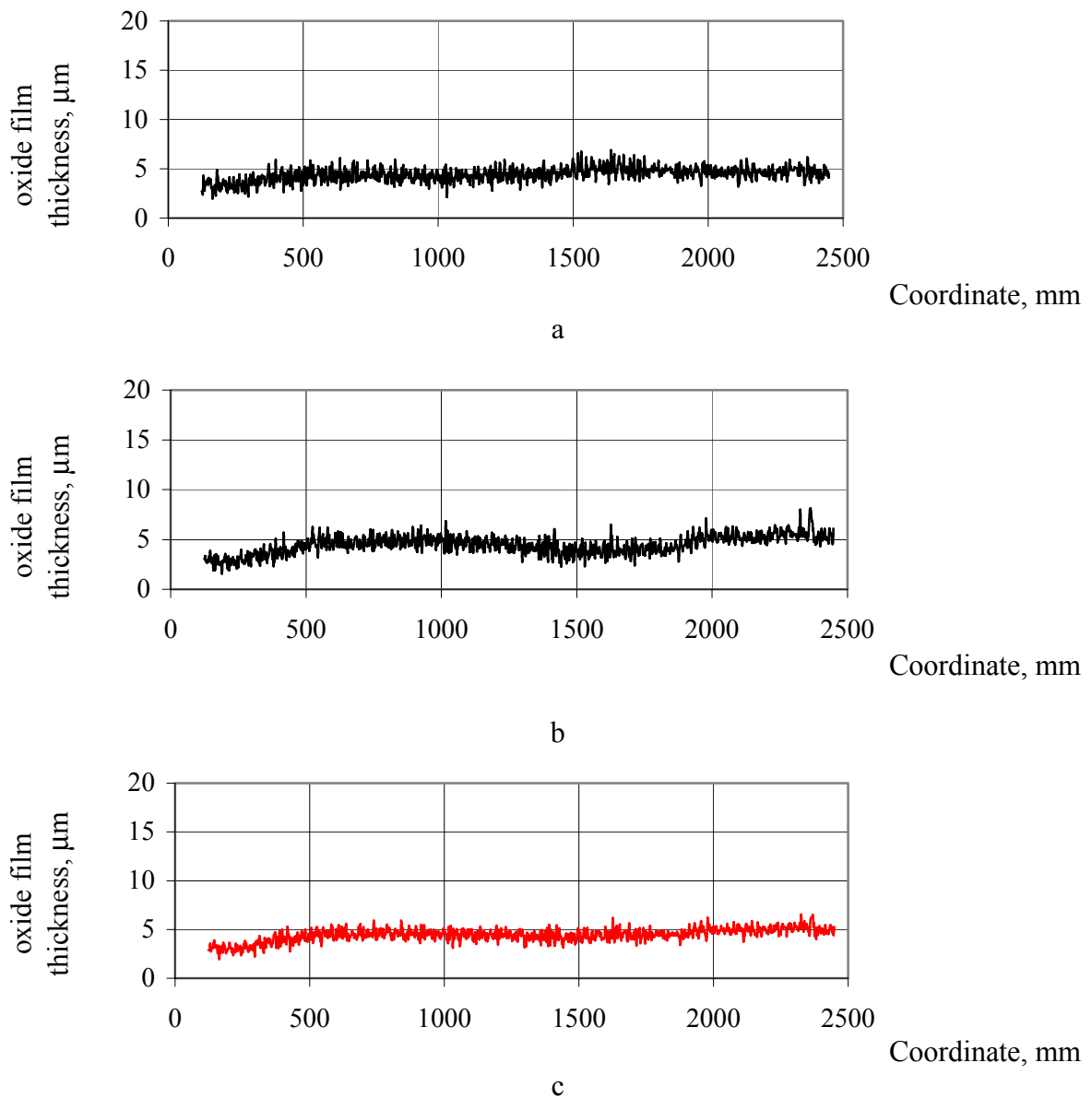
Fig. A2.11. Oxide film thickness in two orientations (a,b) on the cladding outer surface of fuel element No.64 and its average value (c) after thermal tests at 350 ℃.

Fig. A2.12. Oxide film thickness in two orientations (a,b) on the cladding outer surface of fuel element No.64 and its average value (c) after thermal tests at 390°C.
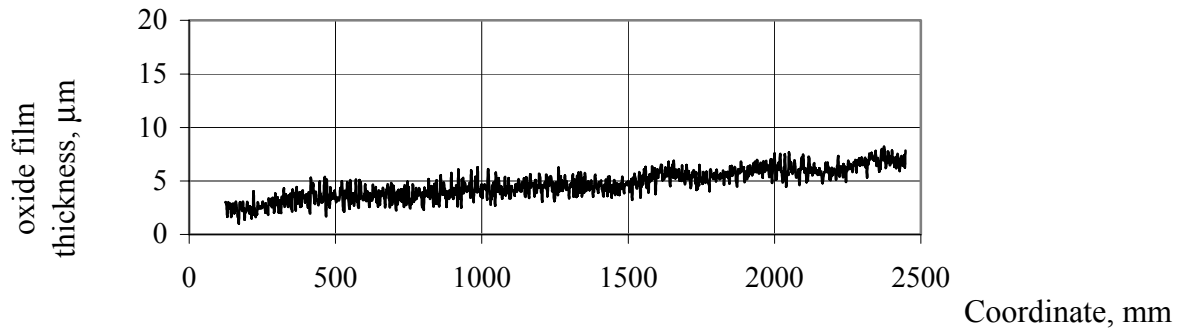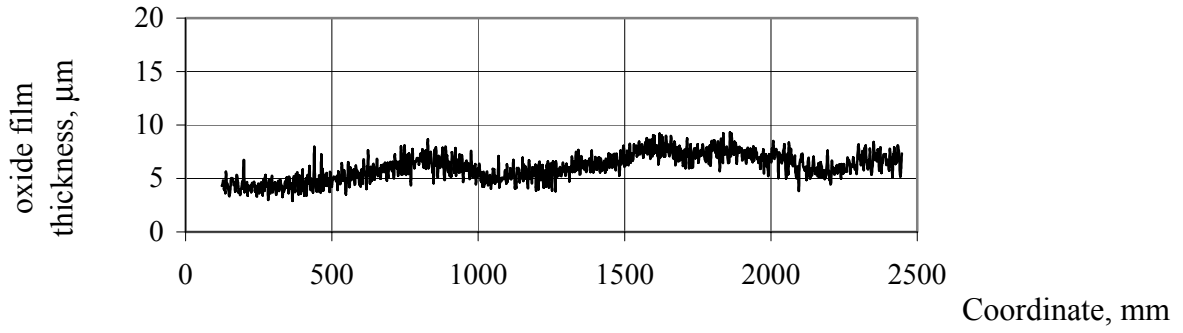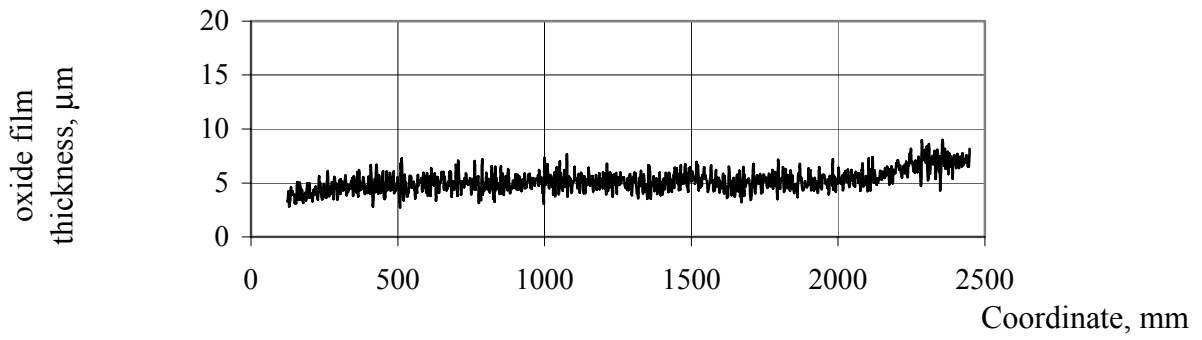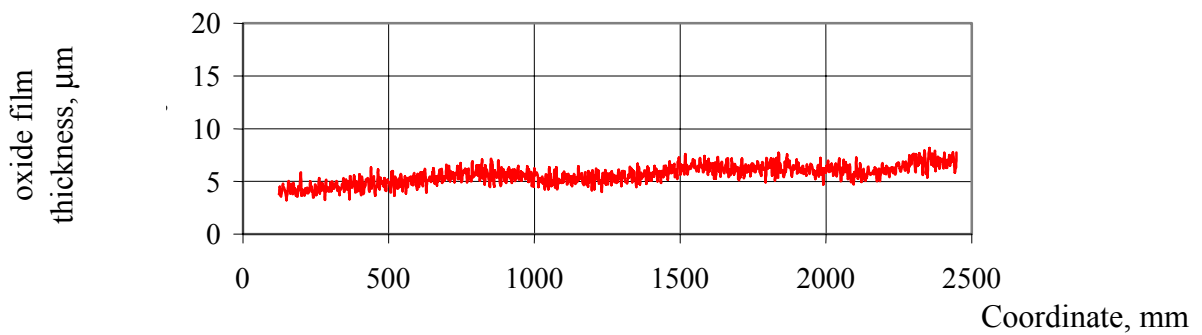
Fig. A2.13. Oxide film thickness in two orientations (a,b) on the cladding outer surface of fuel element No.78 and its average value (c) after thermal tests at 350 ℃.
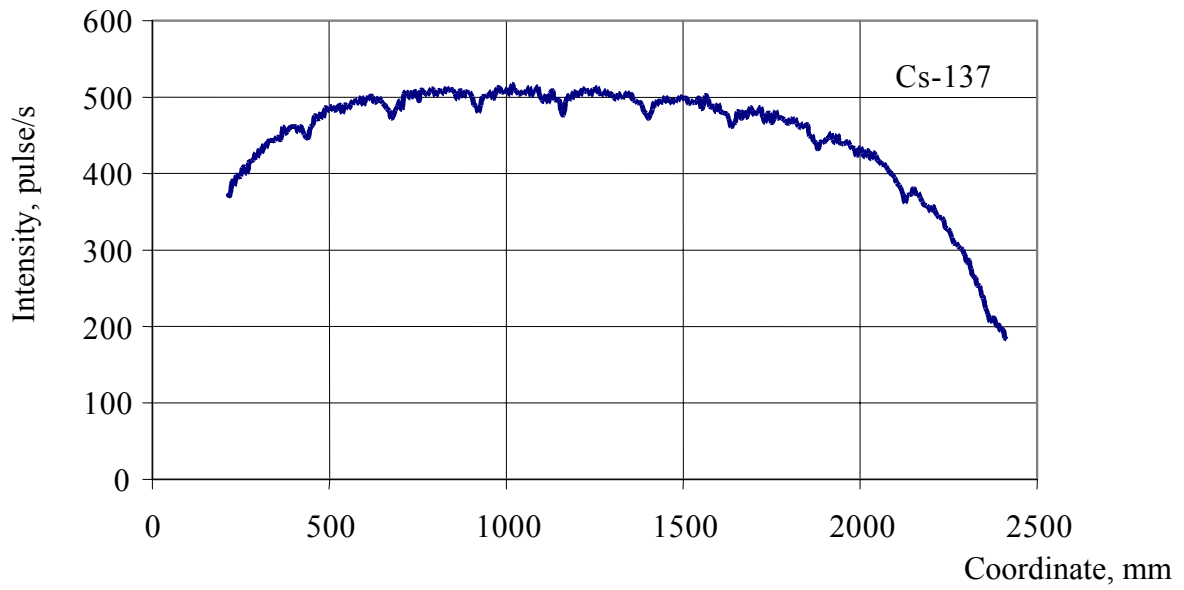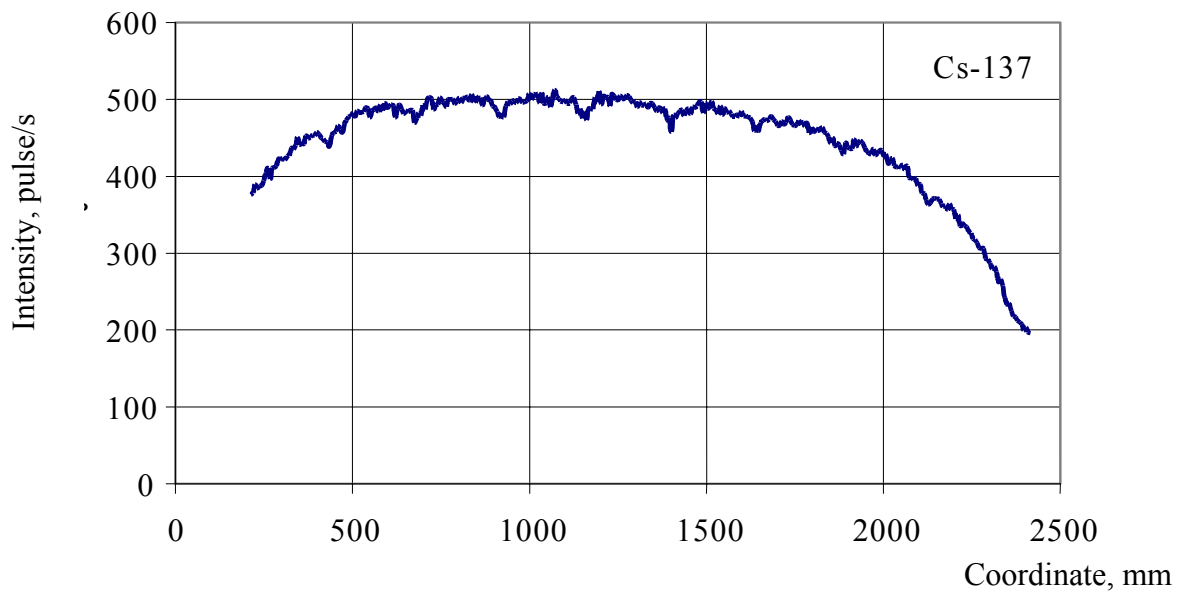
a

b

c

Fig. A2.14. Oxide film thickness in two orientations (a,b) on the cladding outer surface of fuel element No.78 and its average value (c) after thermal tests at 390°C.

5. GAMMA-SCANNING RESULTS OF FUEL ELEMENTS AFTER THERMAL TESTS

a

b
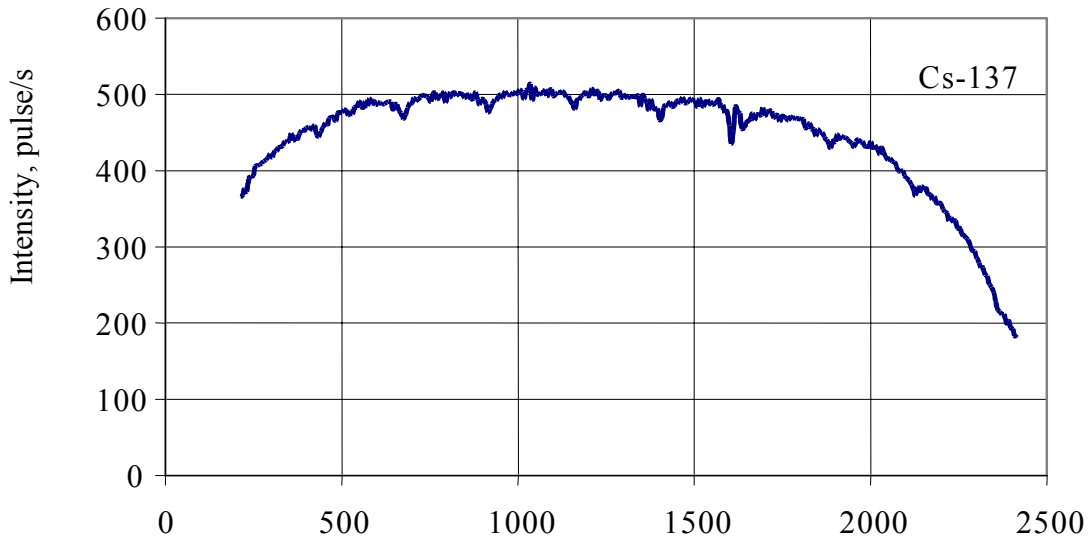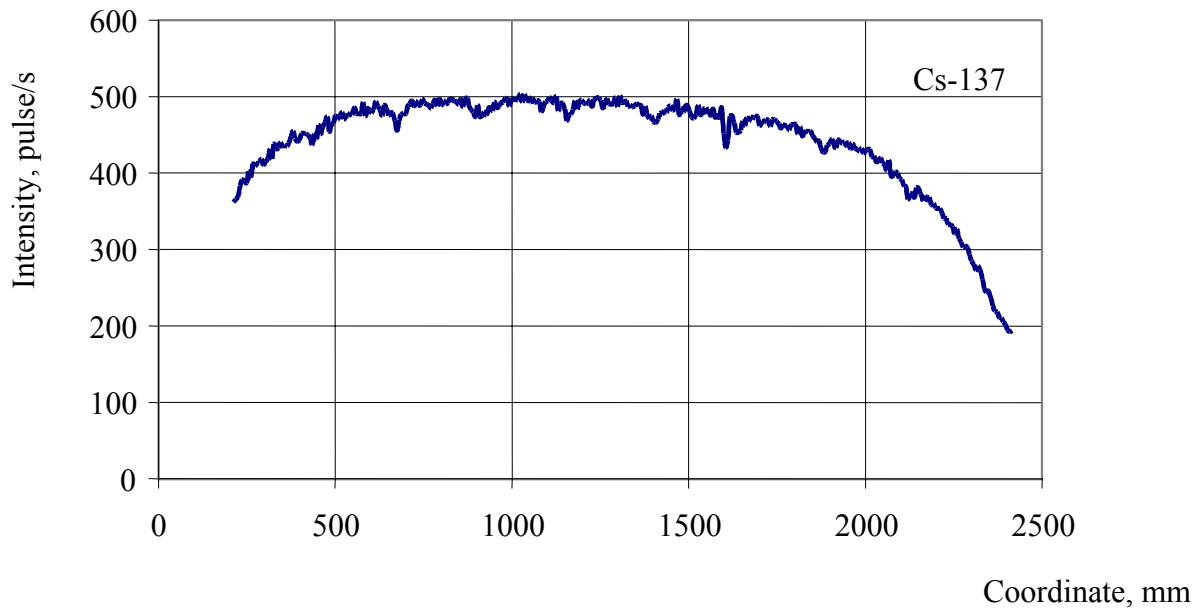
Fig. A2.15. The gamma- scanning results of fuel element No.64 after thermal tests at 350 ℃ (a) and 390 ℃ (b).

a

Coordinate, mm

b

Fig. A2.16. The gamma- scanning results of fuel element No.64 after thermal tests a 350℃ (a) and 390℃ (b).

REFERENCES

[1] MAYUZUMI, M., AND YOSHIKI, N., A method for evaluating maximum allowable temperature of spent fuel during dry storage condition: Safety, Engineering and environmental Aspects (Proc. Int. Sem. Vienna, 1990), IAEA-SR-171, Vienna (1990) 21.

[2] PEEHS, M., et al. LWR Spent Fuel Behaviour. Journal of Nuclear Materials, v.137, No.3 (1986).

[3] BIBILASHVILI Yu.K., KADARMETOV I.M., MEDVEDEV A.V. SOCOLOV F.F., Permissible temperatures of WWER spent fuel under dry storage conditions. Second International Seminar on WWER Fuel Performance, Modeling and Experimental Support, Sandanski, Bulgaria, 21–25 April 1997.

[4] SMIRNOV, A., SMIRNOV, V., et al., The peculiarities of the WWER-440 fuel behaviour at higher burnups, Second International Meeting "WWER Fuel Performance, Modeling and Experimental Support". April 21–25, 1997, Bulgaria.

[5] BEK, E.G., JENIN, A.A., IVANOV, A.V., et al ,"WWER spent fuel rods cladding material", 66 pages with illustrations, Atlas, Novo Sibirsk, in Russian language.

[6] SMIRNOV, A., SMIRNOV, V., et al., Behaviour of WWER-440 and WWER-1000 fuel in a burnup range of 20–48MW.d/kgU, Ibid. [4].

[7] ROGOZJANOV, A. J., KABYLJANSKIJ, G.P., NOVOSELOV, A.E., et al, "Relationships and peculiarities of the Zr-1%Nb alloy steady state creep before, during and after in pile irradiation", Transactions of the SCC RIAR, vol.4, Dimitrovgrad (2000) 17–23, in Russian language.

[8] ROGOZJANOV, A. J., KABYLJANSKIJ, G.P., "Zr-1%Nb alloy out of reactors creep in the components for nuclear energy" Transactions of the 5th International conference of reactor materials, Dimitrovgrad, Sept. 8–12 1997, vol. 2 part1 Dimitrovgrad (1998) 164–195, in Russian language.

[9] ROGOZJANOV, A. J., KABYLJANSKIJ, G.P., NOVOSELOV, A.E., et al , "Radiation and thermal creep of Zr-alloy cladding tubes" Transactions of 6th Russian conf. Of reactor materials, Dimitrovgrad September 11–15 2000, vol.2 part1, Dimitrovgrad (2001) 111–127, in Russian language.

[10] ROGAZJANOV, A. J., NUZHDOV, A.A., "Description of the transient creep stage of Zr-1%Nb alloy cladding tubes", Transactions of SCC RIAR, vol.2, Dimitrovgrad (2001) 10–20.

[11] HEP, J., SHIK, V., VESELY, J., "The characteristics of the WWER-440 SNF in CASTOR 440/84 cask (thermal report)", Skoda JS Plzen, Ae 9864/Dok, June 1999, in Czech language.

[12] ZYMAK, J., VESELY, J., "Prelimary proposal of limit conditions for high burnup WWER-440 SNFdry storage (up to 47 MWd/kgU) in the CASTOR 440/84 type of cask". Skoda-UJP report No. 892, December 1999, in Czech language.

[13] SPILKER, H., PEEHS, M., DYCK, H-P, KASPAR, G., NISSEN, K., "Spent LWR fuel dry storage in large transport and storage casks after extended burnup", Journal of Nuclear Materials, 250 (1997), 63–74.